THE UNIVERSITY OF ALBERTA

RELEASE FORM

NAME OF AUTHOR: Robert Leslie Brooks

TITLE OF THESIS: Polarization Studies Using Beam-Foil Spectroscopy

DEGREE FOR WHICH THESIS WAS PRESENTED: Ph.D.

YEAR THIS DEGREE GRANTED: 1979

THE UNIVERSITY OF ALBERTA

POLARIZATION STUDIES USING BEAM-FOIL SPECTROSCOPY

by

© ROBERT LESLIE BROOKS

A THESIS

SUBMITTED TO THE FACULTY OF GRADUATE STUDIES AND RESEARCH

IN PARTIAL FULFILMENT OF THE REQUIREMENTS FOR THE DEGREE

OF DOCTOR OF PHILOSOPHY

DEPARTMENT OF PHYSICS

EDMONTON, ALBERTA

FALL, 1979

THE UNIVERSITY OF ALBERTA

FACULTY OF GRADUATE STUDIES AND RESEARCH

The undersigned certify that they have read, and recommend to the Faculty of Graduate Studies and Research, for acceptance, a thesis entitled "Polarization Studies Using Beam-Foil Spectroscopy" submitted by Robert Leslie Brooks in partial fulfilment of the requirements for the degree of Doctor of Philosophy.

ABSTRACT

Methods are presented for acquiring and analyzing polarization data taken with the beam-foil light source using a tilted foil. These methods include a self-consistent technique for determining the axis of a plane polarizer, as well as the fast axis and phase of a retarder.

The generalized theory of light emission in the dipole approximation for a cascade-free source using the spin-independence hypothesis is reviewed and extended to include the evaluation of the Stokes parameters. Alignment and orientation are described by excitation parameters using the spherical tensor formalism. These excitation parameters are then related to the Fano-Macek parameters and some consequences and examples of the formalism are examined.

The results of three experiments using neutral Helium are presented. The first examines the polarization of four singlet transitions as a function of foil-tilt angle. The second presents an examination of the spectrum of Helium transitions between doubly-excited states and the polarization vs. tilt angle for four such transitions. The third examines the complications which arise when the polarization vs. tilt angle is measured for the triplet transitions and presents some results for three such transitions.

A survey of the polarization of fifteen Nitrogen II transitions and five Nitrogen III transitions measured at 0° and 60° foil-tilt angle is presented. Complications

arising from unresolved hyperfine structure and partially resolved fine structure are examined in detail.

Experimental evidence for the validity of the spin-independence hypothesis is discussed. An empirical rule for estimating the relative magnitude of the circular polarization fraction at large tilt angle is also presented.

ACKNOWLEDGMENTS

Through almost six years and two degree projects my supervisor, Dr. E.H. Pinnington, has offered guidance, assistance and friendship which have not only made this work possible but enjoyable. His financial support for travel to, and participation in, two international beam-foil conferences is also gratefully acknowledged.

No laboratory work is possible without competent technical assistance. The construction of both the target chamber and polarimeter were performed by Mr. E.A. Foster whose expertise is principally responsible for the excellent precision of the data. The accelerator, vacuum systems and most peripheral equipment were assembled and maintained by Mr. J.H. Woolley. Hearty thanks to both are offered for all of their help.

Special thanks are extended to Dr. Bonnie Edwards who produced the excellent computer graphics used for many of the figures. Helpful discussions with her and encouragement from my wife, one and the same person, have added immeasurably to the quality of this work.

Financial assistance from the Alma Mater Fund and the University of Alberta are gratefully acknowledged.

TABLE OF CONTENTS

CHAPTER PAGE

LIST OF TABLES

LIST OF FIGURES

LIST OF PHOTOGRAPHIC PLATES

CHAPTER I

INTRODUCTION

Beam-foil spectroscopy (BFS) has been a fertile area of experimental atomic phsyics for the past fifteen years. It has recently been chosen as the topic for Volume 1 of Topics in Current Physics (Ba 76) which offers an excellent and comprehensive review of the subject by eleven authors. Another recent review of the entire area has been written by H. G. Berry (Be 77). Five international conferences devoted to beam-foil spectroscopy, each with published proceedings,[1] have stimulated rapid advances and have helped the dissemination of new techniques to laboratories around the world.

BFS under usual conditions utilizes a fast positive ion beam ($v \simeq 0.01c$), at high vacuum, which passes through a thin (3 - 50 μgm/cm^2) exciter foil before being collected in a Faraday cup, which provides the means for monitoring the beam current. The foil (usually amorphous carbon) causes the ions to populate practically all excited states, including those of several different ionization stages. Which ionization stage predominates depends upon the emergent beam velocity. Spontaneous radiative decay of these excited states produces a spectral source with unique characteristics. Many lines, mostly from multiply-excited states, have never

---

[1] Ba 68, MBB 70, Ba 73, SP 76, De 79.

been observed from conventional sources. Collisional line broadening is non-existent due to the high vacuum condition but Doppler broadening when viewing the beam perpendicularly is significant.

The well defined foil location, together with the known beam velocity permit positions along the beam to be simply converted to precise times since foil excitation. By passing light collected perpendicularly from a short longitudinal section of the beam through a monochromator, the intensity of a selected transition may be measured as a function of time since excitation. By starting such a measurement close to the foil and by moving the foil in small increments a decay curve for the selected excited state may be directly measured. Such a curve for the ideal case would decrease in intensity as a single exponential function whose decay constant would be the reciprocal of the mean life of the exicted state. In practice, cascades from higher lying levels and blends from spectral lines of another ionization stage complicate the analysis.

The previous brief description has been given for what might be categorized as classic beam-foil spectroscopy. Spectral identification and mean-life determination are not the only measurements which can be performed with the beam-foil source. Two types of measurements are sensitive to the anisotropic nature of the excited states. One is a quantum-beat measurement in which the light intensity is observed to

be modulated as a function of distance from the foil. The modulation frequency is a consequence of a coherent superposition of closely spaced (in energy) excited levels, usually fine structure or hyperfine structure separations if performed with no external field. The coherence is a consequence of the sudden nature of the excitation which must take place in a time at least as short as the foil passage time. In fact the same phenomenon has been observed with a gas sample in place of a foil so the relevant time is almost certainly the two particle collision time ($\approx 10^{-16}$s) and not the time of passage through the foil (SLMH 79). The amplitude of the modulation depends upon the degree of alignment or orientation present in the excited state. These quantities are measures of the anisotropy of the excited states which also influences the polarization of the emitted light. The determination of this polarization constitutes the second type of measurement alluded to above and is the subject of this dissertation.

The beam-foil excitation mechanism and the way it relates to ion-atom collision studies using gas targets or solid surface targets with glancing collisions has come under extensive scrutiny in recent years. Besides the esoteric interest generated when a new phenomenon is observed, such studies may have practical implications for plasma research where ion-atom charge exchange cross sections are required and where new diagnostic techniques always need development.

The study of surface phenomena by the use of an ion-beam probe can also have practical implications for the solid-state physicist. While such considerations may provide motivation for this research, the area is too new to be able to point convincingly to any practical benefits thus far.

The phenomenon which will be examined in detail is the change of the polarization of the emitted light following beam-foil excitation with the change in the foil-tilt angle. It will be demonstrated that large circular polarization fractions can be observed with a tilted foil. Such large fractions are not restricted to one or two carefully chosen transitions but are of a rather general nature and can be observed in a large selection of transitions though not from all transitions.

The polarization of the emitted light is not just a function of foil-tilt angle but also depends upon foil material, beam velocity, foil temperature, the type of atom or ion excited by the foil and at least some of the quantum numbers of both the excited state and the state to which the transition is made. Measurements to be presented in this project will focus upon the change of polarization with foil-tilt angle for a selection of different Helium transitions having different quantum numbers (Chapter V) and a comparison of polarizations with a perpendicular foil and a 60° tilted foil for a large selection of different Nitrogen transitions (Chapter VI). As many of the other variables as possible

have been kept constant for these measurements and a complete description of experimental parameters is given in Appendix 2 along with the tabulated results.

Chapter II presents a theoretical description of the light intensity emitted via dipole radiation in the absence of cascades. The Stokes parameters, a particularly convenient and complete description of the polarization of light, are then derived from this expression. While none of the material is new, the treatment is in some respects more complete than others which have appeared in print and all of the derivations have been performed by the author.

Chapter III describes the method used for measuring the Stokes parameters. The idea of rotating a retarder before a fixed polarizer had not been used by beam-foil spectroscopists when the decision was made to utilize this method, and had been proven to work satisfactorily as a preliminary step to collecting data before the technique appeared in the literature. The method of data reduction chosen for this type of experiment is somewhat more straightforward than that proposed by others. Methods presented for determining the angles of the polarizing elements and the phase of the retarder were also developed within the course of this project.

Chapter IV describes the experimental equipment, the method of data collection and the error analysis employed. All of the equipment preparation and programming of the new

minicomputer system were performed as part of this project.

Chapter V discusses three experiments performed using neutral Helium. All of them are related to the variation of polarization with changing foil-tilt angle. The first examines the Helium singlets, the second Helium doubly-excited states and the third normal triplets. The results of the first experiment have been published, the second is in preparation and the third will be performed again in a different manner as suggested in the text.

Chapter VI describes the polarization at two different foil tilts of a selection of Nitrogen II and III transitions, and examines many of the complications that occur when performing such measurements of elements more complex than Helium. The spin-independence hypothesis and the matter of partially resolved fine structure are two areas which will be examined in some detail.

CHAPTER II

THEORY OF LIGHT EMISSION

This chapter will treat that aspect of light emission which is relevant to the beam-foil source. A generalized intensity expression will be found which accounts for both a superposition of energy levels as well as non-statistical population of the excited states. From this expression the Stokes parameters or polarization of the emitted light will be derived.

The polarization of radiation spontaneously emitted by an excited atom or ion is dependent upon the relative populations of the magnetic sub-states in the excited state manifold of interest. These relative populations depend upon the excitation mechanism whose spatial symmetries impose constraints upon the relative populations, which in turn will dictate the number of independent parameters needed to describe the excited state. The polarization is further dependent upon the direction of emission but this is a consequence of the non-isotropic nature of the excitation process itself.

One feature of the beam-foil source is that excitation occurs during rapid passage ($<10^{-14}$s) through a thin carbon foil. The excited state is then a coherent superposition of states within an energy band of approximately

0.06 eV (500 cm^{-1}). Quantum beats, or modulations of the emitted intensity with time, may be observed if the energy difference of available states yields frequencies within the band pass of the detection system. A summary of quantum beats in beam-foil spectroscopy has previously been written by the author (Br 75). A theory of light emission applicable to the beam-foil source must be able to account for all of the aforementioned processes.

The theoretical treatment which follows uses a formalism employed by Ellis (El 73) and extends the calculation to an evaluation of the Stokes parameters under general detector orientation. The results so obtained are then compared to those using the Fano-Macek formalism (FM 73) which, while having a different appearance, is an equivalent treatment of the same problem.

It perhaps should be stressed that the Stokes parameters represent a property of the source and depend principally upon source parameters and the direction of emission and, while dependent upon the detector coordinate frame, are independent of the polarimeter or the measurement sequence used to determine them (Chapter III). The polarization vector, $\vec{\varepsilon}$, is a source parameter and as such is an unknown quantity. It can be eliminated by forming the Stokes parameters but in general there is no one-to-one correspondence between a given set of Stokes values and some particular $\vec{\varepsilon}$. This follows from the fact that Stokes parameters

represent an ensemble average which occurs in the derivation by performing a trace over a product of a density matrix and the emission operator. Unpolarized light, for example, occurs naturally in the result while no value of $\vec{\varepsilon}$ can represent unpolarized light. This point of view is not a necessary one to follow, but it permits complete separation of the quantum mechanics of light emission to be treated in this chapter from the measurement of the Stokes parameters which can be treated classically and is the subject of the following chapter.

2.1 Separation of the Intensity Expression

The intensity of light emitted within a solid angle $d\Omega$ can be expressed in the electric dipole approximation as

$$\frac{dI}{d\Omega} = C' \sum_f \left| < f \left| \vec{\varepsilon}^* \cdot \vec{D} \right| \psi_i (t) > \right|^2 \tag{2.1}$$

where the sum is taken over unresolved final states, $\vec{\varepsilon}$ is a complex polarization vector, $\vec{D}$ is the dipole transition operator and $C' = e^2\omega^4/2\pi c^3$ in c.g.s. units. If D is expressed in cm. the above expression has the dimensions of power. $\psi_i (t)$ expresses the time evolution of the initial state created by the foil and contains the unknown factors which are to be determined by measurement. In order to express ψ as a statistical combination of basis states, the density matrix formalism will be used.

First (2.1) may be expressed as

$$\frac{dI}{d\Omega} = T_r \{\rho(t)\, L(\lambda,\vec{\varepsilon})\}/T_r\, \rho(0)$$

where T_r indicates the trace of a matrix. ρ is the density matrix and L is the light emission operator which can be implicitly defined by rewriting the above as

$$\frac{dI}{d\Omega} = C'\, T_r\{(\vec{\varepsilon}^* \cdot \vec{D})^\dagger\, \rho(t)\, (\vec{\varepsilon}^* \cdot D)\}/T_r\, \rho(0). \qquad (2.2)$$

This problem will be solved in detail for the case of unresolved fine structure with no hyperfine structure. Other coupling schemes will be treated in section 2.5. The basis states can then be written as $|\alpha(LS)JM\rangle$. Equation (2.2) can be written in full as

$$T_r\, \rho(0)\, \frac{dI}{d\Omega} = \sum_{\substack{JM \\ J'M'}} \langle\alpha(LS)\; J'M'|L(\lambda,\vec{\varepsilon})|\alpha(LS)JM\rangle$$

$$\times \quad \langle\alpha(LS)JM|\rho(t)|\alpha(LS)J'M'\rangle \qquad (2.3)$$

where

$$\langle\alpha(LS)J'M'|L(\lambda,\vec{\varepsilon})|\alpha(LS)JM\rangle$$

$$= \sum_{J_fM_f} C' \quad \langle\alpha(LS)J'M'|(\vec{\varepsilon}^* \cdot \vec{D})^\dagger|\alpha(L_fS)J_fM_f\rangle$$

$$\times \quad \langle\alpha(L_fS)J_fM_f|(\vec{\varepsilon}^* \cdot \vec{D})|\alpha(LS)JM\rangle \qquad (2.4)$$

The time evolution of the density matrix can be expressed as

$$\rho(t) = e^{-iHt/\hbar}\,\rho(0)\,e^{iHt/\hbar}$$

and hence

$$\begin{aligned}&\langle\alpha(LS)JM|\rho(t)|\alpha(LS)J'M'\rangle\\ &= \langle\alpha(LS)JM|\rho(0)|\alpha(LS)J'M'\rangle \quad e^{-i\omega_{JJ'}t}\, e^{-\Gamma t}\end{aligned} \tag{2.5}$$

with $\omega_{JJ'} = (E_J - E_{J'})/\hbar$ and Γ the reciprocal of the lifetime of the upper multiplet.

The most fruitful way to proceed is to expand the operators $\rho(0)$ and $L(\lambda,\vec{\varepsilon})$ as spherical tensors. This will permit a separation of the geometrical factors contained in $\vec{\varepsilon}$ from the dynamical factors contained in $\vec{D}$. It will also permit the linking of certain geometrical components with certain density matrix elements, thereby allowing a comparison between theory and measurement. Let

$$\rho(0) \equiv \sum_{kq} (-1)^q\, \rho^k_{-q}\, R^k_q \tag{2.6}$$

and

$$L(\lambda,\vec{\varepsilon}) \equiv \sum_{kq} (-1)^q\, \ell^k_{-q}(\vec{\varepsilon})\, L^k_q(\lambda). \tag{2.7}$$

The separation of $L(\lambda,\vec{\varepsilon})$ into two components, $\ell^k_{-q}(\vec{\varepsilon})$ and $L^k_q(\lambda)$ is a direct consequence of the separation contained in the expression $\vec{\varepsilon}^* \cdot \vec{D}$. It is only necessary to convert these

to spherical tensors. The separation of $\rho(0)$ into ρ^k_{-q} and R^k_q may be treated in two different but equivalent manners. The first would claim that the separation is purely formal and that no interpretation be given to R^k_q, their only requirement being that they transform under rotations like angular momentum operators. The second treats the R^k_q explicitly as angular momemtum operators, thereby relating the coefficients of ρ^k_q to certain expectation values of angular momentum. Since the chosen basis states are ones for which J^2 and J_z are "good" quantum numbers, such an interpretation is always possible whether or not R^k_q is treated as an angular momentum operator. For this reason the first interpretation will be used in the following derivation since it is slightly more straightforward.

The task which lies ahead is the evaluation of equation (2.3). The first half of that equation will be taken up in the next section while the second half will be treated in the following one.

2.2 The Light Emission Operator

Any vector $\vec{r}$ can be converted into a spherical tensor of rank 1 using the following convention:

$$r^1_1 = \frac{-1}{\sqrt{2}}(r_x + ir_y)$$

$$r^1_0 = r_z$$

$$r^1_{-1} = \frac{+1}{\sqrt{2}}(r_x - ir_y)$$

It is apparent that $r_q^{1*} = (-1)^q \, r_{-q}^1$. The convention which will be followed here is that spherical tensors formed from real vectors should satisfy

$$r_q^{k*} = (-1)^q \, r_{-q}^k.$$

If the vector is complex, this expression needs to be modified to

$$r_q^{k*} = (-1)^q \, r_{-q}^{k+} \tag{2.8}$$

where r_q^{k+} signifies that the Cartesian components of r be replaced by their complex conjugates.

The inner product $\vec{\varepsilon}^* \cdot \vec{D}$ may be expressed in spherical tensor notation as

$$\vec{\varepsilon}^* \cdot \vec{D} = \sum_q (-1)^q \, \varepsilon_{-q}^+ \, D_q$$

where the superscript 1 is understood. D_q then equals $\left(\frac{3}{4\pi}\right)^{\frac{1}{2}} r_q$ which is the solid harmonic of rank 1.

Using these considerations and invoking the Wigner-Eckart Theorem, equation (2.4) may be written

$$<J'M'|L(\lambda,\vec{\varepsilon})|\,JM> = C' \sum_{J_f M_f} \sum_{q_1 q_2} (-1)^{J'-M'+J_f-M_f}$$

$$\times\ (-1)^{q_1+q_2}\ \varepsilon_{q_1}\ \varepsilon^{+}_{-q_2} \begin{pmatrix} J' & 1 & J_f \\ -M' & -q_1 & M_f \end{pmatrix} \begin{pmatrix} J_f & 1 & J \\ -M_f & q_2 & M \end{pmatrix}$$

$$\times\ <\alpha(LS)J'\,||D||\,\alpha(L_fS)\ J_f><\alpha(L_fS)\ J_f\,||D||\,\alpha(LS)\ J> \qquad (2.9)$$

The reduction of this equation can be found in Appendix 1. The result is

$$<J'M'|L(\lambda,\vec{\varepsilon})|\,JM> = C \sum_{kq} (-1)^{q}\ \ell^{k}_{-q} (-1)^{J'-M'} \begin{pmatrix} J' & k & J \\ -M' & q & M \end{pmatrix}$$

$$(-1)^{L+S+J}\ [J\ J'\ K]^{\frac{1}{2}} \begin{Bmatrix} J' & J & k \\ L & L & S \end{Bmatrix} \begin{Bmatrix} L & L & k \\ 1 & 1 & L_f \end{Bmatrix} \qquad (2.10)$$

where

$$C = C'S = C'\,|<\alpha L\,||D||\,\alpha L_f>|^{2} \qquad (2.11)$$

and S is the usual multiplet strength parameter. The notation $[\ell_1 \ell_2 \cdot\cdot\cdot \ell_n] \equiv (2\ell_1+1)(2\ell_2+1)\cdot\cdot\cdot(2\ell_n+1)$ has been used. Finally the definition of ℓ^{k}_{q} is

$$\ell_q^k = \sum_{q_1 q_2} (-1)^q \, \varepsilon_{q_1} \, \varepsilon_{q_2}^{+} (2k+1)^{\frac{1}{2}} \begin{pmatrix} 1 & 1 & k \\ q_1 & q_2 & -q \end{pmatrix} . \qquad (2.12)$$

2.3 The Density Matrix

The second matrix element in equation (2.3) may be calculated by evaluating the time independent expression of equation (2.5):

$$<\alpha(LS)JM \,|\rho(0)|\, \alpha(LS)J'M'>$$

$$= \sum_{k'q'} (-1)^{q'} \rho^{k'}_{-q'} \quad <\alpha JM \,|R^{k'}_{q'}|\, \alpha J'M'> \quad .$$

The Wigner-Eckart Theorem applied to the above gives:

$$<\alpha JM \,|\rho(0)|\, \alpha J'M'>$$

$$= \sum_{k'q'} (-1)^{J-M+q'} \rho^{k'}_{-q'} \begin{pmatrix} J & k' & J' \\ -M & q' & M' \end{pmatrix} <\alpha J \,||R^{k'}||\, \alpha J'> \, . \qquad (2.13)$$

At this point the spin-independence hypothesis will be invoked. It affords a significant simplification to the equations and no example of its violation using the beam-foil source is known. Ellis (El 77) has recently extended this calculation to those cases for which this hypothesis is not assumed. The reduced matrix element of equation (2.13) may then be written as:

$$\langle\alpha(LS)J \| R^{k'} \| \alpha(LS)J'\rangle = (-1)^{L+S+J'+k'} \frac{[J\,J']^{\frac{1}{2}}}{[S]}$$

$$\times \begin{Bmatrix} J' & J & k' \\ L & L & S \end{Bmatrix} \langle\alpha L \| R^{k'} \| \alpha L\rangle. \tag{2.14}$$

The factor $1/(2S + 1)$ is introduced for convenience. Since the $\rho^{k'}_{q'}$ are unknown parameters, it is permissible to incorporate the value of $\langle\alpha L \| R^{k'} \| \alpha L\rangle$ into the coefficients. Equation (2.13) then becomes

$$\langle\alpha JM |\rho(0)| \alpha J'M'\rangle = \sum_{k'q'} (-1)^{J-M+q'+L+S+J'+k}$$

$$\times [J\,J']^{\frac{1}{2}} [S]^{-1} \rho^{k'}_{-q'} \begin{pmatrix} J & k' & J' \\ -M & q' & M' \end{pmatrix} \begin{Bmatrix} J' & J & k' \\ L & L & S \end{Bmatrix} \tag{2.15}$$

Two additional features regarding the ρ parameters are proven in Appendix 1. The first is that reflection symmetry in the plane containing the beam and lying perpendicular to the foil tilt axis imposes the constraint

$$\rho^k_q = (-1)^k \rho^k_{-q} . \tag{2.16}$$

The second is that the trace of ρ is given by:

$$\mathrm{Tr}\,\rho = (2L + 1)^{\frac{1}{2}} \rho^0_0 \tag{2.17}$$

Equation (2.3) may finally be evaluated by using equations (2.5), (2.10) and (2.15).

$$\mathrm{Tr}\ \rho(0)\ \frac{dI}{d\Omega} = \sum_{\substack{J\,J' \\ M\,M'}} \langle\alpha(LS)J'M'|L(\lambda,\vec{\varepsilon})|\alpha(LS)JM\rangle$$

$$\times\ \langle\alpha(LS)JM|\rho(0)|\alpha(LS)J'M'\rangle\ e^{-i\omega_{JJ'}t}\ e^{-\Gamma t}$$

$$= \sum_{\substack{kq \\ k'q'}} \sum_{\substack{J\,J' \\ M\,M'}} C(-1)^{k+q'} \frac{[J\,J']\,[k]^{\frac{1}{2}}}{[S]} \begin{pmatrix} J' & k & J \\ -M' & q & M \end{pmatrix} \begin{pmatrix} J & k' & J' \\ -M & q' & M' \end{pmatrix}$$

$$\times\ \ell^{k}_{-q}\ \rho^{k'}_{-q'} \begin{Bmatrix} J' & J & k' \\ L & L & S \end{Bmatrix} \begin{Bmatrix} J' & J & k \\ L & L & S \end{Bmatrix} \begin{Bmatrix} L & L & k \\ 1 & 1 & L_f \end{Bmatrix}$$

The sum over M and M' can be performed using

$$\sum_{m_1 m_2} \begin{pmatrix} j_1 & j_2 & j_3 \\ m_1 & m_2 & m_3 \end{pmatrix} \begin{pmatrix} j_1 & j_2 & j_3' \\ m_1 & m_2 & m_3' \end{pmatrix} = [j_3]^{-1}\ \delta_{j_3 j_3'}\ \delta_{m_3 m_3'}$$

$$\times\ \delta(j_1, j_2, j_3)$$

where the third δ symbol means that j_1, j_2 and j_3 must be able to form a triangle. Then

$$\sum_{M\,M'} \begin{pmatrix} J & J' & k \\ M & -M' & q \end{pmatrix} \begin{pmatrix} J & J' & k' \\ M & -M' & -q' \end{pmatrix} = [k]^{-1}\ \delta_{kk'}\,\delta_{q\,-q'}$$

Finally

$$\frac{dI}{d\Omega} = C \sum_{kq} (-1)^{q}\ \rho^{k}_{q}\ \ell^{k}_{-q} \sum_{J\,J'} (-1)^{k} \frac{[J\,J']}{[S]\,[kL]^{\frac{1}{2}}}$$

$$\times\ e^{-\Gamma t}\ e^{-i\omega_{JJ'}t} \begin{Bmatrix} J' & J & k \\ L & L & S \end{Bmatrix}^2 \begin{Bmatrix} L & L & k \\ 1 & 1 & L_f \end{Bmatrix} \Big/ \rho_0^0 \qquad (2.18)$$

All of the geometrical factors occur in the expression

$$\sum_q (-1)^q \rho_q^k \ell_{-q}^k$$

which will be evaluated in the following section. The final result follows with the substitution of that expression into equation (2.18).

2.4 Evaluation of the Stokes Parameters

Figure 1 shows the coordinate frame used for this calculation while Figure 2 shows the actual laboratory reference frame. Though all of the data to be discussed in this work was taken with $\theta = 90°$ and $\phi = 0°$, the more general expression is derived and some consequences are considered in section 2.7. z - lies along the beam axis and the laboratory frame (x, y, z) is to be considered stationary while the detector frame (ξ, η, ζ) is rotated.

The most general polarization vector, $\vec{\varepsilon}$, can be written in the detector frame as

$$\varepsilon_\xi = \cos\psi$$

$$\varepsilon_\eta = e^{i\delta} \sin\psi$$

$$\varepsilon_\zeta = 0\ . \qquad (2.19)$$

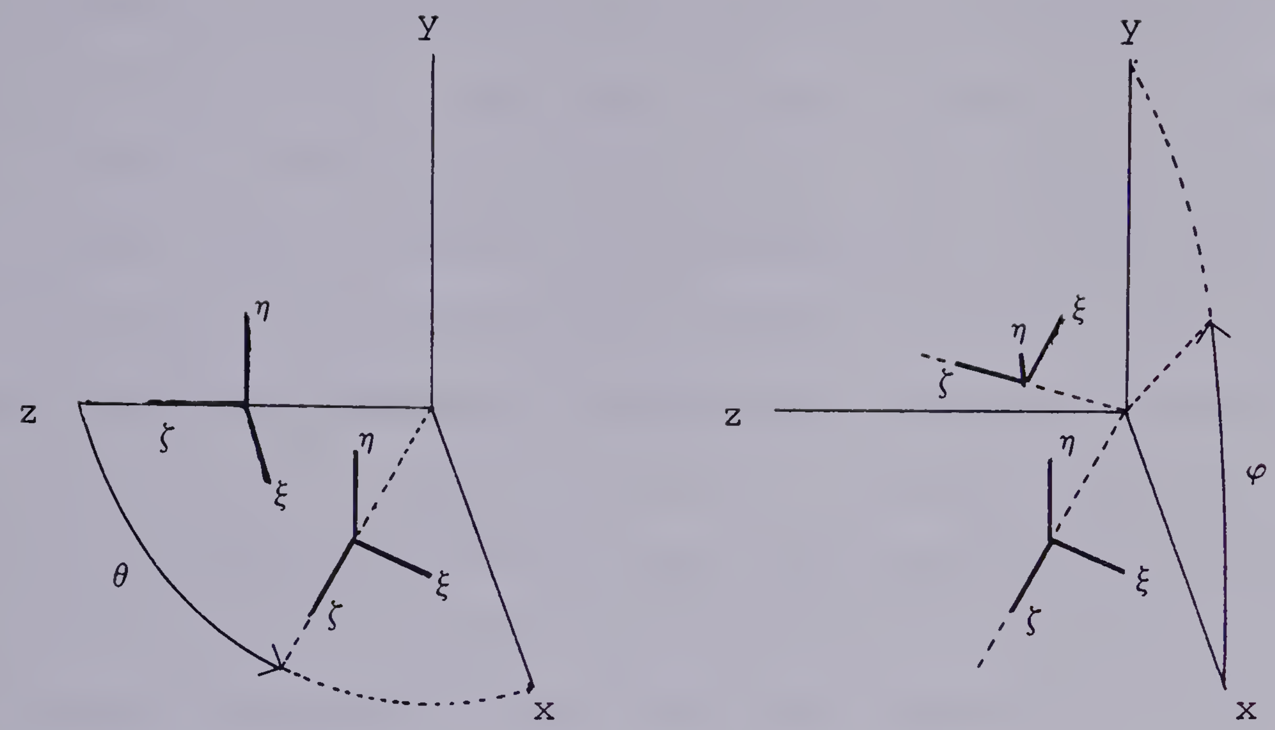

Figure 1. Coordinate Frame

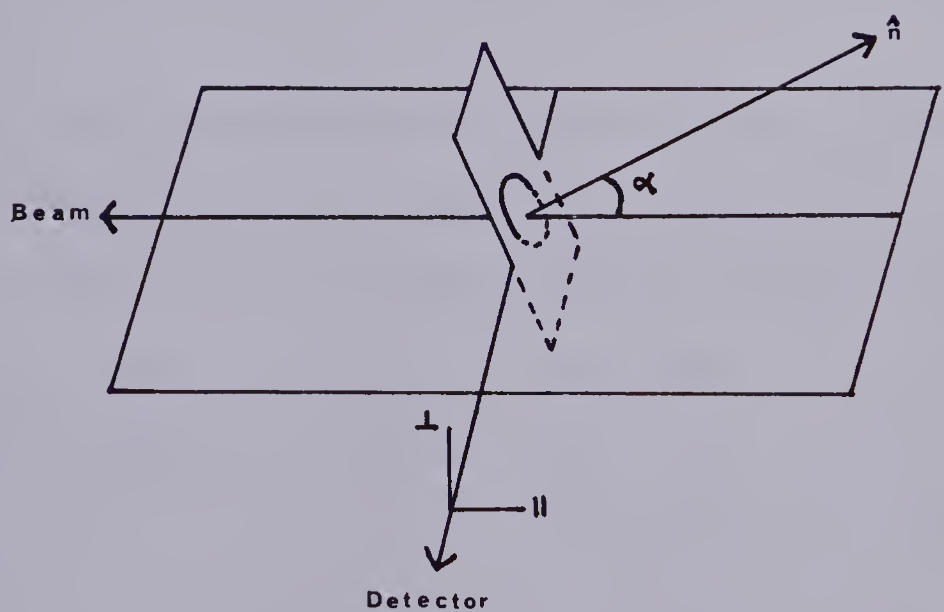

Figure 2. Beam, Foil and Detector Geometry

This vector is transverse to the direction of propagation (ζ) and is a unit vector. Any state of pure elliptical polarization can be chosen by adjusting ψ and δ. The detector frame can be most easily oriented by starting with the two sets of axes coincident and performing a positive rotation about the y-axis through an angle θ, followed by a positive rotation about the z-axis through an angle ϕ. A positive rotation is one for which the positive axis coincided with the direction of advance of a right-handed screw when turned in the direction of rotation. θ and ϕ are not equivalent to the standard spherical coordinates of a vector lying in the ζ direction. Nor are θ and ϕ equivalent to any two of the standard Euler angles. Note that these rotations are such that ξ always lies in the $z - \zeta$ plane. ξ is the axis from which all angles of the polarizing elements (Chapter III) are measured.

One great advantage of using θ and ϕ as defined here is that the transformation from the detector frame to the laboratory frame is particularly simple and given by:

$$\begin{bmatrix} \varepsilon_x \\ \varepsilon_y \\ \varepsilon_z \end{bmatrix} = \begin{bmatrix} \cos\phi & -\sin\phi & 0 \\ \sin\phi & \cos\phi & 0 \\ 0 & 0 & 1 \end{bmatrix} \begin{bmatrix} \cos\theta & 0 & \sin\theta \\ 0 & 1 & 0 \\ -\sin\theta & 0 & \cos\theta \end{bmatrix} \begin{bmatrix} \varepsilon_\xi \\ \varepsilon_\eta \\ \varepsilon_\zeta \end{bmatrix}$$

$$\begin{aligned} \varepsilon_x &= \cos\psi \cos\theta \cos\phi - e^{i\delta} \sin\psi \sin\phi \\ \varepsilon_y &= \cos\psi \cos\theta \sin\phi + e^{i\delta} \sin\psi \cos\phi \\ \varepsilon_z &= -\cos\psi \sin\theta \end{aligned} \tag{2.20}$$

The expression which requires calculation is given by equation (2.12):

$$\ell_q^k = \sum_{q_1 q_2} (-1)^q \; \varepsilon_{q_1} \varepsilon_{q_2}^{+} (2k+1)^{\frac{1}{2}} \begin{pmatrix} 1 & 1 & k \\ q_1 & q_2 & -q \end{pmatrix}$$

This is coupled to ρ_q^k as

$$\sum_q (-1)^q \rho_q^k \ell_{-q}^k \, .$$

This sum can be written using equation (2.16) as

$$\rho_0^0 \ell_0^0 + \rho_0^2 \ell_0^2 + \rho_1^1 (\ell_1^1 - \ell_{-1}^1) - \rho_1^2 (\ell_1^2 + \ell_{-1}^2) + \rho_2^2 (\ell_2^2 + \ell_{-2}^2) .$$

The needed ℓ_q^k values are then given by

$$\ell_0^0 = -1\sqrt{3}$$

$$\ell_0^2 = \frac{1}{\sqrt{6}} (3\cos^2(\psi)\sin^2(\theta) - 1)$$

$$(\ell_1^1 - \ell_{-1}^1) = -\sin(2\psi)\sin(\theta)\cos(\phi)\sin(\delta)$$

$$(\ell_1^2 + \ell_{-1}^2) = i[\cos^2(\psi)\sin(2\theta)\sin(\phi) + \sin(2\psi)\sin(\theta)\cos(\phi)\cos(\delta)]$$

$$(\ell_2^2 + \ell_{-2}^2) = \cos^2(\psi)\cos^2(\theta)\,\cos(2\phi) - \sin^2(\psi)\cos(2\phi)$$

Defining an excitation parameter as

$$\sigma_q^k \equiv \frac{(-1)^{k+1} \rho_q^k}{\sqrt{2k+1}\, \rho_0^0} , \tag{2.21}$$

the general expression for light emission and the principal result of this chapter can be written:

$$I(\psi,\delta) = \frac{A^{\circ}(t)}{\sqrt{3}} - \frac{\sigma_0{}^2 A^2(t)}{\sqrt{6}} (3\cos^2(\psi)\sin^2(\theta) - 1)$$

$$- \sigma_1^1 A^1(t)\sin(2\psi)\sin(\theta)\cos(\phi)\sin(\delta)$$

$$- i\sigma_1^2 A^2(t)[\cos^2(\psi)\sin(2\theta)\sin(\phi) + \sin(2\psi)\sin(\theta)\cos(\phi)\cos(\delta)]$$

$$- \sigma_2{}^2 A^2(t)[\cos^2(\psi)\cos^2(\theta)\cos(2\phi) - \sin^2(\psi)\cos(2\phi)]. \quad (2.22)$$

$A^k(t)$ is defined as

$$A^k(t) \equiv \frac{C\ e^{-\Gamma t}}{\sqrt{2L+1}} \begin{Bmatrix} L & L & k \\ 1 & 1 & L_f \end{Bmatrix} \sum_{J\,J'} B(J,J',k)\cos(\omega_{JJ'}t) \quad (2.23)$$

with

$$B(J,J',K) \equiv \begin{Bmatrix} J & J' & k \\ L & L & S \end{Bmatrix}^2 \frac{(2J+1)(2J'+1)}{(2S+1)} . \quad (2.24)$$

Equation (2.22) gives the intensity of light emitted within a small solid angle centered about the coordinates θ and ϕ. The effect of integrating $dI/d\Omega$ over the solid angle subtended by the detection system only introduces an overall multiplicative constant which is of no concern since no measurement relies upon an absolute intensity. The emitted intensity is a function of the unknown polarization vector,

ξ, or equivalently of the unknown parameters ψ and δ. One can use $I(\psi,\delta)$ to generate the light intensity of any specified state of polarization. In particular the Stokes parameters (to be defined (Equation 3.1) and discussed in the next chapter) can be formed from this expression and then compared to the measured parameters. They will be listed here twice; once as a function of θ and ϕ and again for the normal side-on viewing configuration of θ = 90° and ϕ = 0°.

$$I = [I(\psi=0,\delta=0) + I(\psi=90,\delta=0)]/2$$

$$= \frac{A^{\circ}(t)}{\sqrt{3}} - \frac{\sigma_0^2 A^2(t)}{2\sqrt{6}}(1 - 3\cos^2\theta) - \frac{i\sigma_1^2}{2}A^2(t)\sin 2\theta\sin\phi$$

$$+ \frac{\sigma_2^2}{2} A^2(t)\sin^2\theta\cos 2\phi \qquad (2.25)$$

$$M = [I(\psi=0,\delta=0) - I(\psi=90,\delta=0)]/2$$

$$= \frac{-3\sigma_0^2}{2\sqrt{6}} A^2(t)\sin^2\theta - \frac{i\sigma_1^2}{2} A^2(t)\sin 2\theta\sin\phi$$

$$- \frac{\sigma_2^2}{2} A^2(t)\cos 2\phi(\cos^2\theta + 1) \qquad (2.26)$$

$$C = [I(\psi=45,\delta=0) - I(\psi=135,\delta=0)]/2$$

$$= -i\sigma_1^2 A^2(t)\sin\theta\cos\phi \qquad (2.27)$$

$$S = [I(\psi=45,\delta=90) - I(\psi=135,\delta=90)]/2$$

$$= -\sigma_1^1 A^1(t)\sin\theta\cos\phi \qquad (2.28)$$

$$I = \frac{A^{\circ}(t)}{\sqrt{3}} - \frac{A^{2}(t)}{2}\left[\frac{\sigma_0^2}{\sqrt{6}} - \sigma_2^2\right] \tag{2.29}$$

$$M = \frac{-A^{2}(t)}{2}\left[\frac{3\sigma_0^2}{\sqrt{6}} + \sigma_2^2\right] \tag{2.30}$$

$$C = -i\sigma_1^2 A^2(t) \tag{2.31}$$

$$S = -\sigma_1^1 A^1(t) \tag{2.32}$$

2.5 Consequences of Alternate Coupling Schemes

Expression (2.22) is valid under any spin-independent excitation condition. Equations (2.23) and (2.24) however are peculiar to the case of spectroscopically unresolved fine structure with no hyperfine structure for a cascade free transition. Note the occurrence of $\cos(\omega_{JJ'}t)$ which gives a time dependent oscillation to the intensity. The nature of the beam-foil source is such that this oscillation occurs as a spatial modulation when viewed through a narrow aperture as a function of position downstream from the foil. Whether or not such a modulation can be observed depends upon the fraction of the quantum beat viewed by the aperture. If this fraction were unity or greater, the frequency would be too high and the beat would average to zero. If the fraction were too small the maximum foil travel would be unable to scan over one period and the frequency would be too low to observe. Typical frequency extremes for beam-foil spectroscopy

(beam velocity $\sim$ 0.01c) are 50 MH_z to $10GH_z$. With a focused system the aperture is controlled by the entrance slit width of a spectrometer. A quantum beat which is just resolved using 50 micron slit width would disappear with slits set to 500 microns. The question of resolution can then become a matter of experimental decision.

Equation (2.23) and (2.24) can be altered to account for different angular momentum coupling schemes. The derivations are completely analogous to the one given and therefore only the results will be quoted. For unresolved hyperfine structure with resolved fine structure:

$$A^k(t) = \frac{C\ e^{-\Gamma t}}{\sqrt{2J+1}} \begin{Bmatrix} J & J & k \\ 1 & 1 & J_f \end{Bmatrix} \sum_{FF'} B(F,F',k) \cos(\omega_{FF'}t) \qquad (2.33)$$

$$B(F,F',k) = \begin{Bmatrix} F & F' & k \\ J & J & I \end{Bmatrix}^2 \frac{(2F+1)(2F'+1)}{(2I+1)} \ . \qquad (2.34)$$

The case I = 0 would yield an expression for resolved fine structure alone. Two points should be noted, however. The S which appeared previously in the definition of C (equation 2.11) was the multiplet strength while now it must be regarded as the line strength. Furthermore the reduced matrix element of R which has been set equal to 1 is

$$<\alpha(LS)J||R^k||\alpha(LS)J> \ .$$

This latter choice is not so convenient for comparing polarizations of different fine structure components within

a multiplet. With $<\alpha L \| R^k \| \alpha L> = 1$, as before, one can write for resolved fine structure:

$$A^k(t) = \frac{C\,e^{-\Gamma t}(-1)^k}{\sqrt{2L+1}} \begin{Bmatrix} J & J & k \\ 1 & 1 & J_f \end{Bmatrix} \begin{Bmatrix} J & J & k \\ L & L & S \end{Bmatrix} \frac{(2J+1)}{(2S+1)} \cdot \quad (2.35)$$

Equation (2.33) could be modified in a similar way.

It would be possible to write an expression for both unresolved hyperfine as well as unresolved fine structure, so long as J were a good quantum number. This condition means that the hyperfine intervals would have to be about a factor of 10 smaller than the fine structure intervals. Such an expression would not then be of practical use since usual experimental beam resolution would permit one or the other effect to be observed but not both. If the magnitudes of the intervals were comparable, J would not be a good quantum number and the entire Hamiltonian would have to be diagonalized.

By way of illustration, the expression for S/I for the case of resolved fine structure using (2.35), (2.32) and (2.29) is:

$$\frac{S}{I} = \frac{\sigma_1^1 \begin{Bmatrix} J & J & 1 \\ 1 & 1 & J_f \end{Bmatrix} \begin{Bmatrix} J & J & 1 \\ L & L & S \end{Bmatrix}}{\frac{1}{3^{\frac{1}{2}}} \begin{Bmatrix} J & J & 0 \\ 1 & 1 & J_f \end{Bmatrix} \begin{Bmatrix} J & J & 0 \\ L & L & S \end{Bmatrix} + \left[\frac{\sigma_2^2}{2} - \frac{\sigma_0^2}{(24)^{\frac{1}{2}}}\right] \begin{Bmatrix} J & J & 2 \\ 1 & 1 & J_f \end{Bmatrix} \begin{Bmatrix} J & J & 2 \\ L & L & S \end{Bmatrix}}$$

This is the expression used by Andrä, Fröhling, Plöhm and

Silver (AFPS 76) to describe the circular polarization of 17 Ar II lines excited by 300-keV Ar^+ ions on a copper surface inclined at 1.5° to the beam. (The different sign in the numerator arises from his different viewing position: $\theta = -90°$.) The interesting result is that the polarization of all 17 lines could be adequately described by a single set of σ parameters. While one would expect the cross sections to remain unchanged for the different lines of a multiplet, the fact that a single set could describe the lines originating on 4 different multiplets indicates that $\langle \alpha L \| \mathbb{R}^k \| \alpha L \rangle$ was independent of L for this experiment.

2.6 The Fano-Macek Parameters

An entirely different but equivalent formalism for handling light emission from the beam-foil source was given by Fano and Macek (FM 73) and extended by Macek and Burns (MB 76). They derive an expression analogous to equation (2.22) but with the interpretation that the light intensity is that detected after traversing a polarizer and quarter-wave. One can readily form the Stokes parameters from their expression thereby obtaining the transformation between the σ_q^k and their alignment and orientation parameters. The Stokes parameters are given by

$$I = \frac{2}{3} CSe^{-\Gamma t} \left[1 + \frac{h^{(2)}}{4} (A_0^{col} + 3A_{2+}^{col})\right] \tag{2.36}$$

$$M = \frac{1}{2} CSe^{-\Gamma t} h^{(2)} (A_0^{col} - A_{2+}^{col}) \qquad (2.37)$$

$$C = CSe^{-\Gamma t} h^{(2)} A_{1+}^{col} \qquad (2.38)$$

$$S = CSe^{-\Gamma t} h^{(1)} O_{1-}^{col} \qquad (2.39)$$

Here $h^{(k)}(J_i,J_f) = (-1)^{J_i - J_f} \begin{Bmatrix} J_i & J_i & k \\ 1 & 1 & J_f \end{Bmatrix} \begin{Bmatrix} J_i & J_i & k \\ 1 & 1 & J_i \end{Bmatrix}^{-1}$.

The alignment parameters (A^{col}) are always associated with $k = 2$, while the orientation parameter (O^{col}) is associated with $k = 1$. The above expression is valid for resolved fine structure. For unresolved fine structure $h^{(k)}$ becomes $h^{(k)}(L_i,L_f)$ and each alignment and orientation parameter is multiplied by the appropriate $G^k(t)$ given by:

$$G^k(t) = \sum_{JJ'} \frac{(2J+1)(2J'+1)}{(2S+1)} \begin{Bmatrix} J & J' & k \\ L & L & S \end{Bmatrix}^2 \cos(\omega_{JJ'} t) \qquad (2.40)$$

The extension to unresolved hyperfine structure is performed as before.

To arrive at a transformation connecting the σ_q^k to A^{col} and O^{col}, it is necessary to form the ratios M/I, C/I and S/I in order that different normalization or phase conventions will cancel.

$$\frac{M}{I} = \frac{-A^2(t)/A^\circ(t)[3/2\sqrt{2}\ \sigma_0^2 + \sqrt{3}/2\ \sigma_2^2]}{1 - \frac{A^2(t)}{A^\circ(t)} \left[\frac{\sigma_0^2}{2\sqrt{2}} - \frac{\sqrt{3}}{2} \sigma_2^2 \right]}$$

The analogous expression from (2.36) and (2.37) is

$$\frac{M}{I} = \frac{h^{(2)}\ G^2(t)\ 3/4\ [A_0^{col} - A_{2+}^{col}]}{1 + \frac{h^{(2)}\ G^2(t)}{4}\left[A_0^{col} + 3A_{2+}^{col}\right]}$$

The transformation can then be obtained by equating numerators and denominators. Defining $H^{(k)}$ as

$$H^{(k)} \equiv \frac{A^k(t)/A^\circ(t)}{G^k(t)h^{(k)}}\ , \tag{2.41}$$

the transformation equations, after performing similar calculations for C/I and S/I, become:

$$\begin{aligned}
A_0^{col} &= -\sqrt{2}\,\sigma_0^2\ H^{(2)} \\
A_{1+}^{col} &= \frac{-2}{\sqrt{3}}\ i\sigma_1^2\ H^{(2)} \\
A_{2+}^{col} &= \frac{2}{\sqrt{3}}\ \sigma_2^2\ H^{(2)} \\
O_{1-}^{col} &= \frac{-2}{\sqrt{3}}\ \sigma_1^1\ H^{(1)}
\end{aligned} \tag{2.42}$$

For the case of unresolved fine structure

$$H^{(k)} = \begin{Bmatrix} L & L & k \\ 1 & 1 & L \end{Bmatrix} \Big/ \begin{Bmatrix} L & L & 0 \\ 1 & 1 & L \end{Bmatrix} = -\sqrt{3(2L+1)}\begin{Bmatrix} L & L & k \\ 1 & 1 & L \end{Bmatrix} \tag{2.43}$$

2.7 Some Consequences and Examples

Equations (2.25) to (2.28) represent the results of this chapter in their most general form. Note from Figure 2 that tilting the foil in the opposite direction (α to $-\alpha$) is equivalent to moving the detector to the other side of the beam ($\theta = 90°$ to $\theta = -90°$). C and S change sign under such a transformation while I and M remain invariant. When comparing Stokes parameters between different laboratories, it is important to note their reference frame.

Next consider the circumstance of axial symmetry which applies whenever the foil is perpendicular to the beam. Axial symmetry means that ρ^k_q must remain invariant to any rotation about the z-axis. Reference to Appendix 1 shows this demands $q = 0$. The consequence of this is that $C = S = 0$ and

$$I = \frac{A^\circ(t)}{\sqrt{3}} - \frac{\sigma_0^2 \, A^2(t)}{2\sqrt{6}}$$

$$M = \frac{-3\,\sigma_0^2 \, A^2(t)}{2\sqrt{6}}$$

The next chapter will demonstrate that $\frac{1}{2}(I + M)$ is the intensity passed through a horizontally oriented plane polarizer while $\frac{1}{2}(I - M)$ is that passed through a vertically oriented polarizer. These combinations are

$$I + M = \frac{A^\circ(t)}{\sqrt{3}} - \frac{2\sigma_0^2}{\sqrt{6}} A^2(t)$$

$$I - M = \frac{A^{\circ}(t)}{\sqrt{3}} + \frac{\sigma_0^2}{\sqrt{6}} A^2(t)$$

Since any quantum beat can show up only in the $A^2(t)$ term, the above equations have been used to justify the claim that the beat amplitude in horizontally polarized light is twice that of vertically polarized light and 180° out of phase. This is, however, only approximately true. For some atom having unresolved fine structure with a single beat frequency, $A^2(t)$ takes the form:

$$A^2(t) = A^0(t)\, a_1 (1 + a_2 \cos \omega t).$$

If this expression is put into the above equations and the ratio of beat amplitudes is formed one finds

$$\frac{\text{Horiz. beat amp.}}{\text{Vert. beat amp.}} = \frac{-2(\sqrt{2} + a_1 \sigma_0^2)}{(\sqrt{2} - 2a_1 \sigma_0^2)}$$

For small enough values of a_1 and σ_0^2 this indeed approaches -2. For the 3_S - 3_P transition in Helium (see Chapter V) $a_1 = 5/18$ and $\sigma_0^2 \simeq -0.2$ and the ratio of beat amplitudes is -1.8. The limiting value of -2 can only be achieved when $\sigma_0^2 = 0$; i.e., when no beat is present. This was first pointed out by Wittman, Tillmann, Andrä and Dobberstein (WTAD 72) using a somewhat different theoretical formalism. The value measured for this ratio by Burns and Hancock (BH 73) for the $2s\,^3S$ - $3p\,^3P$ transition of He I is -1.6.

Another consequence which was tested by Burns and Hancock is that if light from the above source is passed through a polarizer with its transmission axis at 54.7° to the horizontal, the quantum beats disappear. Again anticipating a result from the next chapter, the intensity of light which passes through a plane polarizer making an angle γ to the horizontal is

$$I^t = \frac{1}{2}[I + M \cos(2\gamma)].$$

Substituting the values for I and M from above give

$$I^t = \frac{1}{2}\left[\frac{A^\circ(t)}{\sqrt{3}} - \frac{\sigma_0^2 A^2(t)}{2\sqrt{6}}\ (1 + 3\cos(2\gamma))\right]$$

The beats will disappear if $(1 + 3\cos(2\gamma)) = 0$, or $\gamma = 54.7°$.

CHAPTER III

THE MEASUREMENT OF POLARIZATION

Ellipsometry is the term often given to the complete determination of the polarization of a particular light source. The most general state of polarization for any source is said to be partially elliptically polarized. There is no unique convention for the description of such polarization. One choice is to specify the size, azimuth and shape of the polarization elipse; another, the spherical coordinates of the Poincare Sphere. Perhaps the most popular choice, and the one which will be used here, is to describe the polarization by the Stokes parameters using the notation I, M, C, and S of Jones (Jo 41) and Perrin (Pe 42). Other notations appear in the literature but do not seem to be so widely used.

3.1 Definition of the Stokes Parameters

Within classical electromagnetic theory, light may be considered as an oscillation of an electric and magnetic field transverse to the direction of propagation. Specification of the electric field vector is sufficient to completely describe the nature of the radiation. For monochromatic light propagating in the z-direction the electric field may be written:

$$\vec{E} = E_x\,\hat{x} + E_y\,\hat{y}$$

with

$$E_x = a\cos(kz - \omega t)$$

$$E_y = b\cos(kz - \omega t + \delta)$$

Specification of a, b and δ defines the polarization of the light. The electric field magnitude, however, is not a measurable quantity. Only the square of the electric field magnitude, proportional to the light intensity, is measurable. Furthermore, any measurement of light intensity is a time-averaged measurement of an incoherent sum of wave trains each of which is described by the above equations. Polarization must then be specified by the average intensity in the x-direction, the average intensity in the y-direction and the average phase between the two. A particularly convenient way of specifying these parameters as well as the amount of unpolarized light is through use of the Stokes parameters. Define

$$I_p = a^2 + b^2$$

$$M = a^2 - b^2$$

$$C = 2ab\cos(\delta)$$

$$S = 2ab\sin(\delta) \tag{3.1}$$

I_p is the polarized light intensity. M is the horizontal (positive) or vertical (negative) linearly polarized light. C is the linearly polarized light at 45° (positive) or 135° (negative) to the reference axis. S is the right (positive) or left (negative) circularly polarized light.

From (3.1) it is clear that $M^2 + C^2 + S^2 = I_p{}^2$. Three parameters, then, are sufficient to describe polarized light. These are a^2, b^2 and δ or M, C and S. By making the extension

$$I = I_p + I_u \tag{3.2}$$

where I_u is the intensity of unpolarized light,

$$I^2 \geq M^2 + C^2 + S^2 \tag{3.3}$$

and the four parameters, I, M, C and S can describe the state of partially polarized light. These are the Stokes parameters.

3.2 Mueller Calculus

One important advantage of using Stokes parameters is that they may be arranged as a column vector, $\begin{bmatrix} I \\ M \\ C \\ S \end{bmatrix}$, and be operated upon by matrices representing polarizing elements. The formalism was first performed by Mueller (Mu 48) and is known as the Mueller calculus. The sign conventions being adopted here are those of Clarke and Grainger (CG 71).

Only two polarizing elements are of practical concern, the perfect polarizer and the retarder. The former is represented by

$$[\varepsilon]_{pol} = \tfrac{1}{2}\begin{bmatrix} 1 & 1 & 0 & 0 \\ 1 & 1 & 0 & 0 \\ 0 & 0 & 0 & 0 \\ 0 & 0 & 0 & 0 \end{bmatrix} \tag{3.4}$$

while the latter is given by

$$[\varepsilon]_{ret} = \begin{bmatrix} 1 & 0 & 0 & 0 \\ 0 & 1 & 0 & 0 \\ 0 & 0 & \cos\Delta & \sin\Delta \\ 0 & 0 & -\sin\Delta & \cos\Delta \end{bmatrix} \tag{3.5}$$

Δ is the degree of retardance with 90° representing a quarter-wave plate.

Each of these elements has an axis; the transmission axis for the polarizer and the fast axis for the retarder. The input Stokes vector must first be rotated to the reference frame of the element, operated upon by the element, and then rotated back to the reference frame of the input vector. The procedure can be represented as:

$$\begin{bmatrix} I' \\ M' \\ C' \\ S' \end{bmatrix} = [R^{-1}]\ [\varepsilon]\ [R] \begin{bmatrix} I \\ M \\ C \\ S \end{bmatrix} \tag{3.6}$$

The rotation matrix is given by

$$[R] = \begin{bmatrix} 1 & 0 & 0 & 0 \\ 0 & \cos 2\theta & \sin 2\theta & 0 \\ 0 & -\sin 2\theta & \cos 2\theta & 0 \\ 0 & 0 & 0 & 1 \end{bmatrix} \tag{3.7}$$

where θ is the angle between the axis of the optical element and the reference axis of the Stokes vector. For the case of the polarizer this angle may be called γ, and the product of the three matrices appearing in (3.6) can be evaluated to give

$$[\varepsilon(\gamma)]_{pol} = \tfrac{1}{2}\begin{bmatrix} 1 & \cos 2\gamma & \sin 2\gamma & 0 \\ \cos 2\gamma & \cos^2 2\gamma & \tfrac{1}{2}\sin 4\gamma & 0 \\ \sin 2\gamma & \tfrac{1}{2}\sin 4\gamma & \sin^2 2\gamma & 0 \\ 0 & 0 & 0 & 0 \end{bmatrix} \tag{3.8}$$

In like fashion, calling the angle β for the retarder,

$$[\varepsilon(\beta)]_{ret} = \begin{bmatrix} 1 & 0 & 0 & 0 \\ 0 & \cos^2 2\beta + \sin^2 2\beta\cos\Delta & \tfrac{1}{2}\sin 4\beta(1-\cos\Delta) & -\sin 2\beta\sin\Delta \\ 0 & \tfrac{1}{2}\sin 4\beta(1-\cos\Delta) & \sin^2 2\beta + \cos^2 2\beta\cos\Delta & \cos 2\beta\sin\Delta \\ 0 & \sin 2\beta\sin\Delta & -\cos 2\beta\sin\Delta & \cos\Delta \end{bmatrix} \tag{3.9}$$

A polarimeter is a device used to measure the Stokes parameters of a particular light source. It need be nothing more than a retarder followed by a plane polarizer. The relevant matrix expression is

$$\begin{bmatrix} I' \\ M' \\ C' \\ S' \end{bmatrix} = [\varepsilon(\gamma)]_{pol}\,[\varepsilon(\beta)]_{ret}\begin{bmatrix} I \\ M \\ C \\ S \end{bmatrix} \tag{3.10}$$

Only the intensity of the transmitted light is measurable. It is straightforward, using (3.8) and (3.9) in (3.10), to derive an expression for I' which relates the transmitted

intensity (hereafter called I^t) to the input Stokes parameters:

$$
\begin{aligned}
I^t(\gamma,\beta,\Delta) = \tfrac{1}{2}\{ I + M\ & [\cos 2\beta \cos 2(\gamma - \beta) \\
& \quad - \sin 2\beta \sin 2(\gamma - \beta) \cos \Delta] \\
+ C\ & [\sin 2\beta \cos 2(\gamma - \beta) \\
& \quad + \cos 2\beta \sin 2(\gamma - \beta) \cos \Delta] \\
+ S\ & [\sin 2(\gamma - \beta) \sin \Delta]\} \qquad (3.11)
\end{aligned}
$$

I,M,C and S are the Stokes parameters of the source with respect to some (laboratory) reference frame. γ is the angle of the transmission axis of a plane polarizer with respect to that same reference frame. Likewise β is the angle of the retarder's fast axis with respect to the reference frame. Δ is the retardance of the retarder, with $\pi/2$ a quarter-wave and π a half-wave plate.

3.3 Determination of the Stokes Parameters

Equation (3.11) represents the most general expression for the measurement of the Stokes parameters. As a simple example of its use consider the following sequence of measurements. Without a retarder, two measurements are taken with the polarizer at 0° and 90° to the reference axis. These are added to give I and subtracted to give M. Two measurements are then taken with the polarizer axis at 45° and 135°. These are subtracted to give C. Finally, with a retarder in place (fast axis aligned with the reference axis)

two measurements are taken with the polarizer at 45° and 135°, and subtracted to give S.

Two forms of equation (3.11) are required:

$$I_1^t\ (\gamma, \beta = 0,\ \Delta = 0) = \frac{1}{2}\{I + M\cos 2\gamma + C\sin 2\gamma\}$$

$$I_2^t\ (\gamma, \beta = 0,\ \Delta = 90) = \frac{1}{2}\{I + M\cos 2\gamma + S\sin 2\gamma\}$$

The first two measurements when added and subtracted give:

$$I_1^t\ (\gamma = 0) + I_1^t\ (\gamma = 90) = \frac{1}{2}[I + M] + \frac{1}{2}[I - M] = I$$

$$I_1^t\ (\gamma = 0) - I_1^t\ (\gamma = 90) = \frac{1}{2}[I + M] - \frac{1}{2}[I - M] = M$$

The second two measurements when subtracted give:

$$I_1^t\ (\gamma = 45) - I_1^t\ (\gamma = 135) = \frac{1}{2}[I + C] - \frac{1}{2}[I - C] = C$$

The last two measurements when subtracted give:

$$I_2^t\ (\gamma = 45) - I_2^t\ (\gamma = 135) = \frac{1}{2}[I + S] - \frac{1}{2}[I - S] = S$$

Such a sequence of measurements has several disadvantages:

1) By rotating the polarizer the light which is passed to the detector has different polarization for different

parts of the same measurement. Since the detector often consists of a grating spectrograph, whose response is strongly polarization sensitive, a significant source of error is introduced.

2) No polarizer or retarder behaves perfectly and a preferred sequence would be one which incorporates equal rotation increments through 360° so that assymmetries in the device might cancel.

3) A preferred sequence would be one which overdetermines the Stokes parameters so that an error estimate can be obtained.

Each of these objections to the "simple" measuring sequence presented above can be satisfied by rotating the retarder before a fixed polarizer in equal increments through 360°. As an illustration consider equation (3.11) for $\gamma = 0$ and $\Delta = 90°$.

$$I^t(\beta) = \frac{1}{2}\left[I + M\cos^2 2\beta + \frac{1}{2}C\sin 4\beta - S\sin 2\beta\right] \qquad (3.12)$$

Clearly, the minimum number of measurements needed to determine four parameters is four. One such sequence is given by:

$$I^t(0) = \frac{1}{2}[I + M]$$
$$I^t(\pi/8) = \frac{1}{2}\left[I + \frac{M}{2} + \frac{C}{2} - \frac{S}{\sqrt{2}}\right]$$
$$I^t(\pi/4) = \frac{1}{2}[I - S]$$
$$I^t(3\pi/4) = \frac{1}{2}[I + S]$$

Such a sequence satisfies the first objection to the "simple" method but not the second or third. Since a perfect retarder is 180° invariant, a sequence which repeats after 180° might most accurately cancel asymmetries. This requirement can be expressed by defining the sequence as $(2\pi/n)$ with n an even integer. The smallest even value for n which can yield a solution to (3.12) is n = 10. Measurements to be presented in later chapters typically use n = 18 or 36.

The reduction of equation (3.11), for given γ and Δ, can most readily be accomplished by recognizing that it is of the form:

$$I_i^t(\beta_i) = \frac{1}{2}\,[I + M\, f_1(\beta_i) + C\, f_2(\beta_i) + S\, f_3(\beta_i)]$$

This equation is linear in the Stokes parameters and can be solved using standard regression techniques (Be 69). The only requirement is that γ, β, and Δ be accurately known. Further details about the measurement sequence are given in Section 4.3.

3.4 Determination of Polarizer and Retarder Axes

The polarimeter to be described in the next chapter permits front-to-back rotation of the polarizer, the retarder or both. Such a rotation changes the polarizer axis from γ_0 to $-\gamma_0$. Similarly, a front-to-back rotation of the retarder changes its axis from β_0 to $-\beta_0$. The determination of these

axes is based on a self-consistent procedure.

An additional polarizer, P_0, is placed after the source but before the polarimeter. Its axis is chosen somewhere between 0° and 45° so that both M and C are non-zero. An exact determination of the axis position is not needed, the only requirement being that it not be changed during the course of the following measurements. A measurement is then taken of the Stokes parameters using approximate values for γ_0, β_0 and Δ. The retarder is then reversed and a second determination of the Stokes parameters is made. The polarizer in the polarimeter is then reversed and a measurement is made with the retarder forward and reversed. Since the Stokes parameters of the source have remained unaltered, γ_0 and β_0 are adjusted in the fitting program (using $-\gamma_0$ and $-\beta_0$ when the respective components were reversed) until M/I and C/I for all four determinations agree. Although the Stokes parameters so measured will not in general be correct (Δ has yet to be determined), their self-consistency is sufficient to determine the axes' positions.

The value for β_0 so determined will be correct modulo 90°. A change of β_0 by 90° only changes the sign of S. If one does not know, a priori, which is the fast and which the slow axis of a retarder, appeal may be made to a known circular polarizer. Purchasing a right-handed circular polarizer from a reputable optical house may indeed be the only way to determine the sign of S. Such a circular

polarizer, if inserted backward, is a plane polarizer not a left-handed polarizer. There is no mistake the user could make which would change a right-handed circular polarizer into a left-handed one. This method of determining the fast axis was used for these experiments.

3.5 Determination of the Retarder Phase

The phase of the retarder may also be determined by a self-consistent method. An initial polarizer, P_0, is introduced as before with its axis as nearly horizontal or vertical as possible. (The intent is to minimize the value for C.) Two sequences of measurements are taken. The first with the polarizer in the polarimeter crossed with respect to P_0, and the second with the polarizer aligned. The angles are not critical. Usually P_0 has been set by eye with its transmission axis vertical. One data set is acquired with $\gamma = 0°$ and a second with $\gamma = 90°$.

The data sets are analyzed in the usual way with some assumed value for the phase, Δ, of the retarder. If Δ is changed, and the data sets reanalyzed, both I and M change. (With an initial linear polarizer, S is zero and C has been chosen to be small.) What is both interesting and useful is that for the case of crossed polarizers the value of $I - |M|$ remains constant as Δ is changed in the program. For aligned polarizers $I + |M|$ remains constant. Thus the value of M/I for the aligned case changes very rapidly with Δ while for the crossed case it changes rather slowly.

The algorithm to solve for Δ is to choose any reasonable value for the phase, Δ_1, and solve for M/I from the crossed polarizer data set. Adjust the value of Δ for the aligned case until M/I equals its previous value. Use this value for the phase, Δ_2, for the crossed case obtaining a new value for M/I, etc. In practice the procedure converges very rapidly and a special version of our analysis routines performs the algorithm automatically.

The validity of this algorithm rests only on the fact that M/I of the source is independent of the method used to measure it. Its practical usefulness requires that $I - |M|$ and $I + |M|$ be independent of Δ when $S = 0$ and C is small for crossed and aligned polarizers respectively. What follows will indicate how this further condition can be proven for $S = 0$ and $C = 0$ for equally weighted data points. This condition has been observed for properly weighted experimental data within the calculated uncertainties.

Consider the case $\gamma = 0$; equation (3.11) may be written

$$I^t\ (\gamma = 0, \beta_i, \Delta) = \frac{1}{2}\ [I + M\ (\cos^2 2\beta_i + \sin^2 2\beta_i \cos \Delta)]$$

If I_0, M_0 and Δ_0 are the "true" values of the respected parameters then

$$I_0 + M_0\ (\cos^2 2\beta_i + \sin^2 2\beta_i \cos \Delta_0) = I + M\ (\cos^2 2\beta_i + \sin^2 2\beta_i \cos \Delta)$$

This equation is of the form

$$y_i = a + b\,X_i$$

whose solution for equal weights is:

$$a = \frac{1}{C}\left(\sum X_i^2 \sum y_i - \sum X_i \sum X_i y_i\right)$$

$$b = \frac{1}{C}\left(N \sum X_i y_i - \sum X_i \sum y_i\right)$$

$$c = N \sum X_i^2 - \left(\sum X_i\right)^2$$

If the N measurements are chosen such that β_i is equally incremented from 0° to 360°, all of the necessary sums can be performed. The value a + b corresponds to I + M. The result is

$$\gamma = 0° \qquad I_0 + M_0 = I + M \tag{3.13}$$

The equation for $\gamma = 90°$ is given by

$$\gamma = 90° \qquad I_0' + M_0' = I' - M' \tag{3.14}$$

The primes indicate that the parameters appearing in equation (3.14) need not be the same as those in (3.13) since the detector response is not the same for $\gamma = 90°$ as it is for $\gamma = 0°$. However $M_0/I_0 = M_0'/I_0'$.

When the transmission axis of the initial polarizer,

P_0, is chosen to lie along the horizontal, equation (3.14) represents the crossed case and (3.13) the aligned case. If the initial polarizer axis is chosen to lie vertically, M is negative and (3.13) represents the crossed case while (3.14) represents the aligned case.

3.6 Summary

Equation (3.11) expresses the intensity of light, characterized by its Stokes parameters, after passage through an ideal polarimeter. While no such device exists, prism calcite polarizers (10^{-6} attenuation when crossed) and zero-order quartz retarders come very close. Any transmission losses in these devices as well as detector inefficiency would appear in (3.11) as an overall multiplicative constant which would cancel when the ratios M/I, C/I and S/I were formed.

Equation (3.11) need not be considered solely as a mechanism for measuring Stokes parameters. By inserting equations (2.27 to 2.30) for the Stokes parameters the equation directly yields the measurable intensity for any particular polarimeter parameters. Indeed, the most general expression for the detected light intensity would be a function of the polarimeter parameters (γ, β, Δ) and the polarimeter orientation (θ, ϕ). Nothing would be gained by writing down such an unwieldy expression explicitly; particular applications can be generated when required.

CHAPTER IV

DATA ACQUISITION AND ERROR ANALYSIS

4.1 Experimental Equipment

Almost all of the laboratory equipment used for this experiment had been newly acquired prior to the commencement of this work. Space had been set aside within the Radiation Research facility but well apart from the 2MV Van de Graaff accelerator which had been used for all previous beam-foil work. Figure 3 shows a diagram of the laboratory layout.

The 350 KV electrostatic accelerator has an ion source capable of accelerating gases or solids. Maximum beam current registered in a Faraday cup in the target chamber is often in excess of 10 micro-amps. Two stages of electrostatic focusing together with an aperture stop just prior to the target chamber permit good current control.

Vacuum is maintained over approximately 4.5 meters of beam pipe by two 6-inch (15.24 cm) oil diffusion pumps. An additional 2-inch (5.08 cm) pump is connected directly to the target chamber. Pressure in the chamber is kept below $5 \cdot 10^{-6}$ torr (700 micro-Pascals).

The beam is mass analyzed by a 15 k Gauss (1.5 Tesla) magnet from Industrial Coils, Inc. The angle through which the beam is deflected is 15°.

4.1.1 Target Chamber

Designing a new multi-purpose target chamber was an

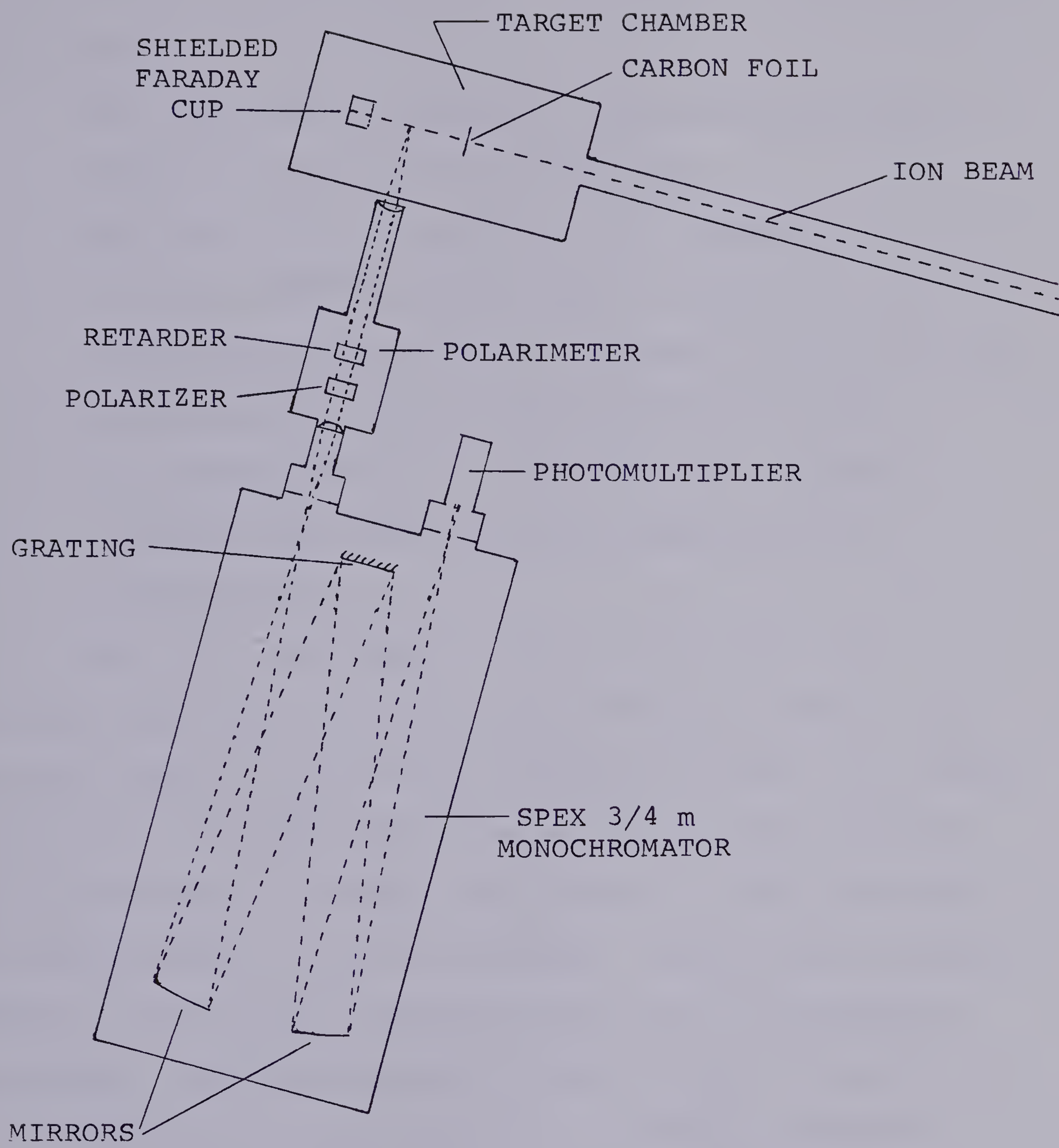

Figure 3. Laboratory Schematic

early priority for this project. Some of the design considerations were:

1) Use with either McPherson or Spex monochromators.
2) Viewing at 90° or 60° to the beam.
3) Foil tilt from 0° to 70° in 10° increments.
4) 12 cm of available foil travel; long enough for quantum beat measurements; movement at any foil tilt.
5) Reproducibility of foil position to 0.01 mm.
6) 40 available foils for changing under vacuum.
7) Optical light pipe positioned near foil for normalization.

The first consideration is not trivial. The McPherson Model 225 is a vacuum monochromator designed for use below 2000 Å. No focusing optics are used in the vacuum ultraviolet. The beam should be as close to the entrance slit as possible to minimize the length of beam viewed by the monochromator. Use of the target chamber with the Spex, however, involves both focusing optics and a polarimeter (see below) inserted between the beam and the entrance slit.

While the target chamber can indeed accommodate viewing at 60° to the beam, the room cannot. There is insufficient space to so mount the polarimeter and monochromator. A future project could resolve this problem by placing mirrors between the polarimeter and the entrance slit of the spectrometer.

All of the design considerations have been satisfied

with the present target chamber. About midway through the project, the tilt mechanism was improved to permit 5° increments to a maximum 80° tilt.

The upper photograph of Plate I shows the black target chamber on the right with the normalizing spectrograph on the left connected by a light pipe. The beam enters the chamber from the right. On the top of the target chamber from the left to right one can clearly see the stepping motor, the foil tilt knob and the foil changing mechanism with the light pipe draped over it. The entire top of the target chamber is removable and with it comes all of the internal mechanism. The lower photograph then shows the inner part of the chamber rigidly attached to the top which is not hanging from the ceiling but rather is resting on a table supported by the two aluminum brackets visible in the top photograph. (The lower photograph is thus upside down.) At the top center of this photograph is the foil-tilt knob with the foil-tilt bracket shown inclined at 45° directly below it (just to the left of the ruler).

The upper photograph of Plate II is a closeup of the foil-tilt bracket but this time shows a foil holder mounted in the bracket with two additional foil holders in the magazine above. Note that each foil holder has an elongated aperture and can accommodate two foils.

Tilting the foil to angles as large as 80° presents obvious problems. With a beam aperture limiting the beam

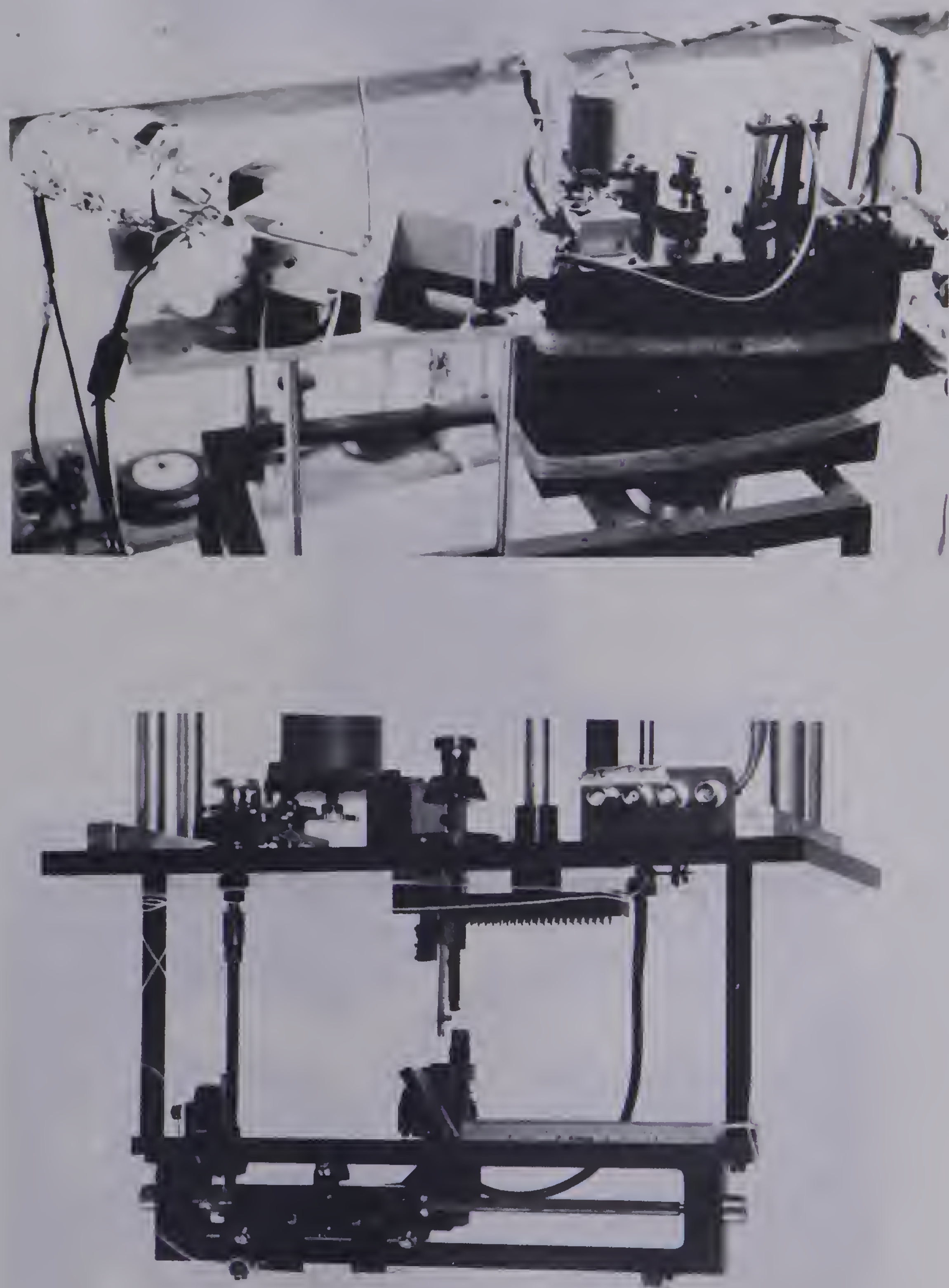

Plate I. The Target Chamber

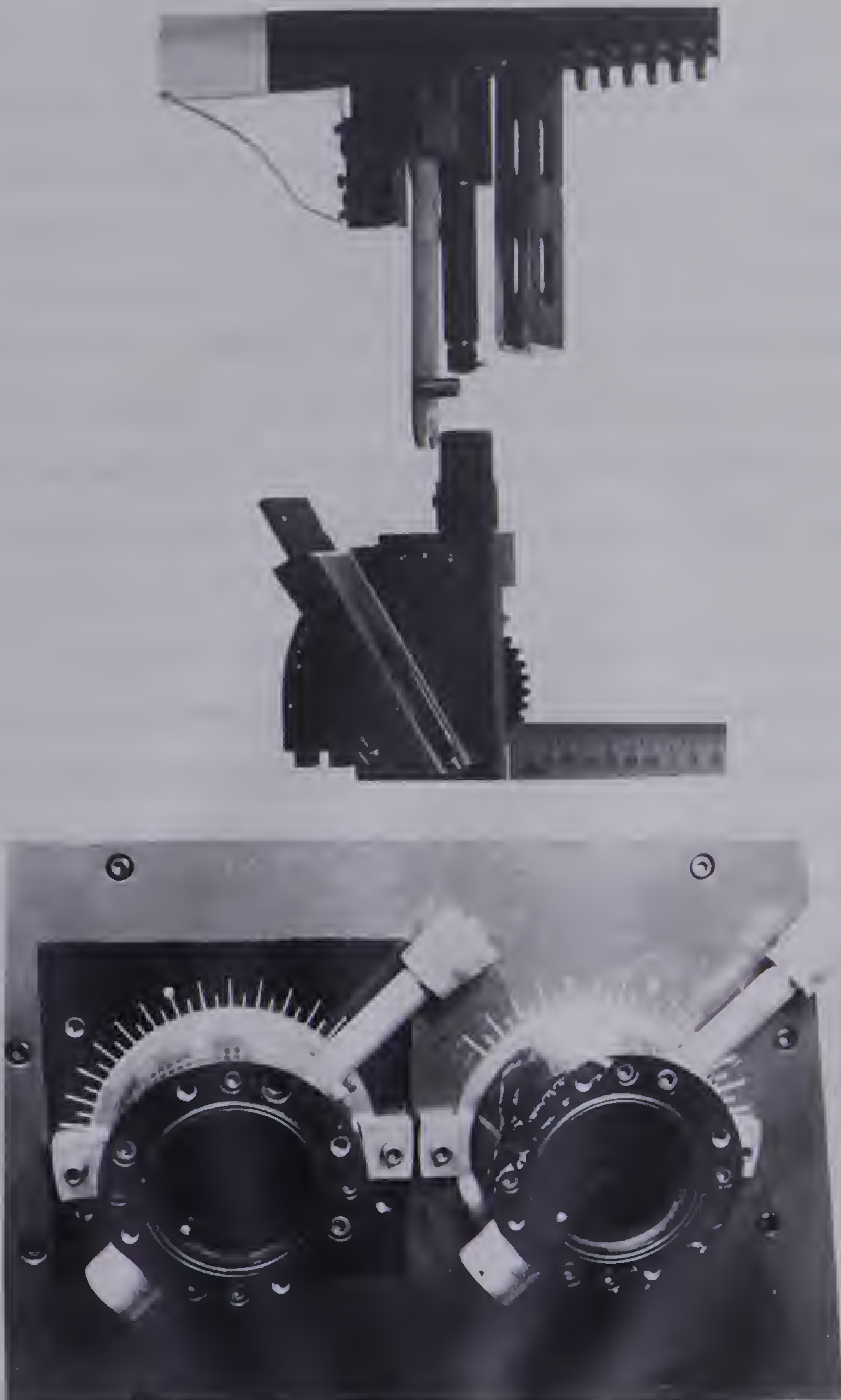

Plate II. Tilted Foil and Spectrometer Slits

diameter to 5 mm, the foil holder must be elongated 15 mm to 5 mm to pass the entire beam at 70° foil tilt. Such a holder would still attenuate about half the beam at 80°. These are ideal values for a holder with zero thickness. In practice about 20% attenuation of the beam current is suffered at 70° and 80% at 80°. Foil lifetimes are also markedly reduced at large tilt angles. Finally, the emergent beam velocity is lowered because of the increased effective thickness of the foil as it is tilted, though for ion beams of the lighter elements this is not a serious problem.

If spatial resolution is important, as it is for lifetime or quantum-beat measurements, the entrance and exit slits of the monochromator must be tilted along with the foil. For the Czerny-Turner design, tilting the slits does not necessarily introduce significant optical aberrations though line broadening is a problem. Exact parallelism of both the entrance and exit slits is more important than was realized during the design stage. The slit tilting modification is pictured in the lower photograph of Plate II. Tilting the slits can also produce a shift in the position of a spectral line caused by the grating not being in perfect vertical alignment. A simple change in the wavelength drive can compensate for this effect. Tilting the slits also increases the beam averaging length if the slit width is not reduced by the cosine of the tilt angle. At 60° the effective averaging length doubles.

4.1.2 Polarimeter

Polarizing elements made from crystal calcite or quartz function best in parallel light. Two fused silica lenses of equal focal length (10 cm) have been employed to focus light from the beam onto the entrance slit of the monochromator. Since the Spex is an f/6.8 system, the maximum usable aperture with 10 cm lenses is 14.7 mm. Both the polarizer and retarder have a 15 mm diameter.

Focusing the system for different wavelengths has been accomplished by mounting both the spectrometer and polarimeter on movable tables connected by a machined screw with a 2 to 1 thread ratio between them. If the polarimeter, including both lenses, moves one unit closer to the beam, the spectrometer moves 2 units, thus maintaining equal distances from the first lens to the beam and from the second lens to the entrance slit.

The good spatial focusing was confirmed by observing the He I quantum beat at 8.77 GHz on the 3889 Å transition. Only for this test measurement were the slits reduced to 100 microns and a foil step size of 50 microns was employed. The beat length is about 0.3 mm and our measured frequency was within 1% of the previously measured value.

The polarizer and retarder are each rigidly mounted inside a cylinder having one hundred gear teeth about its mid-point circumference (Plate III). The cylinder seats in a worm gear whose axis is connected by further gears to a

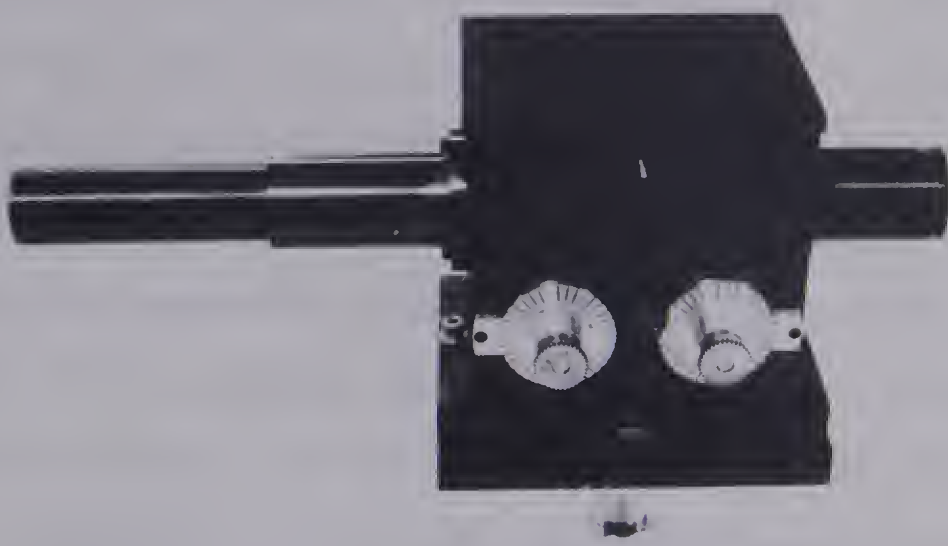

(a) Polarimeter closed.

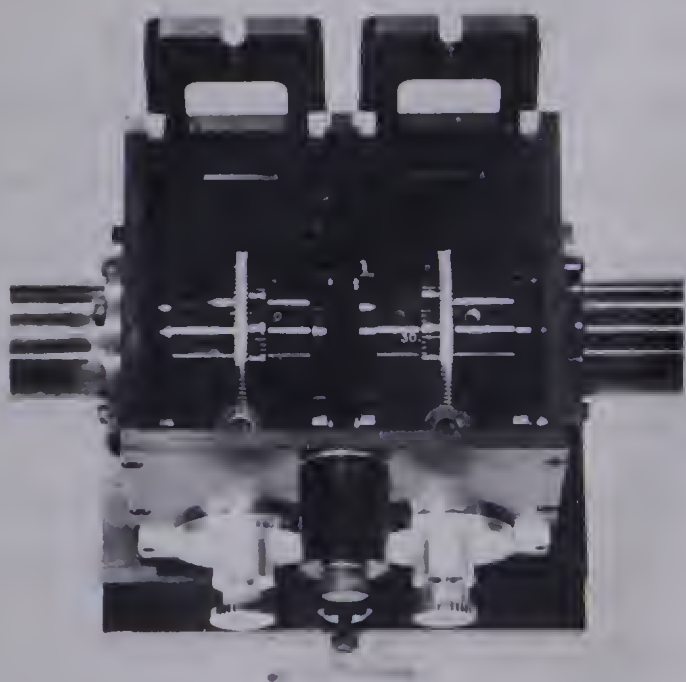

(b) Polarimeter top off as viewed from above. Cylinders in place.

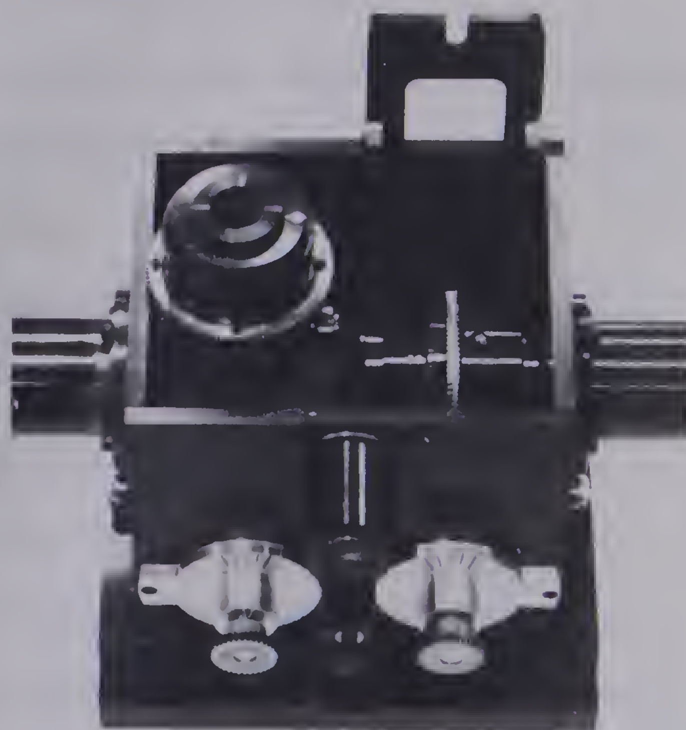

(c) Cylinder removed showing 1/4 λ retarder.

Plate III. The Polarimeter

stepping motor (not present in the photograph). One rotation of the worm gear advances the cylinder by 3.6°. The outer gears connecting the stepping motor allow for 20 pulses to equal one degree rotation of the cylinder. Thus the polarizer and retarder can separately be repositioned to 0.05° and an offset of 0.1° can readily be noticed by visual inspection.

Each cylinder can be removed and rotated, front to back, then reseated in the worm gear effecting an exact 180° rotation about the vertical axis. As described in the previous chapter, this feature is used to determine the polarizer's transmission axis and the retarder's fast axis with respect to the laboratory reference frame.

Two different polarizers were used during the project. Both are 15 mm calcite prism polarizers, one from Oriel Corp., the other from Karl Lambrecht, Inc. The attenuation of calcite in the ultraviolet varies significantly from sample to sample. The only guarantee of obtaining one usable to 2500 Å (50% of maximum transmission) is to specify such a demand before purchase. The Oriel polarizer is usable to 3000 Å while the Lambrecht one is good to 2300 Å.

Two retarders have also been used. One is a quarter wave at 5400 Å from Special Optics, Inc. Both are zero-order quartz retarders with transmission coefficients better than 80% over the entire spectral region of interest (2300 Å to 7000 Å).

4.1.3 Spectrometer and Detector

All measurements have been taken using a Spex Model 1500, 0.75 m Czerny-Turner design monochromotor. Two different gratings have been used. One is a ruled replica with 1200 lines/mm blazed at 5000 Å, while the other is holographic with 2400 lines/mm. The former was used for all measurements above 3500 Å while the latter was used below 3500 Å. Only a physical binding of the wavelength drive above the 3500 Å setting on the holographic grating prevented its use for all measurements. This grating was first tried only after the spectrometer had been carefully aligned. Since repair of the problem would have meant a significant loss of time, it was decided that the two gratings would be used as required and the repair deferred until the project was completed.

Three different EMI photomultipliers, the 6256S, the 9789QB, and the 9658R have been used during this project. The first two have a usable spectral response between 1800 Å and 5500 Å. The 9789QB is a plug-in replacement for the 6256S with a somewhat improved sensitivity. The red sensitive 9658R, mounted in a refrigerated housing, has been used for measurements between 5500 and 7000 Å. Standard photon-counting techniques were employed using Ortec electronics. Dark counts between 1 and 2 per second were typical.

4.1.4 Data Acquisition System

The Tracor Northern TN-11 is a software-controlled,

multi-component data acquisition system configured around a PDP 11/05 minicomputer. It utilizes the Digital Equipment Corp. (DEC) RX-11 dual floppy disk for program and data storage and the DEC DECWRITER terminal for user input and all printing. The "front end" is a TN-1206 four input scalar with external time base. The #1 input must be used as a preset scalar thereby reducing the number of available data inputs to three. The TN-1310 simultaneously controls two stepping motors. One positions the foil in the target chamber while the other rotates either the polarizer or retarder in the polarimeter. All aspects of data input and stepping motor control can be either single-command initiated or directed by a user-written program.

The number of available data channels is variable, limited only by the computer memory size (16K; 2 byte word length) and the executive and program overhead. Typically 1024 data channels, usable as two 512 channel halves, have been selected. One of the powerful features of the system is that the data channels may be allocated in any desired way. For example, the following breakdown of a 512 channel spectrum is typical:

Channel	
0 - 39	Data identification stored as ASCII code
40 - 157	Position of stepping motor
158 - 275	Scalar input #2
276 - 393	Scalar input #3
394 - 511	Scalar input #4 (usually spare)

The normalization signal, connected to scalar #1, can be either time, integrated beam current, or photon counts from a light pipe stationed just behind the foil. The light pipe is connected, without focusing, to a small Jobin-Yvon spectrometer which has a photomultiplier mounted at its exit slit. Usually it is possible to normalize on some strong line from the same ionization stage as the line of interest. The available spectral region is 4000 Å to 5500 Å. The angular acceptance of the light pipe is much greater than that of the spectrometer which causes a significant loss in intensity.

For some starting position of the retarder, photon counts are collected in scalar #2 and time in scalar #3 until the preset of scalar #1 is satisfied (typically about 5 secs). The retarder is then rotated by a stepping motor and the procedure repeated until the retarder has been rotated through 360°. One such cycle represents a single scan and five to ten such scans are summed to form one data set. The recorded time intervals are used to remove background counts from the data. One data set is usually composed of 18 or 36 points from which the Stokes parameters are evaluated.

Figure 4 shows five data samples of the HeI 5016 Å transition. Each were taken using 10° increments of the retarder through 360°. The four peak modulation pattern at 0° foil-tilt is indicative of exclusive linear polarization while the two-peak patterns at 60° is almost entirely circular polarization. The figure convincingly shows how

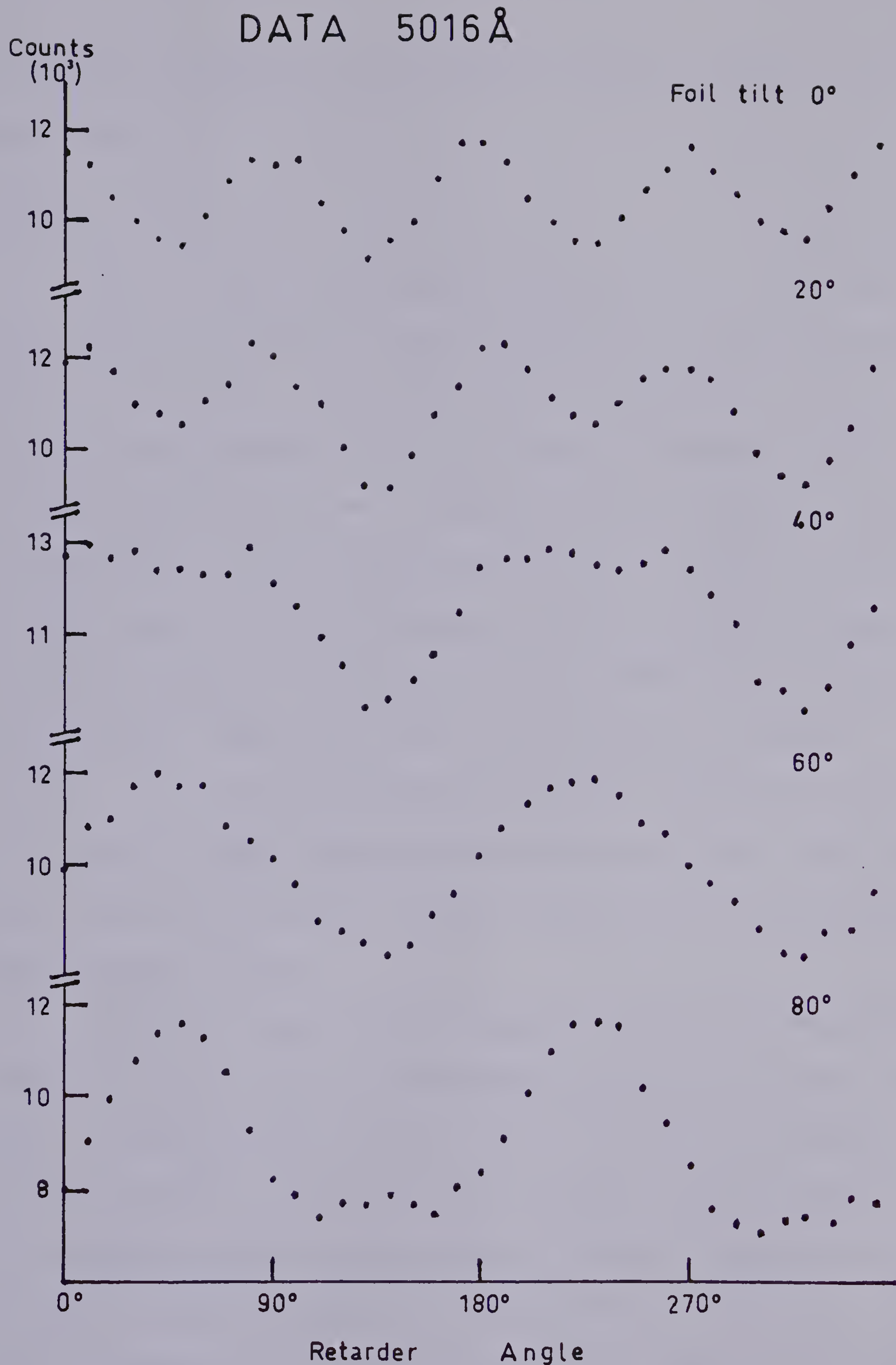

Figure 4. Typical Data Sample. He I

dramatically tilting the foil alters the polarization of the emitted light.

4.2 Random Errors

Several different computer routines are available for analyzing data that can be acquired with the system described in previous sections. Two types of data samples can be collected; polarization data which are collected at some fixed foil position and are a function of the rotation angle of the retarder and decay data which are a function of foil position at some fixed polarimeter setting (which includes no polarimeter present). Included in decay data are quantum-beat data often taken with just a horizontally oriented polarizer. It is not difficult to imagine collecting data as a function of both polarimeter setting and foil position but such data have as yet not been acquired for anything other than feasibility tests.

Optical or beam-current normalization and compensation for the background rate are standard procedure for both types of data. Weighting the data by the inverse of the square root of the number of counts which assumes Poisson statistics and is standard practice for photon counting experiments is also common to both types of data analysis. Initially, then, it came as somewhat of a surprise to find that the polarization data, after being analyzed, showed reduced chi-squared values which were significantly larger than unity whereas decay data showed no such anomaly.

The resolution of this problem came with the realization that optical normalization had not previously been used for decay data and was peculiar to the new target chamber. It is in fact common for the count rate of the normalization detector to be a factor of 2 to 5 smaller than the count rate from the signal detector. This is a consequence of the mismatch of the effective f-value of the light pipe with that of the small monochromator. The normalization signal has an uncertainty proportional to the square root of the number of counts even as the data signal has. These uncertainties should be combined and the data signal weighted accordingly. If the data signal is S_d and the normalization signal is S_n, the uncertainty in the data, σ_d, is given by

$$\sigma_d = S_d \left(\frac{S_d + S_n}{S_d \cdot S_n} \right)^{\frac{1}{2}} \quad ; \qquad (4.1)$$

as $S_n \to \infty$

$$\sigma_d = \sqrt{S_d} \; . \qquad (4.2)$$

To check the effect of using proper weighting, 18 data samples taken in the same manner were analized using both (4.1) and (4.2) for the uncertanties of the data. The reduced chi-squared, χ_ν, which is the usual goodness-of-fit criterion, is defined as

$$\chi^2_\nu = \frac{1}{\nu} \sum_i \left[\frac{1}{\sigma_i^2} [y_i - y(x_i)]^2 \right] \qquad (4.3)$$

where y_i is the datum at position x_i, $y(x_i)$ is the value of the fit at x_i. σ_i is the uncertainty in y_i and ν is the number of degrees of freedom defined as the number of data points minus the number of fitting parameters. The means of the reduced chi-squares for the 18 data samples using the two different methods of weighting were found to be

4.51 ± 1.59	Using (4.2)
1.32 ± 0.52	Using (4.1)

The polarization values themselves were unchanged. The computer estimates of the uncertainties, however, changed significantly. They were found to scale as the ratio of the square roots of the reduced chi-squareds, becoming larger as the reduced chi-squared became smaller.

For the linear least-squares fitting routines, the uncertainties of the parameters do not depend upon χ^2, being determined principally by the uncertainties of the input data. It seems reasonable, then, to multiply the computer estimate of the uncertainty in the final parameters by the square root of the reduced χ^2 (if larger than 1.0) as a means of compensating for improper weighting of the input data.[1] Except for the 18 data samples mentioned above, all of the data acquired for this project used equation (4.2) for the uncertainties. Future data samples will record the necessary information to use equation (4.1).

---

[1]Further support for this procedure will be presented in Section 4.3.

Since the difficulty with large chi-squareds had never been noticed in past years when using beam current normalization for decay data, one might wonder what the advantage is to using optical normalization. The reason why this problem does not arise with beam current normalization is that the current digitizer uses an analog technique to sum huge numbers of ion charges from the beam thereby effectively having no uncertainty from random sources. The reason for using optical normalization is the hope that systematic errors caused by beam fluctuations will be more nearly eliminated. The presence of an additional source of random error is not a problem once the proper method of compensation is known.

4.3 Systematic Errors

Perhaps the most difficult task for an experimental physicist is the elimination of systematic errors. The first step of such a task is the determination of the source of these errors and therein lies the difficulty.

It would be most useful to measure the polarization of a known light source at several different wavelengths. Unfortunately, except for an unpolarized source, such sources are difficult if not impossible to obtain. At 0° foil tilt, both C/I and S/I should be zero. 25 data sets, acquired with a perpendicular foil, were examined and the weighted mean (μ) for S/I was 0.0009 ± 0.0013. The value for C/I was 0.0030 ± 0.0017. The uncertainties assigned to these means have been

calculated using the square root of the variance defined as

$$\chi_\mu^2 = 1/\sum_i 1/\sigma_i^2 \qquad (4.4)$$

where σ_i is the computer determined uncertainty multiplied by the square root of the reduced χ^2 for that particular data set as discussed in the previous section.

There is one possible source of error which exists for C/I that does not exist for S/I and that is the axis determination of the retarder and polarizer. Whereas an incorrect axis value can alter a nonzero measurement of S/I, it has no effect on a zero S/I. Since M/I for these data sets is nonzero, an error in the axis positions of the order of 1° could easily account for the C/I value being as large as it is. However no C/I or M/I values are quoted with an uncertainty smaller than 0.003.

The scatter in these values of C/I and S/I can be estimated by forming a quantity analogous to the χ^2 of equation (4.3). The role of the fitting function is played by the weighted mean, μ. Calling this quantity σ^2, its definition is

$$\sigma^2 = \frac{1}{N - 1}\sum_i (y_i - \mu)^2/\sigma_i^2 \qquad (4.5)$$

where N is the number of points in the sample and the other quantities have been previously defined. σ^2 should be close to one for random scatter about the mean if the weights, σ_i, have been properly assigned. The value of σ^2 for the C/I

sample is 0.59 and for the S/I sample is 1.09. This test indicates that the error assigned to C/I may be too large.

Another test sample of data using zero polarization is offered by an He I transition at 5048 Å which originates from a ^1S term and should therefore be rigorously free from any polarization. The weighted means, over all angles from 0° to 70° in 10° increments for the relative Stokes parameters are:

$$M/I = -0.0006 \pm 0.0030$$

$$C/I = -0.0073 \pm 0.0030$$

$$S/I = -0.0029 \pm 0.0018.$$

These numbers indicate that the assigned uncertainties may be too small. If the scatter of these numbers about the weighted means is examined as before, the values of σ^2 are

$$\sigma^2(M/I) = 0.72$$

$$\sigma^2(C/I) = 0.97$$

$$\sigma^2(S/I) = 1.13 .$$

The scatter indicates that the assigned uncertainties from random sources are correct. To examine systematic errors one could use equation (4.5) with $\mu = 0$. In that case the above values become 0.73, 1.84 and 1.49 respectively which indicates an additional source of error may be present. However, the sample size and the magnitude of the possible error are too small to be definitive.

These studies were performed with a source of known zero polarization and indicate that proper account has been

taken of random errors and that systematic errors, if present are small. One cannot extend the validity of such tests to measurements of non-zero polarization. Repeated measurements of the same transition, with large polarization, scatter about the mean by the amount suggested by their assigned uncertainties. This only indicates that random errors have been properly assigned.

One possible source of error, that has not been thoroughly investigated, is whether the polarization for a given transition varies from foil to foil. How sensitive is the polarization to foil condition and how does it vary as the foil degrades in the beam? One experiment was performed in which a new foil was inserted and each data scan saved individually rather than summed. 12 such scans were recorded before the foil degraded to the point where it would normally have been replaced. No systematic variation in the polarization was recorded though a slight tendency for $|S/I|$ to decrease (≃5%) with foil degradation was noted. No experiment has been performed in which many repeated measurements were taken using different foils. However a significant number of measurements have been repeated once or twice and no serious disagreements have been noticed.

All of the above tests seem to indicate that the precision of the measurements presented in this project are properly indicated by the assigned uncertainties. The matter of accuracy is another question entirely. Without calibration standards it is impossible to determine the accuracy of any

measurement. Of course, the Stokes parameters following a purchased plane polarizer or circular polarizer have been measured and were found to be reasonable. However, these devices are not standards and their polarizing capability varies greatly with the frequency of the transmitted light. The polarization values which have been measured in other laboratories agree with those measured in this project. The procedure of rotating a retarder before a fixed polarizer, when both are high quality elements manufactured to rigid standards, eliminates so many sources of error that one cannot but hope that the accuracy of the recorded values is also properly indicated by the assigned uncertainties.

CHAPTER V

POLARIZATION OF HELIUM

While hydrogen is the simplest atom, the near degeneracy of all quantum states with the same principal quantum number make it unsuitable for experiments probing the differences between states with different orbital quantum numbers. Helium is the simplest atom for such experiments. It offers many transitions in the spectral region 2300Å - 7000Å including some between doubly-excited states. Having no nuclear spin, all transitions are free from hyperfine structure. The singlet and triplet systems are almost non-interacting, at least for all S, P and D states.

The fine structure of Helium is small, being less than about 1 cm^{-1} for all levels. Violation of the Landé interval rule is not an indication of the breakdown of LS-coupling, as it might be in heavier elements, but rather of the importance of the spin-spin and spin-other-orbit interactions (BS 77). While this has been known for some time, only in the past twenty years have the fine structure intervals been measured with sufficient accuracy to challenge the various approximate procedures used to calculate them. Beam-foil spectroscopy has made a substantial contribution towards this endeavor.

Two experiments, both using the quantum beat method,

are worth noting. The first measured the fine structure intervals for the 2s - np sequence (n = 3 to 7; WTAD 72) while the second measured the intervals for the 2p - nd sequence (n = 3 to 8; ACLMM 76). While neither could match the accuracy of other types of experiments for the low lying members of the sequence, both offered the first measurements for higher values of n.

Quantum beats within the triplet states of Helium are easily observed and it is becoming routine to use the beat frequency of 658.6 MH_z for the $^3P_1$ - $^3P_2$ separation observed at 3889Å($2s\,^3S$ - $3p\,^3P°$) as a beam velocity calibration standard. Accurate beam velocity determination is not so important for polarization measurements as it is for mean life or quantum beat frequency measurements.

The first experiment to use a tilted foil was performed by Berry, Curtis, Ellis and Schectman (BCES 74) on the Helium I $2s\,^1S$ - $3p\,^1P°$ transition at 5016Å. It clearly demonstrated that tilting the foil was sufficient to destroy axial symmetry, even on the atomic scale, thereby permitting the observation of circularly polarized light. While the general theory, presented in Chapter II, was formulated prior to this experiment and clearly allows for the observation of circularly polarized light in the absence of cylindrical symmetry, the mechanism and magnitude of the effect is not discussed at all.

Several authors have addressed this problem and a

brief summary of their work will be presented in the following section. The question being raised here is how do the excitation parameters, σ_q^k, depend upon the foil tilt angle? Further questions, which must be answered by any complete theory, would relate to a specification of all experimental parameters (beam velocity, current density, foil temperature, etc.) upon which the excitation parameters depend.

5.1 Tilted Foil Theories

Lewis and Silver (LS 75) were the first to attempt a generalized formalism for tilted foil. Besides the foil-tilt angle, α, their model depends on the size of the interaction region (ϕ) and a second angle, β, which is freely adjustable. The results vary significantly depending upon the assumptions invoked. Two key predictions, that C/I should change sign with increasing foil-tilt angle and that S/I should achieve a maximum before 80° foil-tilt angle has been reached, have not been borne out by experiment. In fairness to the authors they offered reasons why both of the above might <u>not</u> happen.

Lombardi (Lo 75) used a surface electric field model, very similar to Eck's (Ec 73), to demonstrate that failure of Eck's model was not intrinsic to the concepts employed but to some very restricted simplifications used for a particular calculation. However, the Lombardi model has so many parameters that almost any behavior of the polarization with foil tilt can be described.

Herman (He 75) chose to treat the interaction as a

differential collision effect, and while unable to derive explicit relations for the excitation parameters, he was able to express their behavior with foil tilt. However the model is too simplistic to account for many of the observations made to date.

Schröder and Kupfer (SK 76) have treated the problem using electron capture from an electron gas with a steep density gradient. Specifically the problem was solved for a metallic foil and a hydrogen ion beam. When applied to Helium their values for M/I were much larger than observed. However, to their credit, this calculation is ab initio, with no free parameters.

The above theories have used three different treatments to model the beam-foil interaction. Several use an electric field or field gradient at the foil surface, one considers collisions as the ion leaves the foil, and one treats electron capture from a gas with a steep density gradient. The best approach has as yet to be decided.

There is one treatment, by Yehuda Band (Ba 76) which stands out from the others by virtue of its clarity and ready comparison with experiment. The mechanism invoked is also that of a surface potential which is normal to the foil caused by the Fermi energy plus the work function. The potential is expanded in a power series keeping terms to $(V_o/v\cos\alpha)^2$, where V_o is the potential, v the beam velocity and α the foil-tilt angle.

Band expressed his results in terms of six free parameters but a slight rearrangement of the equations easily demonstrates that only five of them are independent (BP 78). In terms of five parameters his results are:

$$\frac{M}{I} = \frac{E \cos^2 \alpha + F}{A \cos^2 \alpha + B} \tag{5.1}$$

$$\frac{C}{I} = \frac{D \sin 2\alpha}{A \cos^2 \alpha + B} \tag{5.2}$$

$$\frac{S}{I} = \frac{\sin \alpha \cos \alpha}{A \cos^2 \alpha + B} \tag{5.3}$$

5.2 Results Using Helium Singlets

Whereas the variation of polarization with foil tilt has been established since 1974, the matter of how this behavior varies from transition to transition for a given element has not previously been examined. An experiment using five Helium singlet transitions, for which quantum beats would not complicate the analysis, was performed for foil-tilt angles from 0° to 70° in 10° increments. The experiment was later repeated for two of the transitions from 0° to 80° in 5° increments. One transition, the $2p\ {}^1P° - 4s\ {}^1S$ at 5045 Å, which should rigorously show no polarization, was used for an indication of systematic errors.

An incident ion energy of 160 KeV was used for all measurements. No attempt was made to compensate for the additional energy loss in the foil as the foil is tilted.

However, the energy loss of Helium is not large and the additional loss at 60° foil tilt is less than 5%.

Figure 5 shows the Stokes parameters for the $^1S - {}^1P$ He I transitions at 5016 Å (2s-3p) and at 3965 Å (2s - 4p). Figure 6 gives the same information for the $^1P^o - {}^1D$ transitions at 6678 Å (2p - 3d) and at 4922 Å (2p - 4d). The smooth curves are least-squares fits to the Band equations (5.1) to (5.3). P_f is the total fractional polarization defined as $[M^2 + C^2 + S^2]^{\frac{1}{2}}/I$.

There is no unique procedure for obtaining the Band parameters from the data. The method chosen was a compromise between rigor and expediency. First the S/I data were inverted (properly weighted after inversion) and a linear least-squares fit for A and B was performed. Using these values, a linear least-squares fit to C/I determines D, while such a fit to M/I determines E and F. This procedure can be criticized on two counts:

1) A and B appear in the equations for all of the Stokes parameters and only the S/I data were used for their evaluation.
2) Inverting equation (5.3), even properly weighted, and minimizing the chi-squared will not in general produce the values of A and B which minimize the chi-squared for equation (5.3) as written. The closer the reduced chi-squared comes to 1.0, the closer the two different ways of evaluating A and B agree. If the fit were very poor,

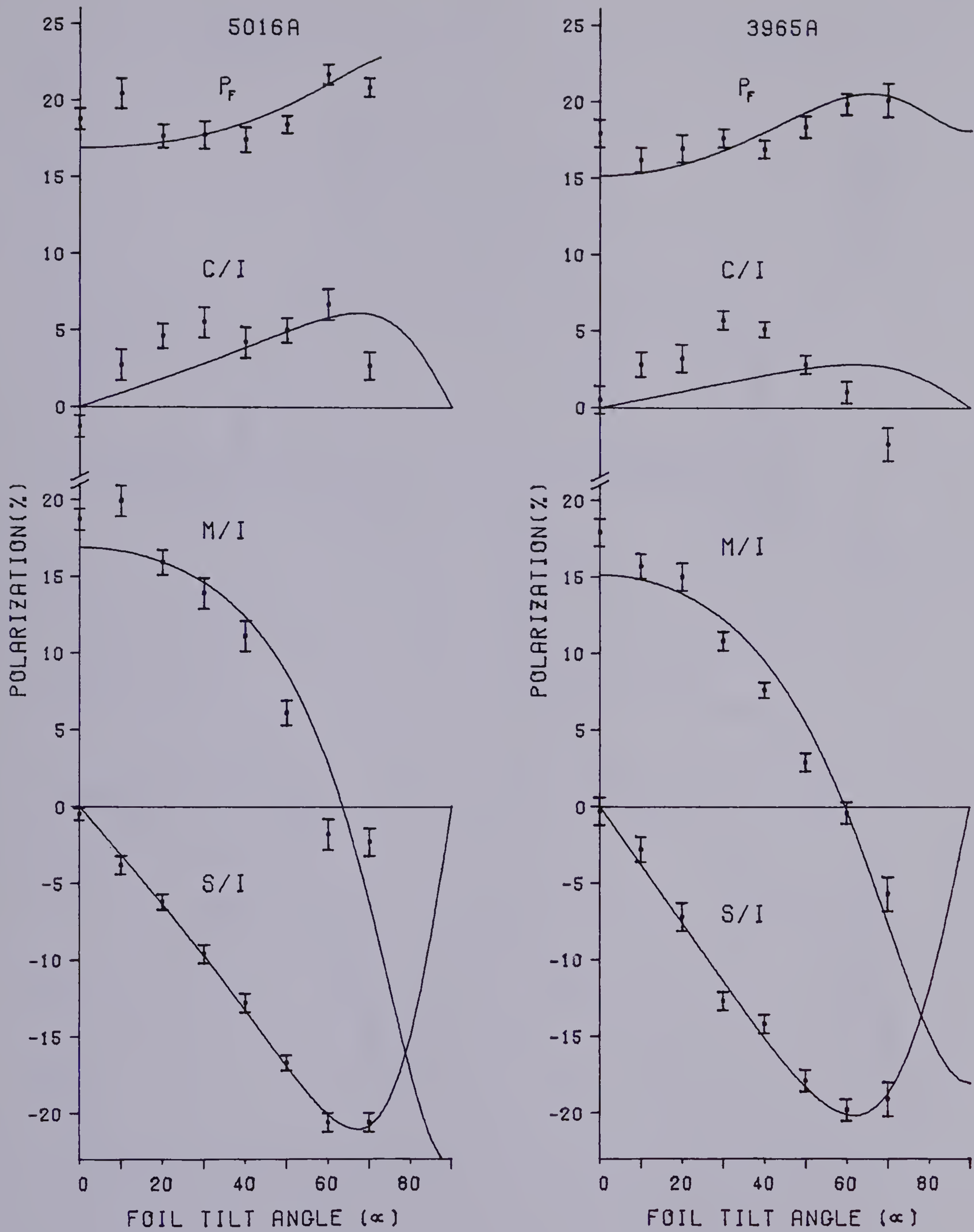

Figure 5. He I Polarization, ^1S - $^1P°$

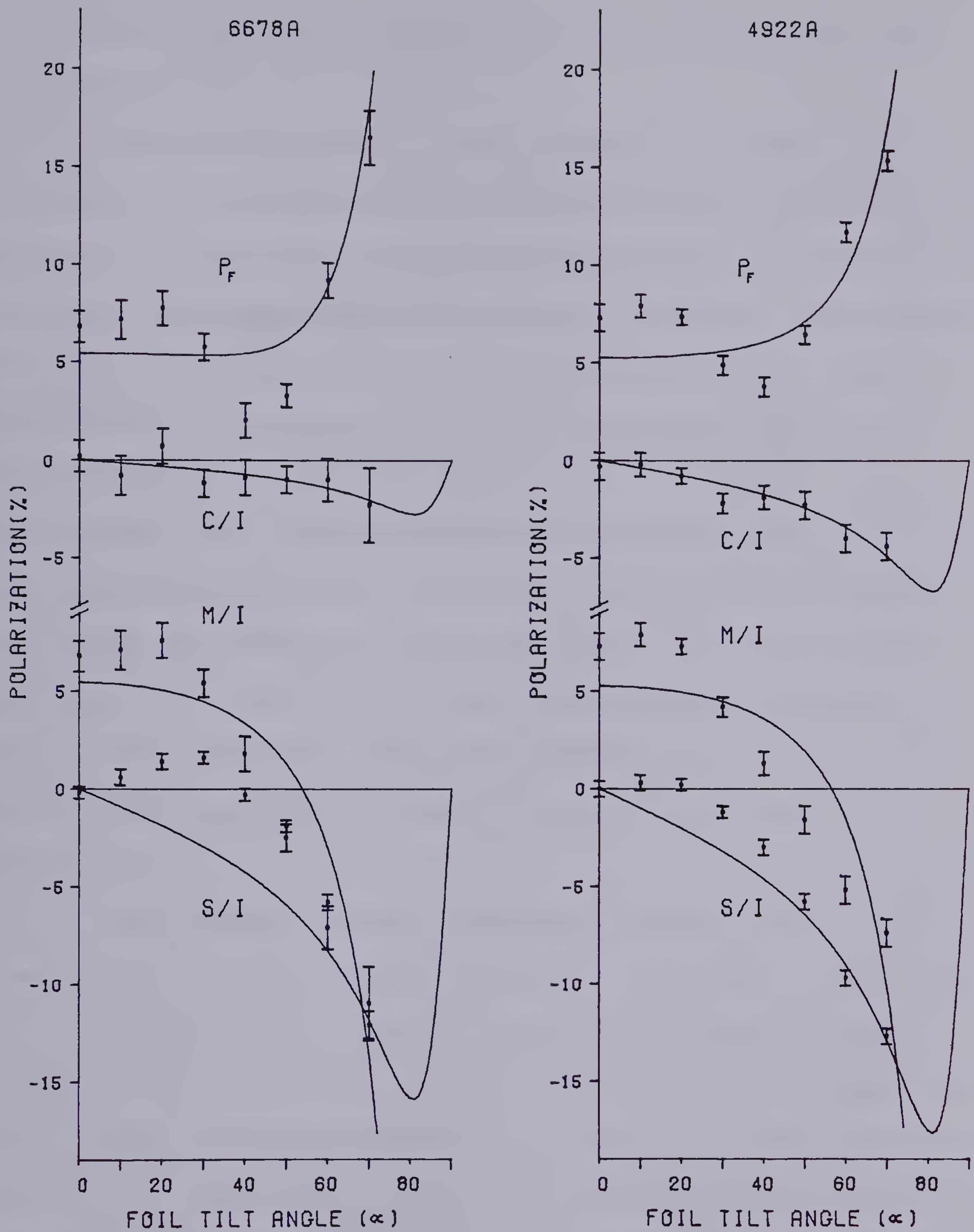

Figure 6. He I Polarization, $^1P^\circ - {}^1D$

the two different values for A and B could differ substantially.

These objections are most relevant if some physical interpretation were being applied to the Band parameters. However, the exercise is being performed solely to find out whether or not some parameters can fit the data. The second criticism only applies if the fit is already poor. The fit cannot get better by applying to A and B the contraint of simultaneously satisfying equations (5.1) and (5.2). In other words, if a set of parameters exists which can fit the data this procedure will find them. If no such set exists, the curves obtained from this method will certainly differ from the curves obtained by some other method but neither set will fit the data. The Band parameters for each of the transitions appearing in Figures 5 and 6 are listed in Appendix 2.

The fits are really quite good for the two ^1S - $^1P°$ transitions with the exception of C/I. The fits for the two $^1P°$ - ^1D transitions, however, cannot be considered satisfactory. One notices two pronounced differences between the results for transitions originating from a ^1D level and those from a $^1P°$. The first is that M/I becomes negative for the former at about 45° foil tilt while for the latter at about 60° foil tilt. The second is that S/I remains close to zero for the ^1D transitions for all foil tilt angles less than about 40° and then becomes rapidly large finally catching up

to the $^1P°$ values for large tilt angle. This feature coupled with the early zero in M/I causes P_f, the total fractional polarization, to achieve a minimum at about 45° for the ^1D transitions while no such minimum occurs for the $^1P°$ ones.

Figure 7 shows the results for the 2s ^1P - 3p $^1P°$ transition at 5016 Å and the 2p $^1P°$ - 4d ^1D one at 4922 Å. The intent in remeasuring these lines was to establish a smooth trend, from 0° to 80° foil tilt for each of the different L states available.[1] The curves are from a cubic spline smoothing routine and represent the best experimental determination of the polarization of these states obtained in this project. The Band theory does not do any better with these results, in fact the larger angle points are even more difficult to fit and a noticeable discrepancy would be visible in the M/I curve for 5016 Å. However, the theory specifically demands higher order terms for large tilt angles so it is unfair to compare these data sets to the Band Theory.

The C/I results are somewhat curious in that, for the $^1P°$ case, they are the ones not well fitted by the theory, while for the ^1D case, they are fitted well indeed.

5.3 Helium Doubly-Excited States

For Helium the only states of practical importance are in fact those for which at least one electron is in the ground state, for the following reason. One finds

---

[1] No transitions in neutral Helium for states with L ≥ 4 occur below 7000 Å.

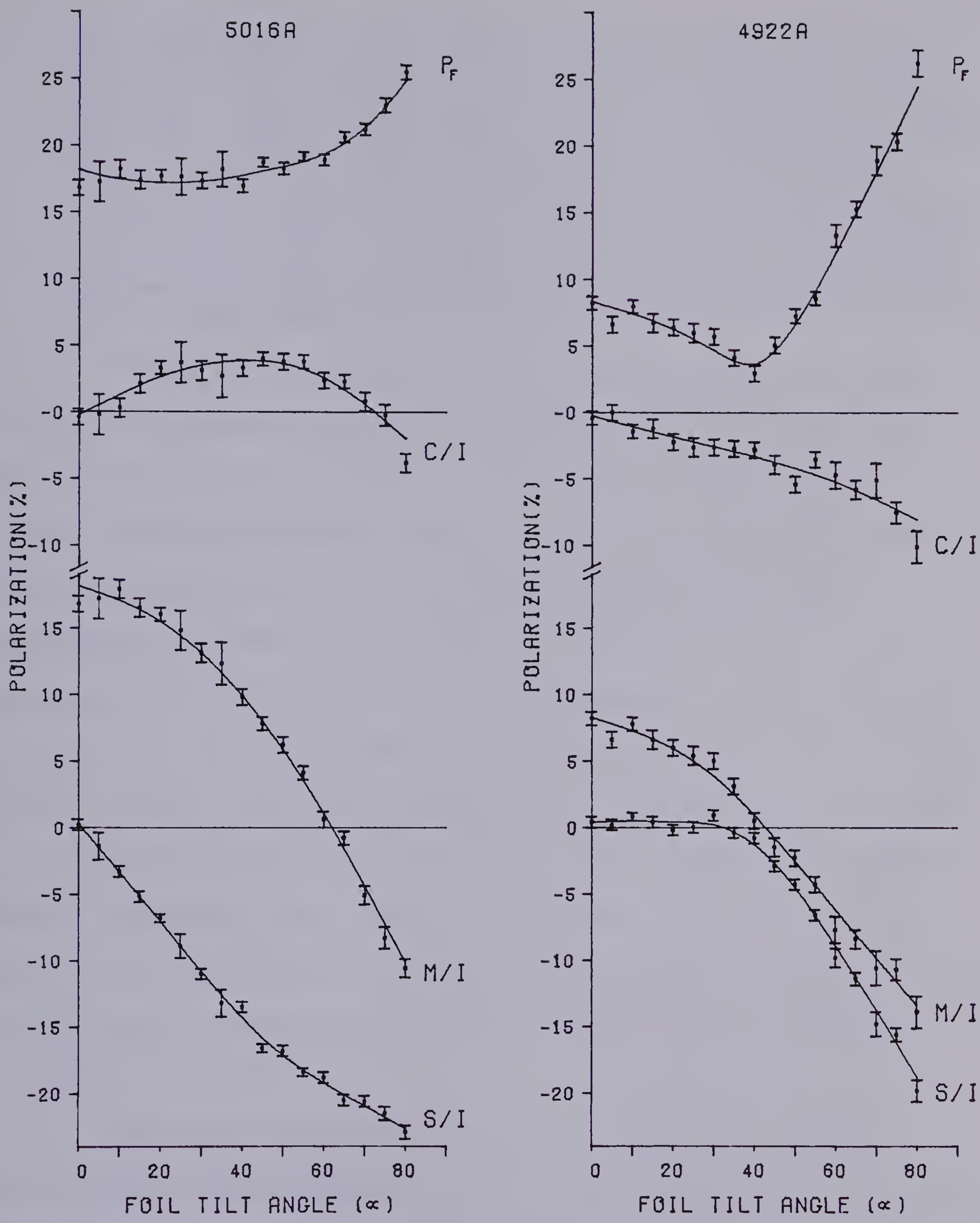

Figure 7. He Polarization, 5016Å and 4922Å

> that the energy of any state in Helium, for which both electrons are excited, is higher than the ground state energy of a He^+ - ion (H-like ion with $Z = 2$) plus a free electron. These states then lie in the continuum and the same holds for all other He-like ions. One can show further that, for such a doubly-excited state in He, dissociation into He^+ plus a free electron (Auger effect) is much more probable than a radiative transition to a bound state of He. Spectral lines involving such doubly-excited He-states are very rare in practice and we shall <u>not</u> consider them any further.

These are the words of Bethe and Salpeter in their classic monograph (recently reprinted, BS 77) on one- and two-electron atoms written in 1957. One of the exciting aspects of the beam-foil light source is that many doubly-excited states in Helium and other elements are easily observable (Be 75). The reason is twofold. While it is correct that all He doubly-excited states lie above the first ionization limit (24.59eV), the selection rules for the Auger effect ($\Delta J = 0$, no parity change; $\Delta L = 0$ and $\Delta S = 0$ for good LS-coupling) prevent autoionization for many of the levels which then radiatively decay. Secondly, even many states which can autoionize do so at a sufficiently slow rate, that radiative decay becomes competitive (Be 75 and references contained therein).

The rule which can be used to determine whether or not a given doubly-excited state in Helium can autoionize is the following. If the parity of the state is the same as the numerical parity of L, the total orbital angular momentum, then the state can autoionize. If the parity is opposite, it cannot. This follows from the above expressed selection

rules for those doubly-excited states below the He II 2p threshold. Above this threshold all states may autoionize.

The primary experimental methods for determining energy levels of doubly-excited states are electron and ion scattering experiments with the observation of resonances (Sc 73). A second technique is the observation of absorption lines using a synchrotron light source (MC 63). Beam foil is the only light source which produces transitions between doubly-excited states observable as emission lines.

Most theoretical treatments of doubly-excited states in He take L and S to be good quantum numbers. However, single configuration designations, such as ns mp, can be misleading when used to describe the autoionizing levels. Several different schemes have been proposed for these levels, but so far none of them has been generally adopted. It should be stressed that the question of notation is not simply a matter of convention. The problem of quantum mechanically describing excited states of atoms and ions from ab initio calculations always involves the explicit or implicit notion of configuration interaction. The labels which one attaches to an energy level then becomes theory dependent. The only labels, for this problem, which must be theory independent are the specification of the energy, the total angular momentum and the parity.

5.3.1 Spectral Analysis

The spectra of Helium between 2200 Å and 3400 Å appears in Figure 8. Eight doubly-excited state transitions

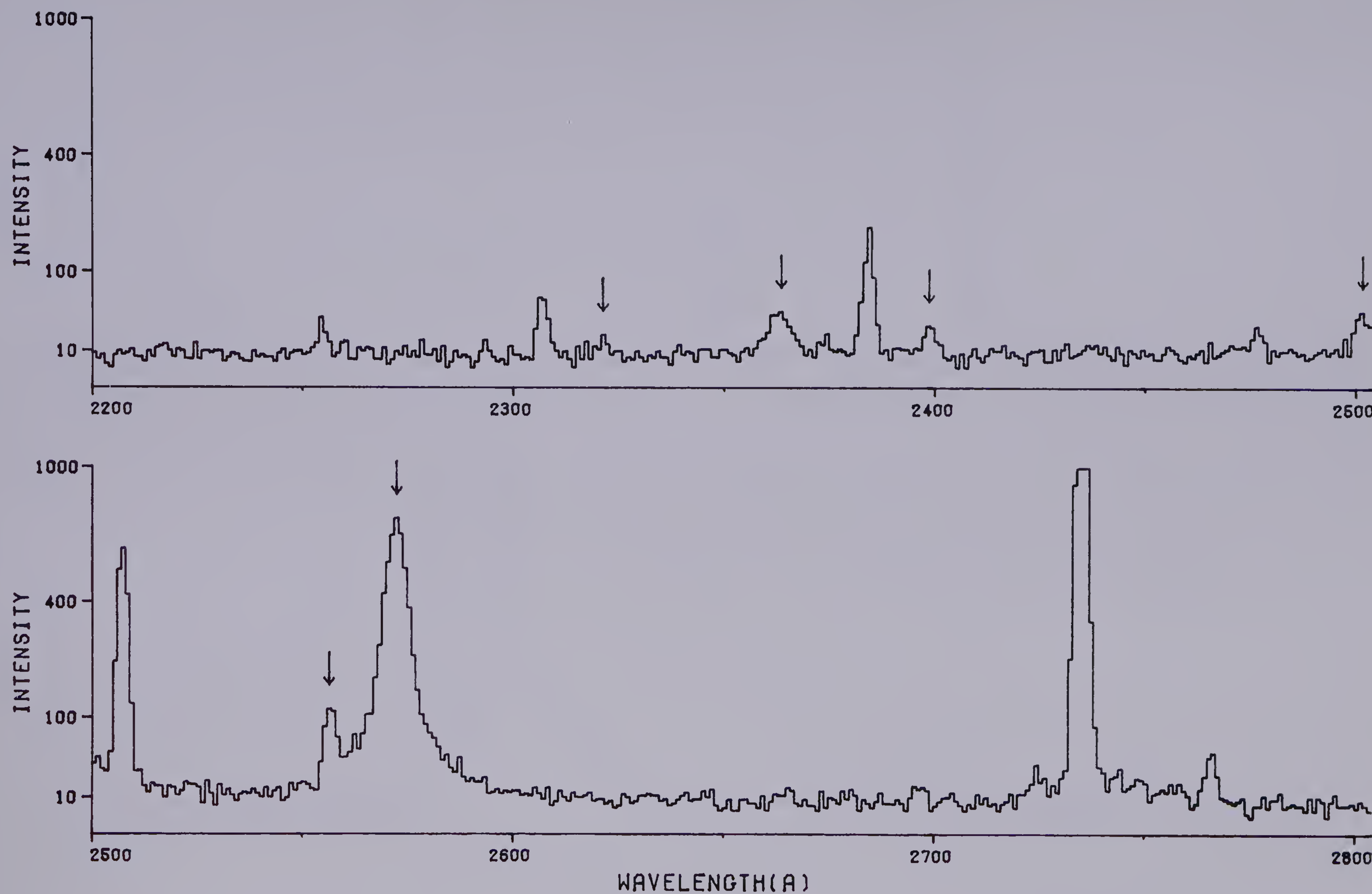

Figure 8a. Helium Spectrum 2200Å-2800Å. Arrows indicate doubly excited state transitions.

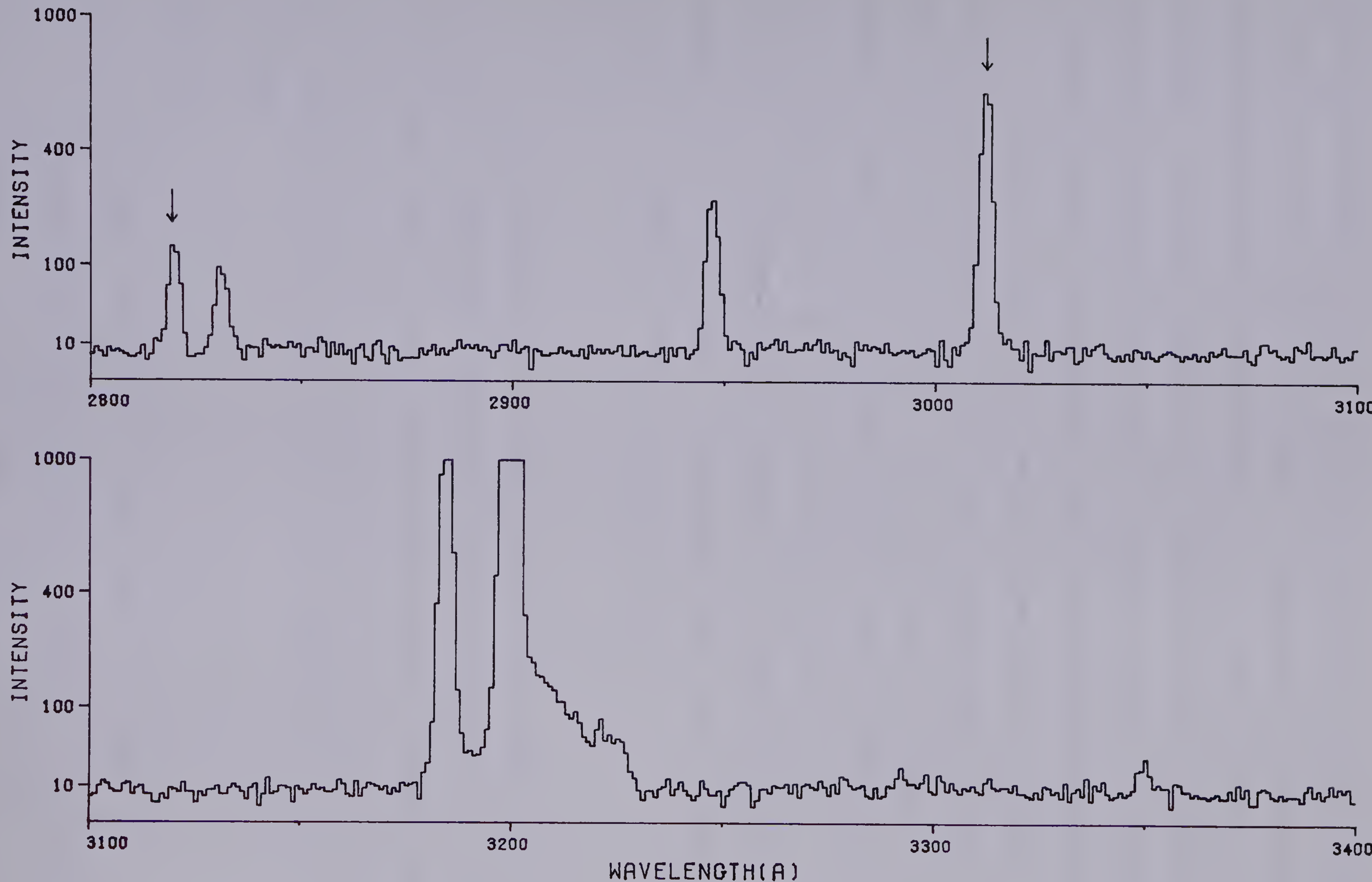

Figure 8b. Helium Spectrum 2800Å-3400Å. See Appendix 2 for experimental conditions.

have been observed within the above spectral region. Five of these are from states forbidden to autoionize by the rules mentioned above and will be referred to as non-autoionizing in what follows. The energy widths of the three permitted to autoionize have been calculated and shown to be narrow, thereby allowing radiative decay to be a competitive if not dominant mode of decay.

Table 1 lists the observed transition wavelengths (air) and the energies of the upper levels after correcting the wavelengths to vacuum. The experimental energies are based on the energies of the 2s2p $^3P°$ level of 470310 ± 50 cm^{-1} (Ma 73) and of the $2p^2$ ^3P level of 481301.5 ± 1.2 cm^{-1} (TW 71).[1] The theoretical values [2] are from two recent papers and the agreement is impressive when one considers that the theoretical values are ab initio.

^3P - $^3D°$

Four transitions of the type $2p^2$ ^3P - 2pnd $^3D°$, for n = 3 to 6, have been observed of which the first two, at 3014 Å and 2562 Å, have been measured using a tilted foil. Only radiative decays are permitted for this sequence, and the lifetime of the 2p3d $^3D°$ has been measured as 0.11±0.01ns (IT 78).

$^3P°$ - ^3P

Only one transition of this type, the 2s2p $^3P°$ -

---

[1]Using a conversion factor of 1.239852(3) 10^{-4}eV/cm^{-1}.

[2]Using 1 au = 27.2116eV; $E(He^{++})$ = 79.0058eV.

TABLE 1

Observed Doubly-Excited Transitions and Energy Levels

Transition (Å)	Designation	Energy of Upper Level (eV)		
			Theory	
		This Exp.	Ca 78	LAC 77
Autoionizing				
2577.7 ± 0.5	$2s2p\ ^3P^o - 2p3p\ ^3D$	63.120(6)	63.125	63.136
2818.0 ± 1.0	$2p^2\ ^3P - 2p3d\ ^3P^o$	64.073(2)	64.076	64.079
2504.4 ± 2.0	$2p^2\ ^3P - 2p4d\ ^3P^o$	64.625(4)	64.624	64.626
Non-autoionizing				
2363.6 ± 2.0	$2s2p\ ^3P^o - 2p3p\ ^3P$	63.556(7)	63.557	63.585
3014.3 ± 1.5	$2p^2\ ^3P - 2p3d\ ^3D^o$	63.787(2)	63.789	63.795
2561.8 ± 1.5	$2p^2\ ^3P - 2p4d\ ^3D^o$	64.513(3)	64.513	64.516
2400.4 ± 2.0	$2p^2\ ^3P - 2p5d\ ^3D^o$	64.838(4)	64.838	64.839
2321.1 ± 2.0	$2p^2\ ^3P - 2p6d\ ^3D^o$	65.014(5)	65.012	65.013

2p3p ^3P at 2364 Å, has been observed and that only weakly. Higher members of this series would have transitions below 2050 Å and would almost certainly be too weak to be seen. Radiative decay is the only mode available to such states.

^3P - $^3P°$

The $^3P°$ energy levels have recently been studied by Lipsky and Conneely (LC 76) who classified them into three types labelled (N,na), (N,nb) and (N,nc). N is the He II threshold below which the state exists. n represents the quantum number of the outer electron and a, b, c designate series of similar line width. The transition $2p^2$ ^3P - 2p3d $^3P°$ at 2818 Å, has its upper state labelled $^3P°(2,3c)$ while the $2p^2$ ^3P - 2p4d $^3P°$ at 2504 Å has its upper state labelled $^3P°(2,4c)$. The c series has the narrowest width being $3.3 \cdot 10^{-6}$eV for (2,3c) and $1.8 \cdot 10^{-6}$eV for (2,4c). The transition observed by Berry, Desesquelles and Dufay (BDD 72) at 3470 Å and labelled by Martin (Ma 73) as $2p^2$ ^3P - 2,3; sp(-) $^3P°$, has its upper state designated as (2,3b) by Lipsky and Conneely. Their width of $4.5 \cdot 10^{-5}$eV corresponds to a very short lifetime of 0.01 ns which might explain why the line is so weak.[1] The next member of the c series, (2,5c), would not likely be observed since the transition at 2504 Å is already extremely weak.

---

[1]Not observed in a spectral scan of that region.

$^3P^\circ$ - ^3D

The strongest doubly-excited state spectral line in the visible or near ultraviolet is from the 2s2p $^3P^\circ$ - 2p3p ^3D transition at 2578 Å. Recently Conneely and Lipsky (CL 78) have included the ^3D terms in their analysis and classify the 2p3p ^3D as (2,3a) ^3D using the same notation as above. Their calculated width of $2.14 \cdot 10^{-4}$eV is much too broad to allow for an observable radiative decay. The width of this level has been calculated by several other authors and a comparison of their results for this level is presented in Table 2. The beam-foil lifetime has been measured as 0.115 ± 0.006ns (IT 76) and 0.14 ± 0.02ns (BDD 72).

TABLE 2

Theoretical Energies and Widths of 2p3p ^3D

Author	Classification	Energy (eV)	Width(Γ) (eV)	Lifetime ($\hbar/\Gamma$ in ns)
COHB 67	^3D 3+	63.141[a]	$1.4 \cdot 10^{-6}$	0.46
AM 67	^3D 3-	63.157[a]	$1.2 \cdot 10^{-5}$	0.05
BT 75	^3D 1	63.120[b]	$2.7 \cdot 10^{-6}$	0.24
LC 78	^3D (2,3a)	63.136	$2.1 \cdot 10^{-4}$	0.003

a. values quoted in eV
b. using the value quoted in Rydbergs

Given the strength of the spectral line at 2578 Å, one might expect to observe a transition from a higher energy level of the same kind. Using the energy levels of Callaway (Ca 78) the next transition (2s2p $^3P°$ - 2p4d ^3D) is predicted at 2081 Å. An experiment, in progress at the time of writing, has unmistakenly identified a transition at that wavelength.

5.3.2 Polarization Results Using Tilted Foil

Only two of the observed doubly-excited state transitions are sufficiently intense to allow a complete sequence of polarization measurements from 0° to 80° foil-tilt angle. The first is the 2s2p $^3P°$ - 2p3p ^3D transition at 2578 Å and the second is the $2p^2$ ^3P - 2p3d $^3D°$ transition at 3014 Å. The results for these transitions are presented in Figure 9.

The first striking feature is that M/I for both transitions is essentially constant with tilt angle but of opposite sign. The 3014 Å transition is the only one in Helium to show a negative value for M/I at 0° foil tilt. In fact it is one of the few non-hydrogenic transitions of any element to show negative M/I for a perpendicular foil.[1]

S/I for both transitions shows the same trend with foil tilt, this being somewhat intermediate between the behavior of the $^1P°$ and ^1D curves of neutral Helium. S/I did obtain a value of nearly -40% at 80° foil tilt for the 2578 Å transition, which is one of the largest polarization fractions ever measured with a tilted foil.

---

[1] One O VIII transition at 36 MeV has shown negative M/I (CHLPB 77). Also see Chapter VI.

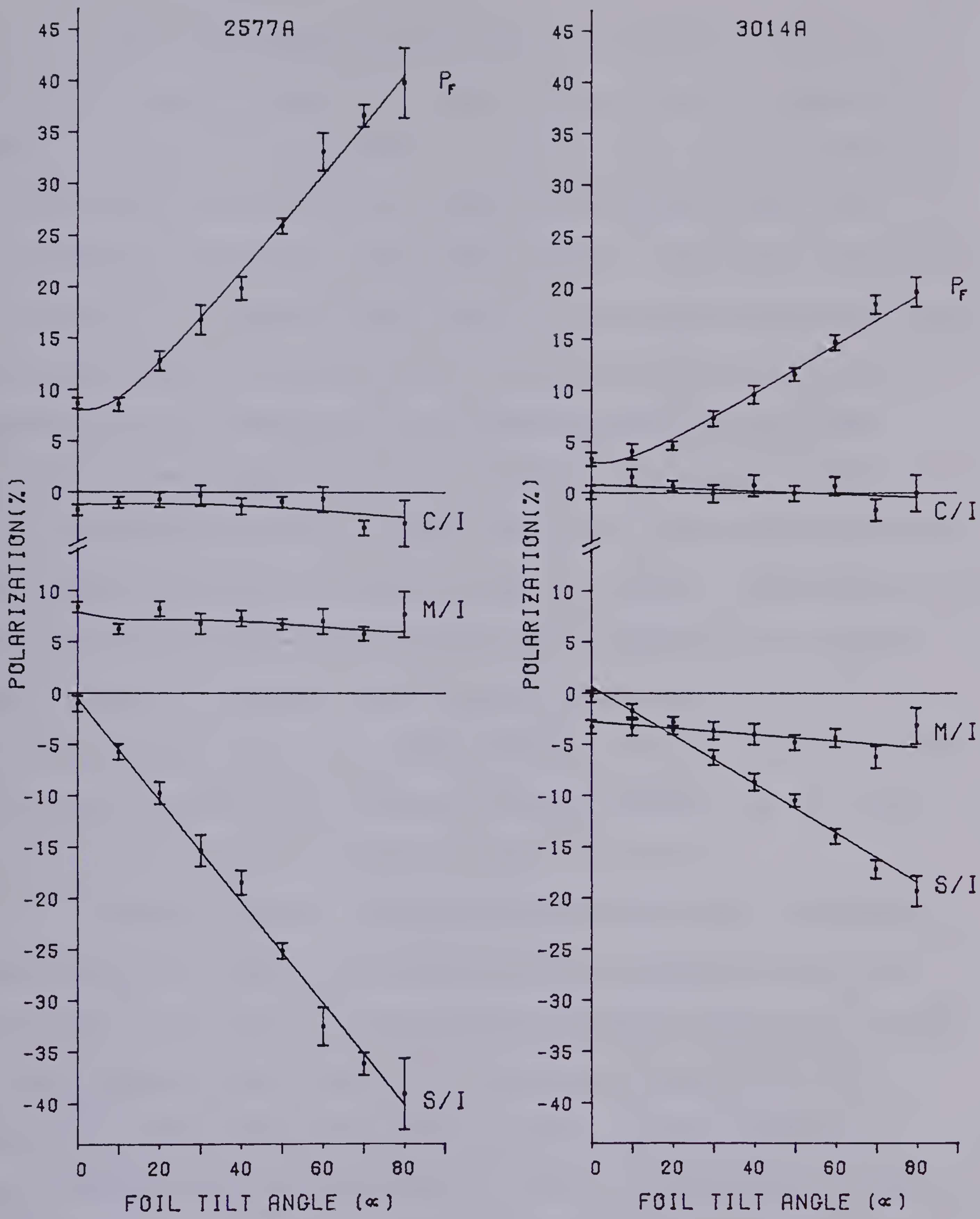

Figure 9. He** Polarization, 2577Å and 3014Å

Two much weaker lines have also been measured at 0°, 20°, 40° and 60° foil tilt. The values appear in Appendix 2. One is the $2p^2\ ^3P - 2p3d\ ^3P°$ at 2818 Å. All of the polarization values at all four tilt angles are quite small and consistent with their value being zero. The other transition is the $2p^2\ ^3P - 2p4d\ ^3D°$ at 2562 Å. The upper state is simply the next higher member of the $^3D°$ which gave rise to 3014 Å transition and might then be expected to yield the same polarization. However, this line is in the wing of the line at 2578 Å which is very broad, and hence some fraction of the observed intensity is coming from that line. The polarization values for 2562 Å at each of the four measured tilt angles may be satisfactorily reproduced by admixing 70% of the 3014 Å values with 30% of the 2578 Å values. Because of this blending problem, the tabulated values should not be taken as the polarization values for this transition.

There are two complications which exist for doubly-excited state transitions which did not exist for Helium singlets. The first is that because these transitions arise from triplet levels there is unresolved fine structure present which causes the polarization to be a function of the distance downstream from the foil. The second is that these transitions arise from such short-lived states that taking a polarization measurement at any position other than that of maximum intensity is simply not possible. With a beam energy of ≃160 KeV and a lifetime of 0.1 ns, the light

intensity drops to 1/e of its value in 0.3 mm which is less than the averaging length (due to slit width) of 0.5 mm. Without knowing the fine structure separation it is impossible to know whether one is measuring some average value for the polarization or some peak value. The difference can be quite significant and will be discussed in a later section when the triplet states of neutral Helium are considered.

Some conclusions can be drawn from the polarization of Helium doubly-excited states which will be further elaborated upon after the Nitrogen measurements have been presented.

1) Not all non-S states of Helium show alignment or orientation with a tilted foil. The transition from the 2p3d $^3P°$ level shows no polarization through 60° foil tilt.
2) S/I can uniformly change in magnitude with foil tilt while M/I remains constant.
3) Identical S, L, and L_f quantum numbers of two different excited states are not sufficient to infer similarity of the polarization of the emission lines from these states. However, if in addition, all of the ℓ_i quantum numbers in the configuration designation are the same, no evidence exists that the polarizations will not be similar.

5.4 Helium Triplets

The behavior of the polarization of the doubly-excited states of Helium with foil tilt angle is markedly different from that of the singlet states. Whether this

difference is caused by their being triplets or by being doubly-excited could be answered in two obvious ways. One could measure either doubly-excited singlet transitions or normal triplet ones. The latter method has been chosen since, in practice, no doubly-excited singlet transitions are of measurable intensity.

Besides their ability to clarify the above point, the neutral Helium triplet transitions contain further information, by virtue of their fine structure, which can be exploited. Thus far it has only been possible to consider the change in polarization with foil-tilt angle. What is of interest are the excitation parameters, σ_q^k, which were treated in detail in Chapter II. Because there are four such parameters, and the relative Stokes parameters constitute three measurements, it is not possible to determine the σ_q^k from a single set of measurements. However, if the Stokes parameters were measured along a quantum beat, several different techniques might be employed to extract all of the excitation parameters.

5.4.1 Polarization of Helium Triplet Transitions

In order to compare the polarization of Helium triplet transitions to that of the singlets, some care must be exercised about the position along the phase at which the measurement is taken. Figure 10 shows the polarization against foil-tilt angle for the 2s ^3S - 3p $^3P°$ transition at 3889 Å and the 2s ^3S - 4p $^3P°$ transition at 3188 Å. The first

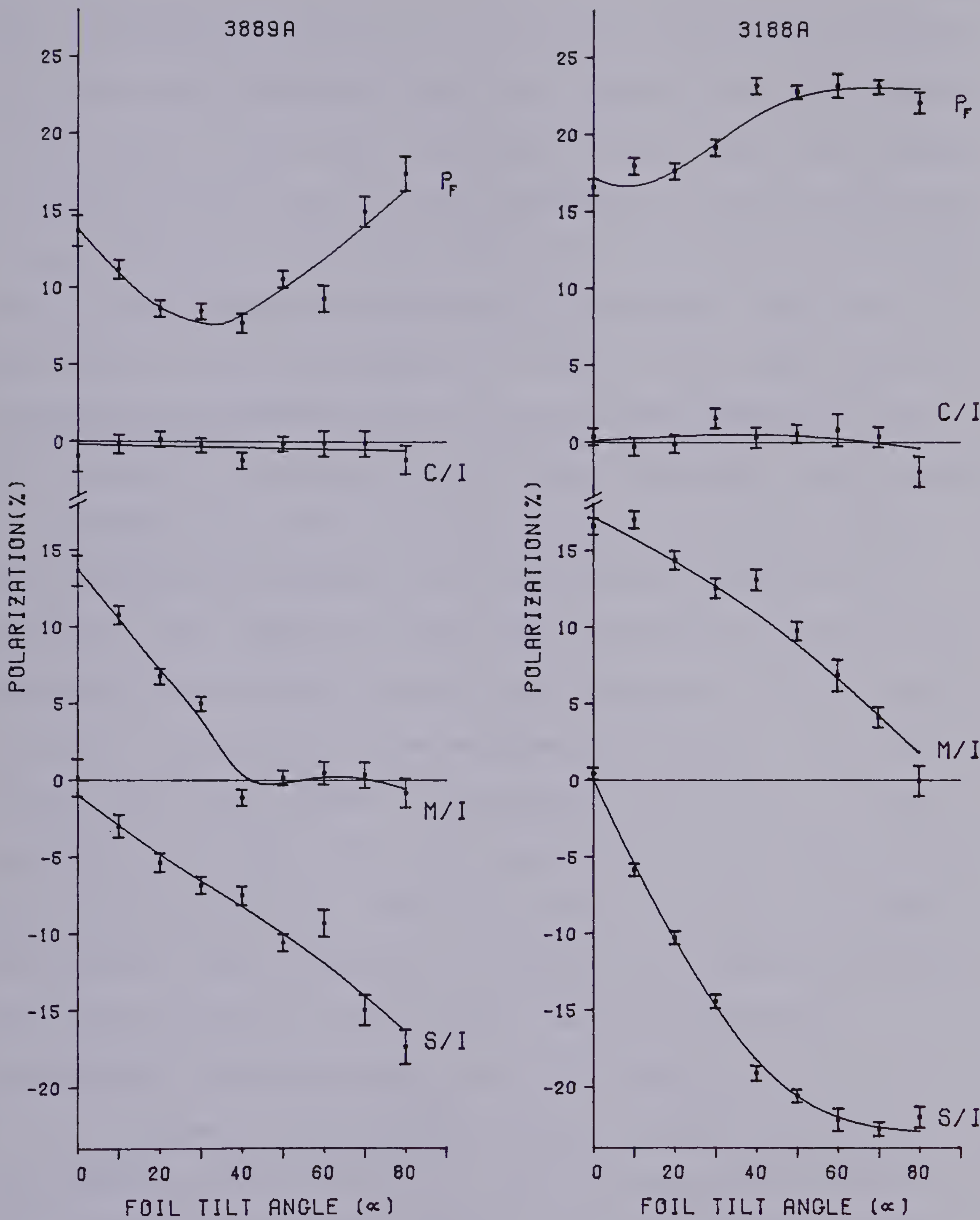

Figure 10. He I Polarization, ^3S - $^3P°$

has a quantum beat length of 4.3 mm (2.8 mm/ns beam velocity; 658.6 MH_z beat frequency) while the second has a beat length of 10.4 mm (269 MH_z beat frequency). The longer beat length of 3188 Å coupled with visual inspection of the beat pattern at each foil-tilt position made it easy to take each measurement at the maximum of the phase of the beat. Such was not the case for the measurements at 3889 Å. Not only were the measurements taken off the beat maximum but the phase from tilt angle to tilt angle was not kept constant. This was not an oversight but rather an overcompensation for an effect which shifts the apparent foil position as the slits are tilted. The axis about which the foil tilts is vertically displaced from the axis about which the slits tilt by about 0.26 mm. The foil must then be moved by 1.26 mm × tan α to observe the same segment of the beam at foil tilt α as was observed at 0° foil tilt. For many polarization measurements the distance from the foil is not critical and is adjusted for maximum light intensity. A pattern of intuitive adjustment had developed which in fact (as was afterwards discovered) overcompensated for this effect.

Figure 11 again shows the polarization at 3188 Å but compares it to the 2s $^3P°$ - 3d ^3D transition at 5876 Å. Clearly the polarization patterns are very similar to the analogous singlet transitions. Most importantly, S/I for the ^3D transition stays very close to zero for foil tilts less than 40°. This feature is independent of the phase at

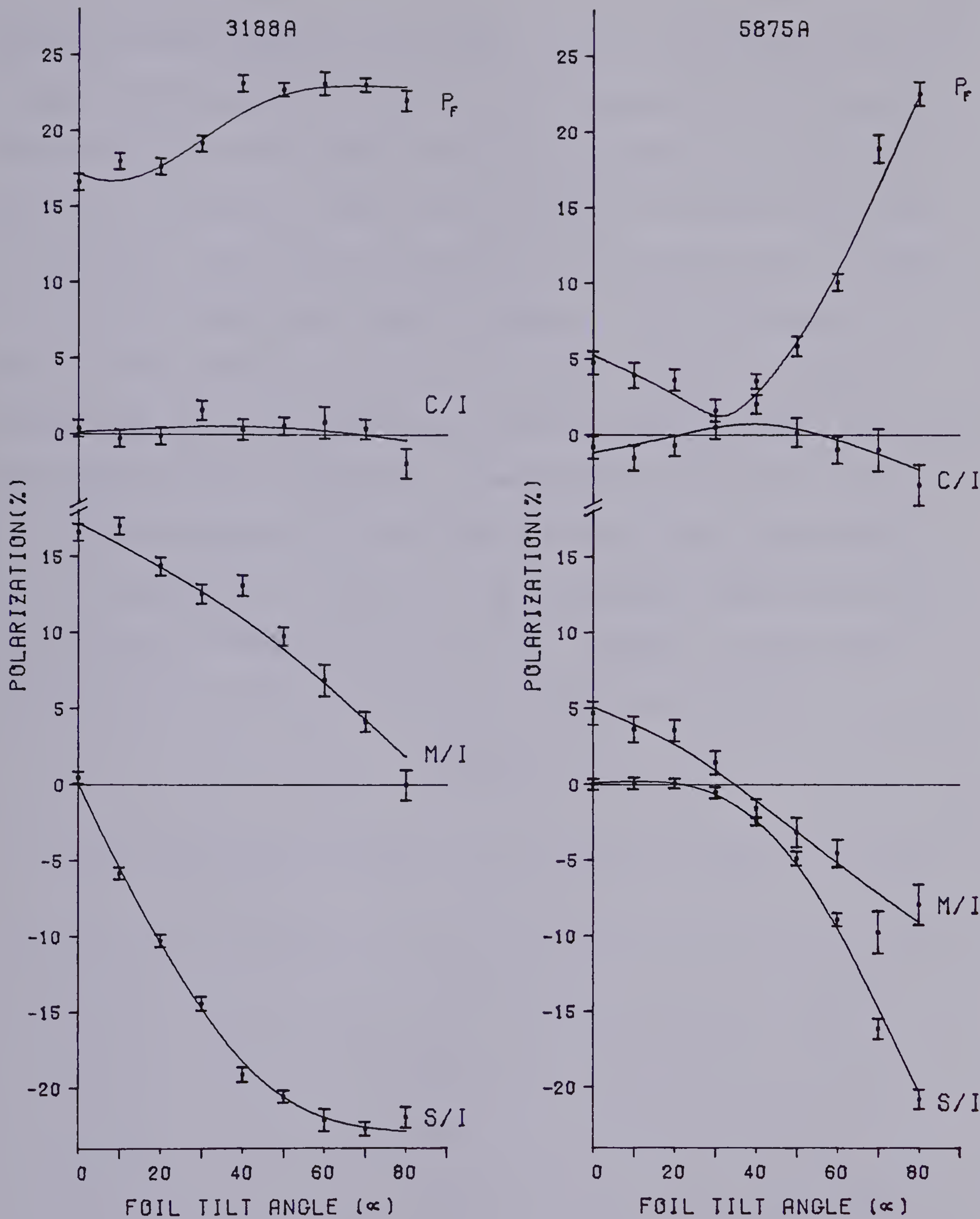

Figure 11. He I Polarization, 3188Å and 5875Å

which the meaurements were taken since, as will be shown in a later section, S/I does not change sign along the phase. The beat length for this transition is about 2.1 mm (1325 MH_z beat frequency) which would make it somewhat difficult to maintain equal phase positions at different tilt angles. In fact the data were taken in exactly the same manner as that for the 3889 Å transition without regard to phase. Unlike the $^3S - {}^3P°$ transitions where position along the phase can dramatically change the polarization, the $^3P° - {}^3D$ transition have polarizations which are not so phase sensitive. This is partially a result of the different fine structure separations between the ^3D and $^3P°$. Table 3 lists these separations for the 3p $^3P°$ and 3d ^3D terms in Helium.

TABLE 3

Fine Structure Intervals of Two Helium Triplet States

J - J'	3p $^3P°$	3d ^3D
1 - 0	8114 MH_z	--
2 - 0	8772	--
2 - 1	658.6	1325 MH_z
3 - 1	--	1401
3 - 2	--	76

The relevant expression for the beat amplitudes, from

Chapter II, is

$$\sum_{JJ'} B(J,J',k)\cos(\omega_{JJ'}t)$$

with $B(J,J',k)$ given by equation (2.24). For the $^3P°$ term both the 1-0 and the 2-0 components in the above sum may be set to zero, since the frequency is sufficiently high that the acceptance length of the spectrometer entrance slit averages over many periods. For the ^3D term all six components (including the $J = J'$ components) in the sum need to be considered. The low frequency (3-2) component may be included with the $J = J'$ components which have no cosine term. The reason is that for distances up to 5 mm from the foil $\cos(\omega_{3-2}t) > 0.99$. The 3-1 component has a coefficient 4/35 as large as the 2-1 component and has not been observed with the beam foil source. Hence this component may be dropped.

The intensity of M light is proportional to $A^2(t)$ while that of S light is proportional to $A^1(t)$. These expressions for each of the transitions take the form:

$$A^1(t)[^3S - {}^3P°] = C_1[^3S - {}^3P°]e^{-\Gamma t}[1 + 5/9\cos(\omega_{21}t)]$$

$$A^1(t)[^3P° - {}^3D] = C_1[^3P° - {}^3D]e^{-\Gamma t}[1 + 1/9\cos(\omega_{21}t)]$$

$$A^2(t)[^3S - {}^3P°] = C_2[^3S - {}^3P°]e^{-\Gamma t}[1 + 9/5\cos(\omega_{21}t)]$$

$$A^2(t)[^3P° - {}^3D] = C_2[^3P° - {}^3D]e^{-\Gamma t}[1 + 35/111\cos(\omega_{21}t)]$$

The constants C_1 and C_2 depend upon the particular

transition but are of no particular interest to this discussion. The beat amplitudes for M light or S light may be read directly from the coefficient of the cosine term of $A^2(t)$ and $A^1(t)$ respectively. Clearly the beat amplitudes of the ^3D transitions are much smaller than those for the $^3P°$. Hence the polarization along the phase will not change for M/I by more than about 25% and for S/I by more than about 12% from the average values for the ^3D transitions. Such error bars would not significantly alter the appearance of the ^3D polarization curves in Figure 11. The case of the $^3P°$ transitions is radically different. For M/I the polarization values vary by 180% from the average values which means that even the sign could be measured incorrectly. (of course these percentages ignore the effect of the denominator in the expression for M/I and S/I, but this is not large since the lead constant dominates that term.)

It is thus possible to understand the differences shown in Figure 10 between the variation of polarization with tilt angle for the transitions at 3889 Å and 3188 Å in terms of a change in phase between one measured point and the next. However, possible future experiments, such as those to be discussed is Section 5.4.3, should include measurements to test whether the differences between the two transitions shown in Figure 10 persist when the phase effects discussed here have been eliminated. The only proper way to perform these measurements for triplet states for which the quantum

beat frequencies are such that they can effect the results significantly is to determine the Stokes parameters as a function of both foil tilt and foil position. The results of such measurements for the 3889 Å and 3188 Å transitions at two tilt angles are discussed in the following section.

5.4.2 Determination of the Excitation Parameters

The Stokes parameters have been measured at 9 points along the phase at both 0° and 60° foil-tilt angles for the 3889 Å transition of He I. They have likewise been measured at 8 points along the phase for the 3188 Å transition. Since both of these transitions are $^3S - {}^3P°$, the equations relating the Stokes parameters to the phase and to the excitation parameters have identical constants and may be written for M/I and S/I as:

$$\frac{M}{I} = \frac{a\ \sigma_M[1 + 9/5\ \cos(\omega t - \phi)]}{1 + a\ \sigma_I[1 + 9/5\ \cos(\omega t - \phi)]} \tag{5.4}$$

$$\frac{S}{I} = \frac{b\ \sigma_1^1[1 + 5/9\ \cos(\omega t - \phi)]}{1 + a\ \sigma_I[1 + 9/5\ \cos(\omega t - \phi)]} \tag{5.5}$$

with

$$\sigma_M = \frac{3\sigma_0^2}{\sqrt{6}} + \sigma_2^2 \tag{5.6}$$

$$\sigma_I = \frac{\sigma_0^2}{\sqrt{6}} - \sigma_2^2 \tag{5.7}$$

$$a = \frac{-5}{12\sqrt{3}} \qquad\qquad b = \frac{\sqrt{3}}{2}$$

With ω fixed to the respective beat frequency, σ_M, σ_I, σ_1^1 and ϕ can be adjusted to yield a minimum in the chi-squared. ϕ would be zero if the foil position were accurately known. For 0° foil tilt, both σ_1^1 and σ_2^2 are zero by cylindrical symmetry so only (5.4) can be used to determine σ_0^2. For 60° foil tilt both (5.4) and (5.5) are applicable and the equations can be fitted together or separately. The fitting routine used in this work employed a non-linear least-squares grid search algorithm by Bevington (Be 69).

One can see from equations (5.4) and (5.5) that the polarization is not so sensitive to σ_I as to the other parameters so long as $|\sigma_I|$ is small enough to avoid a pole. This parameter will then usually have a larger uncertainty than the others. The best determination of all the parameters can be obtained by simultaneously fitting M/I, C/I, and S/I to their theoretical expressions. In practice, the measured values of C/I are too small to yield reliable values of σ_I, so these values have been excluded. The consequence is that $i\sigma_1^2$ (or A_{1+}^{col}) has not been determined but is certainly very small.

Figure 12 shows M/I at 0° and 60° foil tilt and S/I at 60° foil tilt as a function of foil position for the 3889 Å transition of He I. Figure 13 gives the same information for the 3188 Å transition. The smooth curves are plots

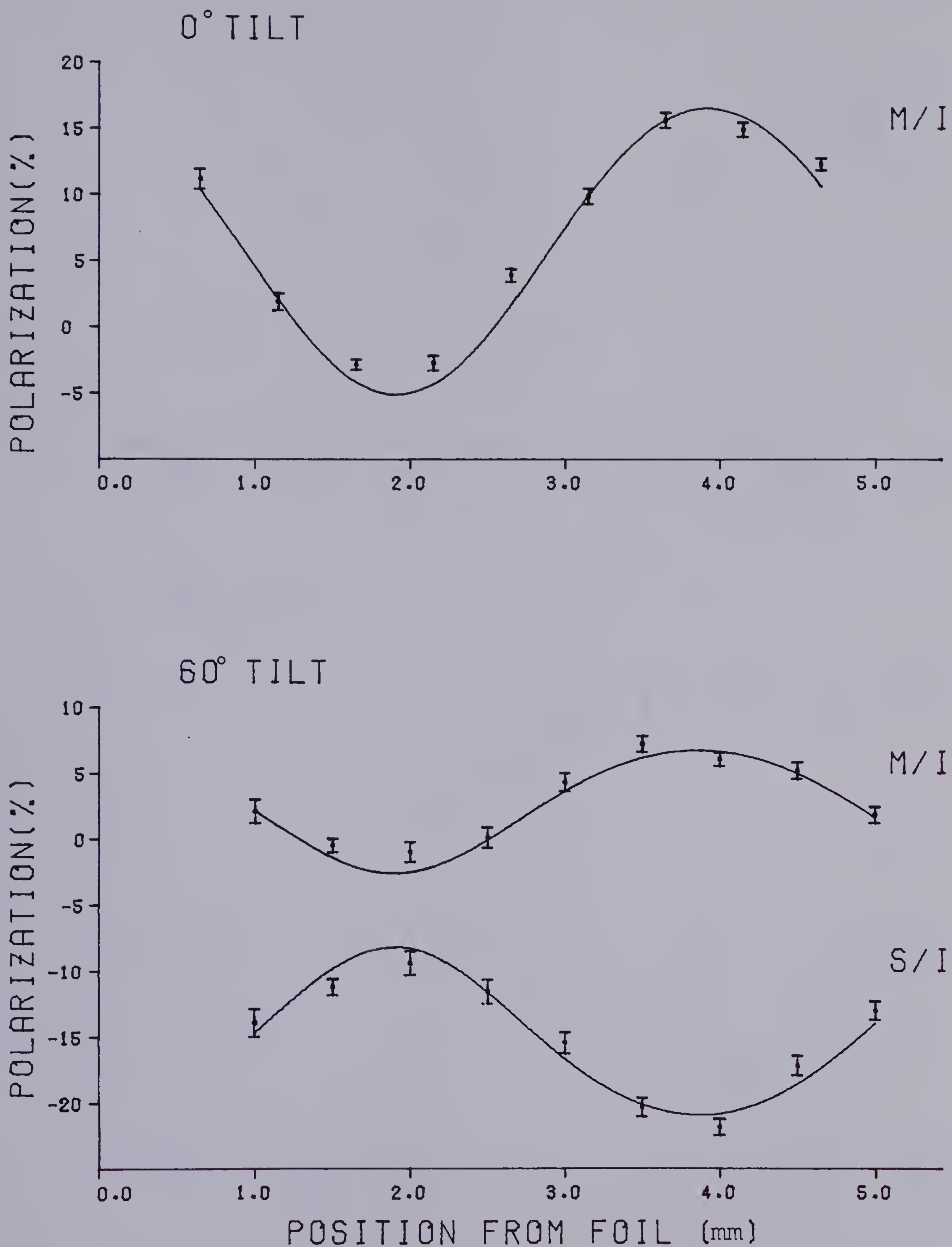

Figure 12. Polarization vs. Foil Position, He I 3889Å

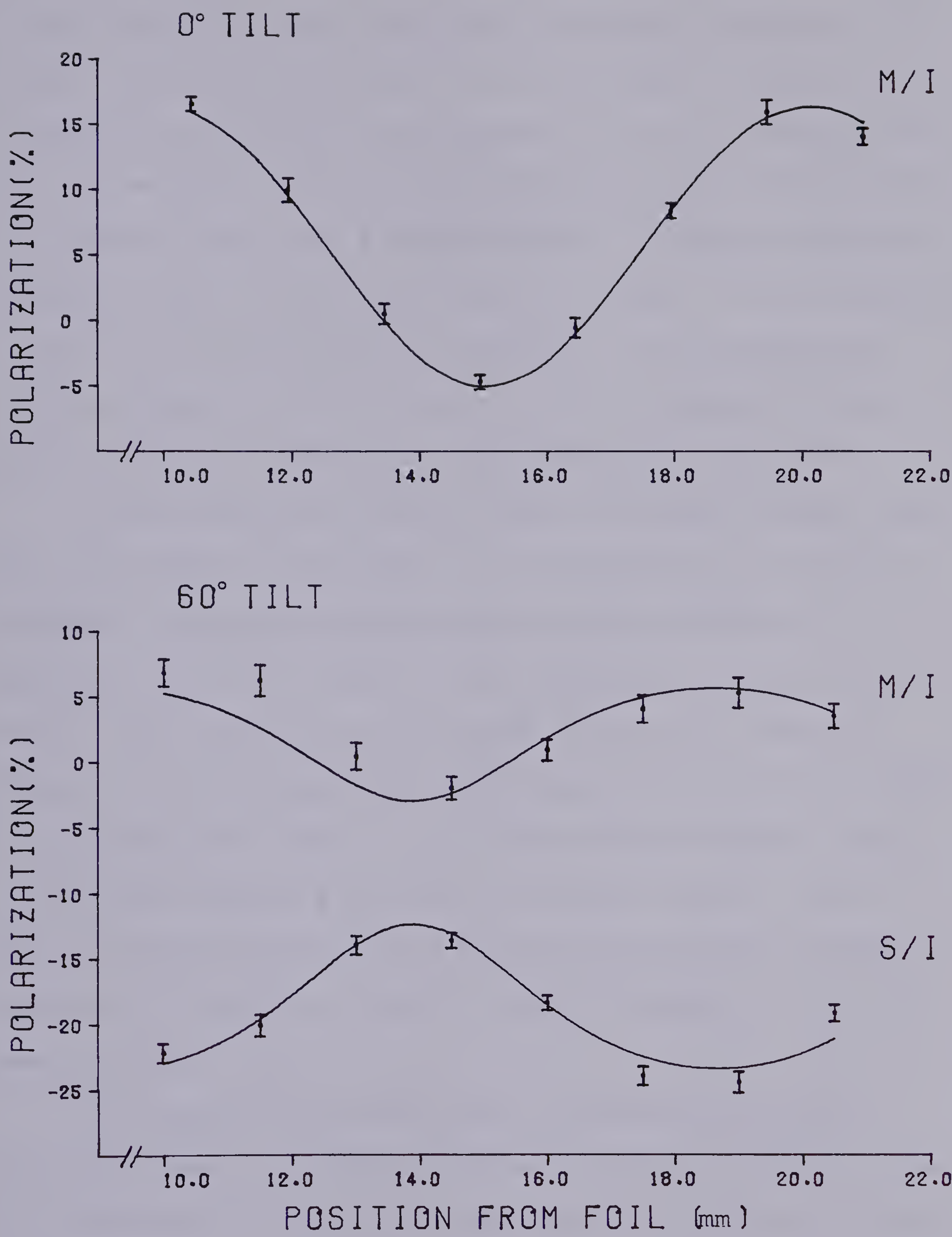

Figure 13. Polarization vs. Foil Position, He I 3188Å

of equations (5.4) and (5.5) The horizontal axis gives distance from the foil in mm. An improvement in the fit can be obtained by allowing the frequency to vary as well as the other parameters. This is not surprising since the data have been acquired over only a single period. The most extreme instance is the 60° foil tilt case of 3188Å. A 23% reduction in the χ^2 can be obtained by increasing the frequency 9%. The phase shifts by 51° yet both σ_M and σ_1^1 change by less than 1%. Even σ_I, the worst case, changes by only 3%.

Since the foil position does not change between data sets, one could use the phase as an indication of the best frequency. Since the quantum beats of the 3889Å He I transition have been used for the accelerator energy calibration, the frequency of the 3188Å transition could be adjusted until the phases of 3188Å agree with those of 3889Å. The parameters for this fit lie intermediate between those of the known frequency and free frequency cases. Table 4 lists the sigma parameters as determined from this method. The curves of Figures 12 and 13 use the parameters for the known frequency case.

No uncertainties have been included with Table 4 since the computer determined uncertainties are smaller than the difference in parameters determined by different fitting procedures. These differences are only significant for σ_I, resulting partly from the form of the equations but more importantly from taking too few data points. Alternate

TABLE 4

Excitation Parameters for Two Helium Triplet Transitions

Transition λ (Å)	Foil Tilt (Deg)	Frequency (MHz)	Phase (Deg)	σ_M	σ_I	σ_0^2	σ_2^2	σ_1^1
3889	0	658.6	-9	-0.26	-0.09[a]	-0.21		
3889	60	658.6	-6	-0.13	-0.39	-0.32	+0.26	-0.19
3889	60[b]	683	+5	-0.13	-0.38	-0.31	+0.25	-0.20
3188	0	269	-9	-0.26	-0.09[a]	-0.21		
3188	60	269	-14	-0.13	-0.82	-0.58	+0.58	-0.27
3188	60[c]	273	-6	-0.13	-0.81	-0.57	+0.57	-0.27
3188	60[b]	293	+37	-0.13	-0.79	-0.57	+0.56	-0.27

a. not a free parameter

b. frequency a free parameter

c. phase chosen to match 3889 Å

methods for taking data and analyzing it will be considered in the following section.

It is worth drawing attention to the peak M/I values in Figure 12, viz. 0.16 at 0° tilt and 0.07 at 60° tilt, and in Figure 13 viz. 0.17 at 0° tilt and 0.07 at 60°, while the corresponding S/I values at 60° are -0.22 and -0.24 respectively. The excellent consistency between these values strongly supports the suggestion made in Section 5.4.1 that the disagreement between the curves shown in Figure 10 was due to phase shift from one measured point to another in the 3889 Å data and that, in reality, the polarization versus foil tilt trends for the transitions at 3889 Å and 3188 Å are very similar.

The only other experiment performed on Helium using a tilted foil which has determined the Fano-Macek (F-M) alignment and orientation parameters was recently reported by Burns, Hight and Greene (BHG 79). Using a technique to be described below, they have measured these parameters for the 3889 Å transition at each foil-tilt angle from 0° to 75° in 5° increments. The conversions between the F-M parameters and the sigma parameters for a ^3S - $^3P°$ transition are given by:

$$A_0^{col} = \sigma_0^2/\sqrt{2} \qquad A_{2+}^{col} = -\sigma_2^2/\sqrt{3}$$

$$A_{1+}^{col} = i\sigma_1^2/\sqrt{3} \qquad O_{1-}^{col} = \sigma_1^1/\sqrt{3} \ . \tag{5.8}$$

Table 5 compares the results for the 3889 Å transition in He I. It is difficult to attribute the disagreement at 60° foil tilt to any one cause. The most striking discrepancy between the Burns et al. results and other results is a maximum in S/I versus foil tilt at about 45°. Certainly the Helium singlets do not show a maximum and neither do the triplets at 3188 Å or 5876 Å (Figure 11). The A_0^{col} and A_{2+}^{col} parameters of Burns et al. predict a zero beat amplitude in the M/I light at 60° foil tilt while this experiment clearly demonstrates a non-zero value (Figure 12).

TABLE 5

Alignment and Orientation for He I 3889 Å

Experiment	Foil Tilt	A_0^{col}	A_{2+}^{col}	O_{1-}^{col}
BHG 79	0°	-0.15		
This Work	0°	-0.15		
BHG 79	60°	-0.055	-0.056	-0.052[a]
This Work	60°	-0.23	-0.15	-0.11

a. sign changed to compensate coordinate frame

It should be stressed that whereas the disagreement in the alignment-orientation parameters seems large, the disagreement in the predicted polarization values, which are the measurable parameters, are not nearly so large. For

example if one assumes that the excitation parameters are the same for triplets as for singlets, the polarization of the singlets could be predicted using the equations of Chapter II. The Burns et al. values for A_0^{col} and A_{2+}^{col} predict M/I values for the singlets that are in good agreement with the curves of Figure 5. (Not so, however, for S/I evaluated from O_{1-}^{col}.) By contrast our measured values at 0° and 60° for the 3188 Å transition agree well with the 3188 Å curve of Figure 10. The amount by which the $^1P°$ curves of Figure 5 differ from the 4p $^3P°$ curve of Figure 10 is thus an indication of the discrepancy between the Burns et al. triplet experiment and the results presented here.

Such comparisons are qualitative and based on too few measurements to be particularly meaningful. What has become clear is that straightforward application of equations (5.4) and (5.5) is not the best method for evaluating the excitation parameters since the laboratory time required to use the procedure adopted in this section at 10° foil-tilt intervals from 0° to 80° becomes prohibitive if the necessary additional data points at each tilt angle were acquired. Some ideas on how such measurements might be taken and how they have been taken elsewhere will be discussed in the following section.

5.4.3 Alternative Methods for Measuring Excitation Parameters

One of the problems with the method of the previous section was that σ_I was not accurately determined. If the

Stokes parameters were measured at different positions downstream from the foil quickly enough to complete 30 or 40 points on one foil with identical normalization at each point, the individual I, M, C and S values might be used rather than the normalized values, M/I, C/I and S/I. Such a measurement sequence would demand that only 4 or 5 retarder positions be used at each foil position so that an entire run could be completed in less than one hour. Several such runs could be separately analyzed with the final values resulting from the mean. The entire procedure would then be repeated for each foil-tilt angle of interest.

Two combinations of I and M eliminate σ_2^2 and σ_0^2 respectively. From equations (2.29) and (2.30) one can find that

$$I + M = \frac{A^0(t)}{\sqrt{3}} - \frac{2\,\sigma_0^2\, A^2(t)}{\sqrt{6}} \tag{5.9}$$

$$I - \frac{M}{3} = \frac{A^0(t)}{\sqrt{3}} + \frac{2}{3}\,\sigma_2^2\, A^2(t) \ . \tag{5.10}$$

Considering the first of these equations, the values for $A^0(t)$ and $A^2(t)$ may be substituted for a ^3S - $^3P°$ transition in Helium to yield:

$$I + M = \frac{Ce^{-\Gamma t}}{9}\left[1 + \frac{5\ \sigma_0^2}{9\sqrt{2}} - \frac{\sigma_0^2}{\sqrt{2}}\cos(\omega t)\right].$$

If the data were fitted to a function of the form,

$$I + M = Ce^{-\Gamma t}[1 + B_0 \cos(\omega t - \phi)] \tag{5.11}$$

one could solve for σ_0^2 in terms of B_0. The result is

$$\sigma_0^2 = \frac{-\sqrt{2}\, B_0}{(1 - 5/9\, B_0)} \quad . \tag{5.12}$$

The introduction of the phase factor, ϕ, is solely to account for uncertainty in the foil position and should be carefully monitored so that a 180° phase shift does not occur. Using this technique, the quantum beat amplitude directly yields the excitation parameter, σ_0^2, independent of normalization factors. This idea was first put forward by Burns, Hight and Greene (BHG 79) in a slightly modified form to be considered below.

σ_2^2 may be treated in an exactly analogous fashion using equation (5.10). Calling its beat amplitude, B_1, one obtains

$$\sigma_2^2 = \frac{+\sqrt{3}\, B_1}{(1 - 5/9\, B_1)} \tag{5.13}$$

The situation for σ_1^1 or $i\sigma_1^2$ is not so clean, being complicated by the appearance of both σ_0^2 and σ_2^2. Considering the case of circularly polarized light, the relevant expression from Chapter II is:

$$I + S = \frac{A^0(t)}{\sqrt{3}} - \frac{\sigma_I}{2} A^2(t) - \sigma_1^1 A^1(t).$$

Here σ_I is defined by equation (5.7). It is to be treated as a known parameter. After substituting for A^0, A^1 and A^2, this becomes

$$I + S = \frac{Ce^{-\Gamma t}}{9} [1 - \frac{5\sqrt{3}}{36} \sigma_I + \frac{\sqrt{3}}{2} \sigma_1^1 + \frac{\sqrt{3}}{2}(\frac{5}{9} \sigma_1^1 \frac{-\sigma_I}{2}) \cos(\omega t)].$$

Again fitting this equation to one of the form of (5.11),

$$I + S = C_2 e^{-\Gamma t}[1 + B_2 \cos(\omega t - \phi)],$$

yields the following expression for σ_1^1:

$$\sigma_1^1 = \frac{\sqrt{3}\ B_2 + (3/4)\ \sigma_I (1 - 5/9\ B_2)}{5/6 (1 - 9/5\ B_2)} . \tag{5.14}$$

Finally, for completeness, with B_3 as the beat amplitude for I + C, one can derive:

$$i\sigma_1^2 = \frac{-\sqrt{3}\ B_3 - (3/4)\ \sigma_I\ (1-5/9\ B_3)}{3/2\ (1 - 5/9\ B_3)} .$$

The beat amplitudes appearing in all of the expressions like equation (5.11) need to be corrected for the finite averaging length imposed by the geometry of the detection system. Only if this averaging length were less than about 1/10 of a beat length could it be ignored. The matter of determining a proper beat amplitude after compensating

for a finite averaging length, has been treated by the author elsewhere (Br 75).

It is interesting to note that the single parameters M, C and S cannot be used to determine the excitation parameters. For example,

$$S = \frac{Ce^{-\Gamma t}}{3\sqrt{3}}\, \sigma_1^1 [1 + 5/9 \cos(\omega t)]$$

and the beat amplitude is 5/9 independent of σ_1^1 and therefore independent of foil tilt. This consequence was checked by Burns et al. (BHG 79) and they found excellent agreement with their measurement.

An alternative method for determining the excitation parameters, and the one employed by Burns et al. in their experiment, is to note that a single configuration of a polarimeter always yields I plus some combination of M, C and S. A horizontally oriented plane polarizer without a retarder passes ½[I + M] so the analysis following equation (5.9) carries through unchanged. Similarly a polarizer oriented at 45° to the reference axis passes ½[I + C] and if a retarder is first inserted the system passes ½[I + S]. No combination can pass C[I - M/3] with C any constant. But this is no significiant drawback since the derivation performed above can be altered for any polarimeter configuration so that ½[I - M], the combination passed by a polarizer aligned vertically, can be used as the fourth measurement.

This technique has one clear advantage over the one suggested at the beginning of this section. Data can be acquired as a function of foil position without changing the polarimeter configuration thereby allowing a single run to be performed in much less time, alleviating the problem of foil breakage and improving the efficiency of data collection. Any time spent in rotating a retarder, for instance, is time when data are not being collected and can significantly reduce the duty cycle. The disadvantage is that the data can be analyzed only by the procedure presented in this section. That is, the Stokes parameters cannot be determined since the various scans would have been acquired with different foils and no normalization is sensitive enough to guarantee that I is identical for every scan. If the Stokes parameters were acquired, as suggested previously, then not only could this method be used but the method of Section 5.4.2 could also be applied and any disagreement between the two might be indicative of systematic errors.

CHAPTER VI

POLARIZATION OF NITROGEN

Nitrogen is an easy element to accelerate and offers a large number of spectral lines in the visible and near ultraviolet. It was the subject of many early beam-foil investigations, culminating in the thorough study by Desesquelles[1] which included both the classification of spectral lines and the determination of mean lives. The region above 2000 Å has recently been reexamined for some N II and N III transitions (BCOWPM 78).

The intent of this work was to perform a survey of the polarization of as many spectral lines as possible at both 0° and 60° foil tilt. Large polarization fractions may prove to be a useful tool for cascade-free mean-life measurements or for spectral identification. Since orientation is possible only with a tilted foil, the only method at present for determining whether or not significant polarization fractions might in general be expected is to measure as large a sample as possible. A second motivation was the possibility of measuring the polarization from transitions analogous to the Helium doubly-excited states. Such transitions exist in N II by considering the closed 1s and 2s shells as having no effect on the polarization.

[1] Ph.D Dissertation; De 71.

All of the Nitrogen data were taken using an N^+ beam at 260 KeV. At this energy only N II and N III transitions have measurable intensities. The spectra appear in Figure 14. While every sufficiently intense line was considered a candidate for this experiment, many had to be excluded because of line blending. The measurements utilized 500 micron slits which yield a line width of about 6 Å at 0° tilt and 10 Å at 60° tilt. The consequence is that the fine structure is only partially resolved, which significantly complicates the interpretation of the results. This matter will be considered in some detail in Section 6.2.1

The polarization was measured for 15 transitions in N II and 5 transitions in N III. The results are presented in Table 6 which lists the transitions by the multiplet designations and notes the wavelength of the strongest line of the multiplet. The values have been taken from Striganov and Sventitskii (SS 68) (corrected for typographical errors).

The transitions which have been included in Table 6 are not entirely free of blends. The listed transition should, however, account for over 80% of the intensity based on careful consideration of the spectrum or acquisition of a higher resolution spectrum. Of particular note are the transitions of N II at 4530 Å, which is blended with a N III line, and at 5001 Å which is blended with both a 3s ^{5}p - 3p ^{5}P° and a 3s ^{3}P° - 3p ^{3}S transition in N II.

Polarization measurements of Nitrogen are complicated

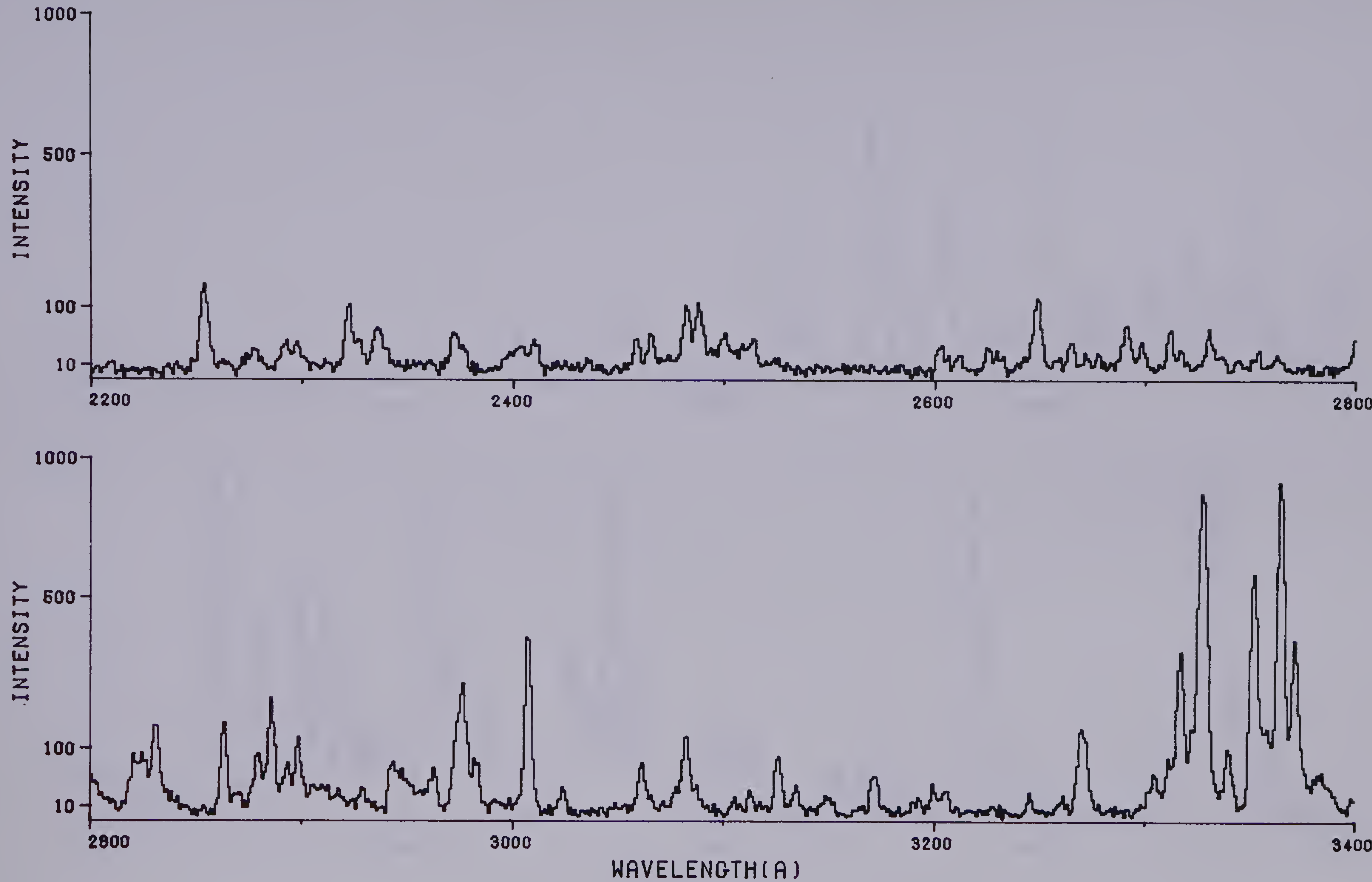

Figure 14a. Nitrogen Spectrum 2200Å-3400Å. See Appendix 2 for experimental conditions.

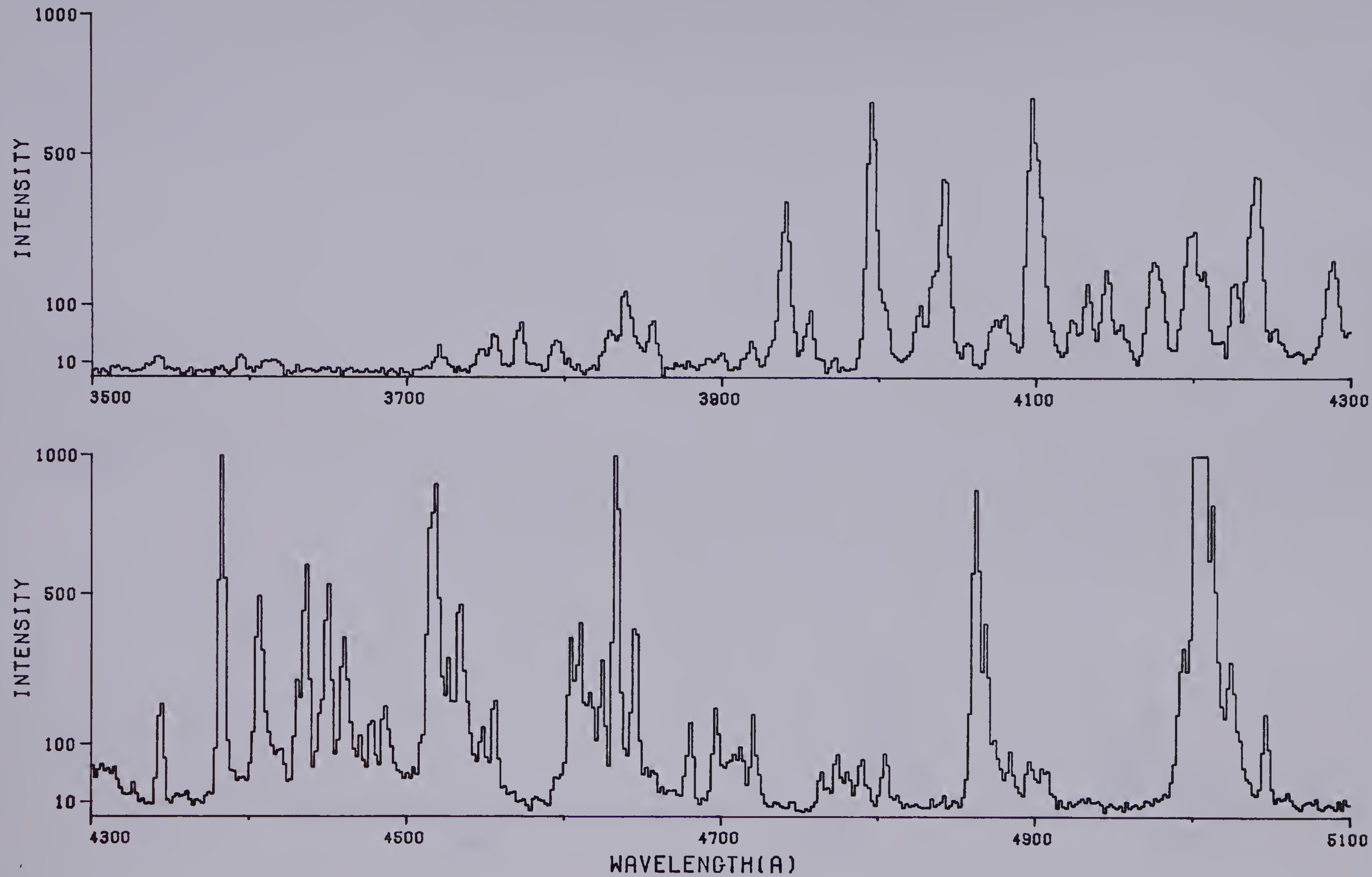

Figure 14b. Nitrogen Spectrum 3500Å-5100Å.

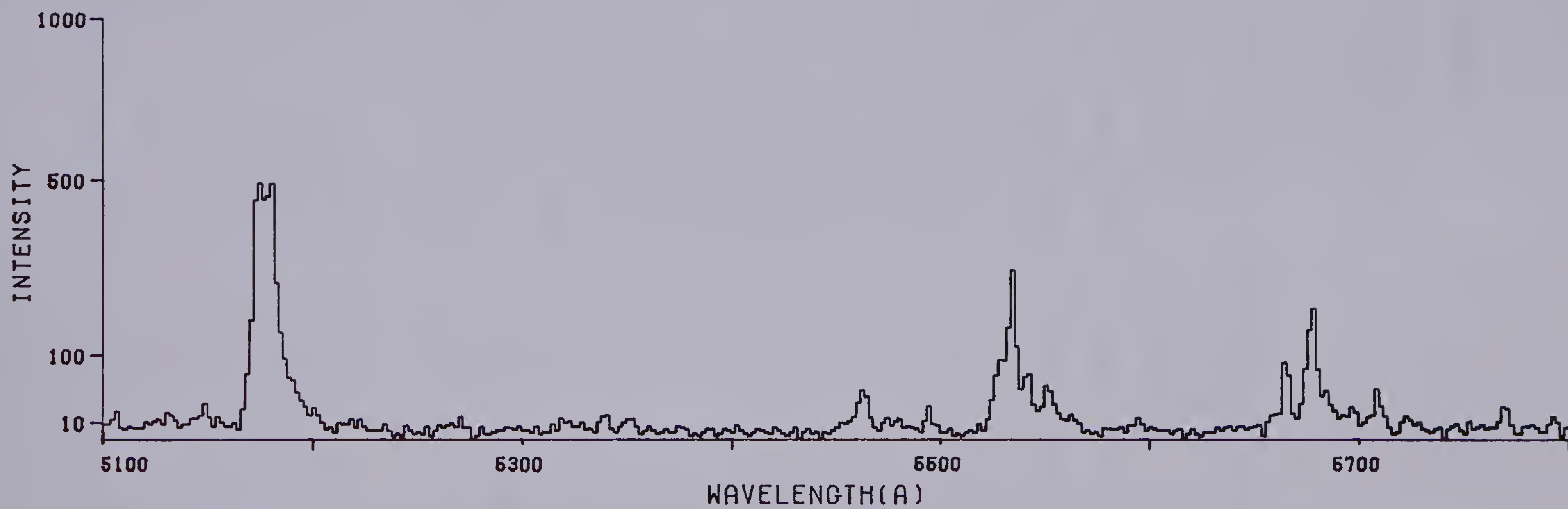

Figure 14c. Nitrogen Spectrum 5100Å-5800Å.

TABLE 6

Nitrogen Polarization

(a) N II

λ(Å)	Desig.	0°	60°		
		M/I(%)	M/I(%)	C/I(%)[a]	S/I(%)
5680	$3s\ ^3P° - 3p\ ^3D$	2.6 ± 0.9	4.0 ± 0.8	-1.8	-11.3 ± 0.4
5535	$3s\ ^5P - 3p\ ^5D°$	6.0 ± 1.3	4.5 ± 0.9	-1.2	-10.1 ± 0.5
5045	$3s\ ^3P° - 3p\ ^3S$	-3.1 ± 2.8	2.4 ± 1.2	0.0	0.2 ± 0.8
5001	$3p\ ^3D - 3d\ ^3F°$	5.8 ± 0.6	5.7 ± 0.6	-2.7	-19.0 ± 1.0
4803	$3p\ ^3D - 3d\ ^3D°$	-6.3 ± 1.0	-4.1 ± 1.4	-2.4	- 6.3 ± 1.0
4631	$3s\ ^3P° - 3p\ ^3P$	0.4 ± 0.6	1.2 ± 0.7	-1.0	- 3.0 ± 0.5
4530	$3d\ ^1F° - 4f\ G\ (9/2)$	1.8 ± 1.0	-1.9 ± 2.0	-1.3	- 9.3 ± 1.4
4447	$3p\ ^1P - 3d\ ^1D°$	7.1 ± 0.9	7.4 ± 1.8	-3.0	-19.3 ± 1.6
4403	?	6.2 ± 1.8	4.2 ± 0.9	-1.6	-16.0 ± 0.7
4433	$3d\ ^3P° - 4f\ D\ (5/2)$	2.3 ± 0.9	0.9 ± 1.9	-2.7	- 3.1 ± 1.6
4242	$3d\ ^3D° - 4f\ F\ (7/2)$	4.4 ± 0.7	2.0 ± 0.6	-2.3	- 7.8 ± 0.5
4146	$3s\ ^5P - 3p\ ^5S°$	-0.3 ± 0.9	0.5 ± 0.6	0.0	- 0.9 ± 0.6
3995	$3s\ ^1P° - 3p\ ^1D$	4.2 ± 0.7	2.9 ± 0.6	-2.5	-11.9 ± 0.7
3329	$3p\ ^3D - 4s\ ^3P°$	-1.0 ± 0.8	-1.1 ± 1.1	0.4	3.5 ± 0.7
3007	$3p\ ^1P - 4s\ ^1P°$	4.7 ± 1.0	-0.3 ± 1.1	-0.5	- 3.7 ± 0.9
(b) N III					
4861	$3p\ ^4D - 3d\ ^4F°$	-0.9 ± 1.1	5.2 ± 1.4	-4.3	-13.2 ± 0.9
4515	$3s\ ^4P° - 3p\ ^4D$	1.4 ± 0.6	2.8 ± 2.4	-1.9	-10.3 ± 1.7
4379	$4f\ ^2F° - 5g\ ^2G$	3.9 ± 0.7	1.3 ± 1.3	-4.3	-14.1 ± 1.1
4097	$3s\ ^2S - 3p\ ^2P°$	2.2 ± 0.9	0.0 ± 0.8	-0.5	- 8.2 ± 0.8
3367	$3s\ ^4P° - 3p\ ^4P$	-0.5 ± 1.4	-0.5 ± 1.1	-0.5	- 1.8 ± 0.7

a. uncertainties same as M/I

by the possibility of unresolved hyperfine structure caused by the angular momentum of the nucleus ($I = 1$). Hyperfine-structure quantum beats have been measured in both N IV and N III.[1] In one experiment (BCES 75) a tilted foil was used which permitted the observation of the $F = 1$ to $F = 0$ interval which cannot be observed using a perpendicular foil.

Most of the discussion in this chapter will be concerned with the measurements of transitions in N II, and there are two reasons to suspect that any unresolved hyperfine structure will not be significant. The first is that the Fermi contact term contributes about 20% to 50% toward the energy separation of the intervals. This term is non-zero only for unpaired s-electrons and only one N II transition in Table 6 ($2s2p^2\,3s\,^5P - 2s2p^2\,3p\,^5D°$), with an upper term having $L \neq 0$, has such an electron. The second reason is that the remaining interactions scale as $\langle 1/r^3 \rangle$, which decreases as the ion charge becomes less positive. Reasonable estimates based upon an extrapolated value for the hyperfine structure constant indicate that frequencies in N II would be too low to be measurable and hence may be ignored.

About half of all the transitions in Table 6 having an upper term that is not $L = 0$ gave S/I values at 60° foil tilt between 10% and 20%. No transition gave an M/I (or C/I) larger than 8% and fewer than half had values larger than 5%. This demonstrates that production of significant orientation

---

[1] BCES 75, SDG 75 and SCDD 76.

is a general feature of beam-tilted-foil excitation and not one restricted to simple elements such as Helium.

The remainder of this chapter will discuss certain aspects of Table 6 in detail and show that at least some of the more prominent features can be explained by the theory of Chapter II.

6.1 N III Results

The first two transitions for N III listed in Table 6 are the ones whose hyperfine structure have been measured using the quantum-beat technique (SCDD 76). The measurements were taken with a perpendicular foil but the polarization values for 0° tilt for these lines are so low that one would not expect the quantum beats to be observable. In fact a quantum beat measurement was performed during this project on the N III 4861 Å transition and no beats with an amplitude greater than 0.8% were observed. The resolution of this apparent inconsistency is offered by the beam energy which for previous workers was 2 MeV while for this experiment was 250 KeV. Alignment has been shown to have a strong energy dependency so it is not surprising for us to measure such a small value at this energy. The S/I value at 60° was found to be -13.2%, suggesting that it would be interesting to perform a quantum-beat measurement at 60° foil tilt.

Two transitions in N III, with measurable intensities, occur between states with closed 1s and 2s shells. These are 4f $^2F°$ - 5g ^2G at 4379 Å and 3s ^2S -3p $^2P°$ at 4097 Å. Both

of these are analogous to the singly-excited states of Helium in that a single electron determines the orbital angular momentum. Figure 15 presents the polarization of these lines as a function of foil tilt.

Though only four points were taken for the 4097 Å transition, two features clearly emerge. The first is that M/I is very small for all tilt angles and the second is that the shape of the S/I curve is similar to the $^1S - ^1P°$ transitions in Helium though the magnitude is about half as large.

The $^2F° - ^2G$ results look as though they may be slightly perturbed by unresolved hyperfine structure. (The fine structure for this transition is the smallest of all the measured Nitrogen lines, $\simeq 0.2$ cm^{-1}, but this should still be too wide to affect the measurements seriously.) Again there is no pronounced change in M/I, unlike the Helium singlets. S/I, like the doubly-excited Helium states, appears intermediate to the $^1S - ^1P°$ results and those of $^1P° - ^1D$.

6.2 N II Results

Two of the prominent features of Table 6 are the two transitions which show polarization of opposite sign to the others in the same column. One is the positive S/I value of 3329 Å and the other is the negative M/I value of 4803 Å (other negative M/I values are within 2 standard deviations of zero). This latter transition is analogous to the Helium doubly-excited state transition at 3014 Å in that the upper term is also a 2p3d $^3D°$, and also showed a negative M/I value.

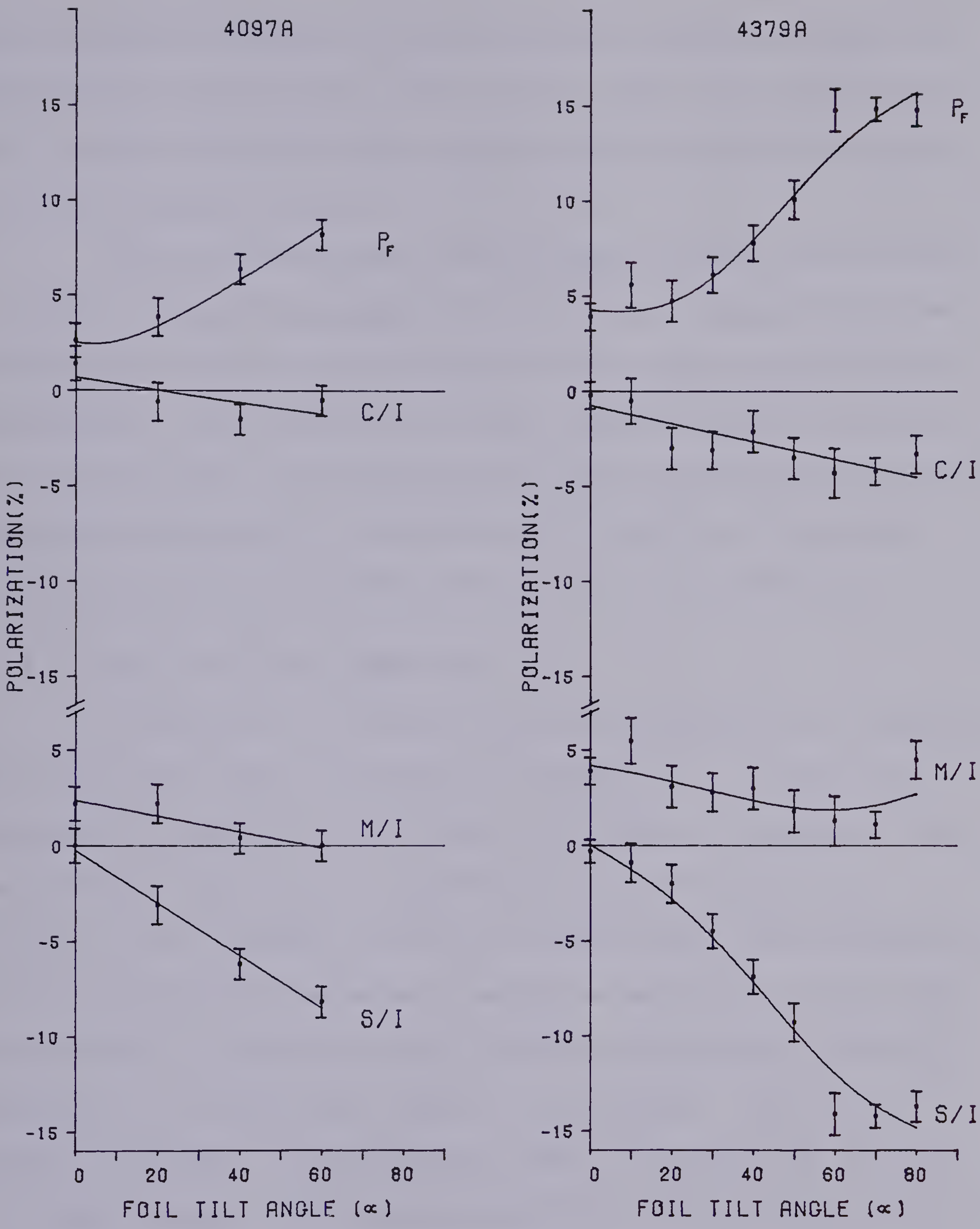

Figure 15. N III Polarization, 4097Å and 4379Å

The results of Chapter II will be used to explain these two features in the Nitrogen table and to show that the negative M/I value in Nitrogen does not arise from an alignment parameter of opposite sign.

There are two upper S terms in Table 6 which show no polarization. These will be examined in some detail and will be shown to strongly indicate the validity of spin-independence for this experiment. The consequence of spin-independence will be tested by examining six transitions whose upper terms appear as both singlets and triplets. But first the question of partial resolution of the fine structure needs to be examined.

6.2.1 Fine Structure Resolution

Polarization formulae for both unresolved and resolved fine structure were presented in Chapter II. It would be possible to derive an expression for partially resolved fine structure, valid for LS-coupling and incorporating the relevant line strength factors, but its application would not be straightforward because it would be necessary to know the instrumental lineshape before relative intensities could be assigned to neighboring lines of a multiplet. The instrumental lineshape is problematic since it depends on how well the spectrometer had been refocused for a moving light source (SL 73). The Spex spectrometer did have provision to make this adjustment but, in practice, it is difficult to make and furthermore this adjustment would be different at each wavelength. The task would be further complicated by tilting the

slits, which not only changes the instrumental linewidth but also shifts the line center. (A much finer adjustment of the slit angle than was available in this work would have been necessary to maintain the slits exactly parallel as they were rotated.) In view of the considerable experimental difficulty involved in implementing the rigorous procedure for partially resolved fine structure, the relevant formula has not been presented.

The compromise which has been adopted is to use the formula for unresolved fine structure for the evaluation of the excitation parameters (Section 6.2.2), then to see what polarization values are predicted for each of the lines of a multiplet using the formula for resolved fine structure. As will be subsequently demonstrated, the polarization value for the multiplet can be obtained by averaging the individual polarization values for the lines weighted by the line-strength factor. This method is not exact but the error seems to be only a few percent.

For unresolved fine structure, then, the applicable equation for $A^k(t)$ from Chapter II is equation (2.23). The fine-structure quantum beats are completely unresolved so that only $J = J'$ terms can be non-zero. $A^k(t)$ then becomes

$$A^k(t) = \frac{Ce^{-\Gamma t}}{\sqrt{2L+1}} \begin{Bmatrix} L & L & k \\ 1 & 1 & L_f \end{Bmatrix} \sum_J \begin{Bmatrix} J & J & k \\ L & L & S \end{Bmatrix}^2 \frac{(2J+1)^2}{(2S+1)} . \tag{6.1}$$

Only the ratio $A^k(t)/A^0(t)$ for $k = 1$ or 2 appears in the

expression for the relative Stokes parameters. From Chapter II these may be written for M/I and S/I as:

$$\frac{M}{I} = \frac{-\sqrt{3}/2\ \sigma_M\ A^2(t)/A^0(t)}{1 - \sqrt{3}/2\ \sigma_I\ A^2(t)/A^0(t)} \tag{6.2}$$

$$\frac{S}{I} = \frac{-\sqrt{3}\ \sigma_1^1\ A^1(t)/A^0(t)}{1 - \sqrt{3}/2\ \sigma_I\ A^2(t)/A^0(t)} \tag{6.3}$$

where σ_M and σ_I are the same as in Chapter V, i.e.,

$$\sigma_M = \frac{3\ \sigma_0^2}{\sqrt{6}} + \sigma_2^2$$

$$\sigma_I = \frac{\sigma_0^2}{\sqrt{6}} - \sigma_2^2.$$

The ratio A^k/A^0 has been compiled in Table 7 for those values of S, L and L_f which appear in Table 6. (L_f represents the angular momentum of the final or lower term.) The program for evaluation of the 6-j symbols was written by Caswell and Maximon (CM 66) and is available through the U.S. National Bureau of Standards.

One natural constraint placed on σ_I is that it be small enough for the denominator in (6.2) or (6.3) always to be positive. Thus the sign of A^k/A^0 is directly related to the sign of the relative Stokes parameters. The only positive value of S/I appearing in Table 6 occurs for the 3p ^3D - 4s $^3P°$

TABLE 7

A^k Ratios for N II and N III

S	L	L_f	A^1/A^0	A^2/A^0
0	1	0	-1.0000	1.0000
0	1	1	-0.5000	-0.5000
0	2	1	-0.8660	0.5916
0	4	3	-0.7906	0.4432
1/2	1	0	-0.7778	0.3333
1/2	4	3	-0.7711	0.4103
1	1	0	-0.5000	0.2778
1	1	1	-0.2500	-0.1389
1	1	2	0.2500	0.0278
1	2	1	-0.6896	0.2800
1	2	2	-0.2299	-0.2800
1	3	2	-0.7296	0.3437
3/2	1	1	-0.2111	-0.1233
3/2	2	1	-0.5592	0.1630
3/2	3	2	-0.6588	0.2500
2	2	1	-0.4330	0.1569

transition at 3329 Å and this is the only positive value in the A^1/A^0 column of Table 7. There are four negative values for A^2/A^0, one of which corresponds to the 3p ^3D -3d $^3D°$ transition at 4803 Å. Of the remaining three, only one contradicts Table 6, since the other two show M/I values close to zero. This one is the 3p ^1P - 4s $^1P°$ transition at 3007 Å which will be one of the triplet-singlet pairs considered in the following section. It seems that the alignment for this state is opposite in sign to the others which might be attributed to the valence electron being in an s state.

6.2.2 Triplet-Singlet Pairs

If one assumes spin-independence, the results of Chapter II indicate that the excitation parameters should be the same for all excited states having the same configuration and the same total orbital angular momentum. By this reasoning triplet-singlet pairs of the same excited state (the lower state need not be the same) should have identical excitation parameters. At 0° foil tilt the two measured M/I values can be used to solve for the single unknown, σ_0^2. At 60° tilt the M/I and S/I values for each member of the pair constitute four measurements while σ_0^2, σ_2^2 and σ_1^1 constitute three unknowns. Of course, C/I could be included at 60° tilt with the added parameter $i\sigma_1^2$. C/I is not a particularly interesting parameter and could only become one if for some measurement it were large when both M/I and S/I were small. This has never been observed which accounts for the fact that it is frequently ignored and justly so.

Three triplet-singlet pairs are available for consideration. The pair at 4803 Å/4447 Å, one at 5680 Å/3995 Å and one at 3329 Å/3007 Å. The multiplet designations for these transitions appear in Table 6. At 0° foil tilt both σ_2^2 and σ_1^1 are zero. Only M/I is non-zero and a single excitation parameter, σ_0^2, must be used to describe the polarization. The column of Table 8, marked M/I at 0°, gives the measured polarization and the value obtained from equation (6.2) for each of the triplet-singlet pairs. The value of σ_0^2 used for the fit, for each of the pairs, then appears in part (b) of Table 8. Likewise for 60° foil tilt the measured values, as well as those obtained by using equations (6.2) and (6.3), appear in part (a) of Table 8 while the three non-zero parameters, σ_0^2, σ_2^2 and σ_1^1 used for the fit appear in part (b). No uncertainties are listed for the excitation parameters since the partial resolution of the fine structure is almost certainly the greatest source of error which is not reflected by the computer estimates from the fit.

Bearing in mind that the fitting procedure is one that employs one free parameter to fit two measurements or three parameters to fit four measurements, some interesting features, nonetheless, emerge from Table 8. The first is that the signs are correct for all measruements if one takes into account the quoted uncertainties of the measured values. The second is that the agreement in the M/I value at 0° is really quite good. This agreement is more difficult to

TABLE 8

N II Triplet-Singlet Comparison

(a) Polarization Values

λ(Å)		0°	60°	
		M/I	M/I	S/I
4803	Exp.	-0.063	-0.041	-0.063
	Fit	-0.040	-0.042	-0.063
4447	Exp.	0.071	0.074	-0.193
	Fit	0.081	0.073	-0.193
5680	Exp.	0.026	0.040	-0.113
	Fit	0.021	0.021	-0.114
3995	Exp.	0.042	0.029	-0.119
	Fit	0.044	0.035	-0.117
3329	Exp.	-0.010	-0.011	0.035
	Fit	-0.003	0.000	0.035
3007	Exp.	0.047	-0.003	-0.037
	Fit	0.048	-0.002	-0.037

(b) Excitation Parameters for Fit

λ(Å)	0°	60°		
	σ_0^2	σ_0^2	σ_2^2	σ_1^1
4803/4447	-0.132	-0.266	+0.163	-0.147
5680/3995	-0.070	-0.711	+0.764	-0.120
3329/3007	+0.092	+1.135	-1.397	-0.077

achieve than the excellent agreement in the S/I column which results from these measurements having smaller relative uncertainties (and therefore greater weights) which forces all of the disagreement into the 60° M/I column. But even in the 60° M/I column only one pair in three shows genuine disagreement with the measurements. The fit predicts that M/I for 3995 Å should be greater than for 5680 Å whereas the measurements indicate the opposite. The last interesting feature, and one mentioned previously, is that σ_0^2 and σ_2^2 for the 3329 Å/3007 Å pair are of opposite sign to the other pairs and are probably of opposite sign to every other N II transition in Table 6.[1] This is not a consequence of any one or two of the six measurements but is a consistent feature of all of them.

The problem of partially resolved fine structure can now be reexamined. The first question which needs to be answered is, why is the agreement of Table 8 as good as it is? The triplet transition, 3p ^3D - 3d $^3D°$, which has been labelled with the wavelength 4803, will be considered in detail. Its fine structure is typical and it is the most difficult of the three to interpret. There is a 34 Å separation between the shortest wavelength of the multiplet and the longest. Table 9 lists these wavelengths, with the initial and final J quantum numbers (J_f - J_i), and the relative line strengths as given by Condon and Shortley (CS 70). The predicted

---

[1]This statement is a certainty only for the 0° values.

polarization for each line using the resolved fine-structure formula of Chapter II (equation 2.35) is also given. The excitation parameters, for 60° foil tilt listed for 4803 Å/ 4447 Å in Table 8, have been used. The value for the singlet transition at 4447 Å has been included for completeness but of course the two different formulae, one for the polarization of a multiplet and one for the polarization of a line, yield the same result for singlets.

TABLE 9

Line Polarization for One N II Triplet Transition

$J_f - J_i$	λ(Å)	Strength	M/I	S/I
3-2	4810	12.5	+0.012	+0.120
3-3	4803	100	-0.081	-0.056
2-1	4794	12.1	+0.008	+0.109
2-2	4788	55.8	-0.045	-0.066
2-3	4781	12.5	+0.052	-0.179
1-1	4780	36.2	-0.045	-0.118
1-2	4774	12.1	+0.039	-0.172
		Average:	-0.045	-0.062
1-2	4447	100	+0.073	-0.193

The values marked "average" were obtained by weighting the listed polarization by the line strength factors and by

then evaluating the mean. These averages are very close to the multiplet values given in Table 8. Certainly the spectrometer has not detected light from any more than the first three lines. The averages, weighted as before, for these lines are M/I = -0.063 and S/I = -0.022. These numbers differ substantially from the measured values which indicates that, at least for this triplet at 60°, the procedure of using the multiplet value is not satisfactory.

At 0° foil tilt the situation is significantly simpler. The line at 4803 Å would have been resolved from its nearest neighbors. The singlet at 4447 Å would also be well resolved. If one applies the formula for resolved fine structure and uses a value for σ_0^2 of -0.116, one obtains M/I = -0.064 for 4803 Å and M/I = +0.071 for 4447 Å which are in excellent agreement with the measured values.

If one examines the triplet transitions at 5680 Å and at 3329 Å, one finds that averaging the polarization for those lines that have not been resolved either gives good agreement with the multiplet values (60° tilt) or gives somewhat better agreement with the measured values (0° tilt). For neither transition is the agreement worse than that of Table 8.

The conclusion which can be reached is that the theory of Chapter II is able to describe the coarse features of Table 6 despite the complication of partially-resolved fine structure. As mentioned previously, a detailed

examination using a formula for partially-resolved fine structure is not warranted unless data were acquired with the added information needed to determine the spectrometer resolution at the wavelength and tilt angle of the measurement.

6.2.3 Transitions from S Terms

Two transitions, the 3s $^3P° - 3p\ ^3S$ at 5045 Å and the 3s $^5P - 3p\ ^5S°$ at 4146 Å, have upper terms with L = 0 and might, from the results of Chapter II, be expected to show no polarization. This conclusion is a direct result of the spin-independence hypothesis. Recently Ellis (El 76) has shown that, if this hypothesis is not invoked, non-zero polarization from an S state is possible if the state is not a singlet and if the fine structure is resolved. These conditions are satisfied by both of the above transitions. The fine structure components for the triplet occur at 5045 Å(2-1), 5011 Å(1-1) and 5003 Å(0-1) where $J_f - J_i$ appear in parenthesis. The three quintet components occur at 4146 Å(3-2), 4134 Å(2-2) and 4124 Å(1-2). The two transitions, as listed in Table 6, show no polarization larger than 2 standard deviations from zero.

One cannot conclude from the null result that spin-independence is necessarily a valid hypothesis for the Nitrogen transitions. On the other hand, a straightforward measurement, which could have shown the invalidity of the assumption, failed to do so.

CHAPTER VII

DISCUSSION AND CONCLUSION

That tilting the exciter foil in beam-foil spectroscopy induces significant orientation for a large number of excited states has clearly been demonstrated. Future experiments may utilize this technique solely as a source of oriented excited states. Both quantum-beat and lifetime experiments can be designed which require such a special light source. The circular polarization fraction increases with foil tilt and the question as to whether an optimum angle exists for tilted-foil measurements may arise. The results with the Helium $^1P° - {}^1D$ transitions (Figure 6) indicate that 60° foil tilt provides a much larger circular polarization fraction than does 45° tilt. Angles larger than 60° suffer from short foil lifetime and significant attenuation of the beam velocity. Thus it seems that 60° is an optimum angle for performing tilted-foil measurements.

7.1 Comments on the Polarization of Helium

The results of the Helium singlet experiment demonstrate that the differences between $^1S - {}^1P°$ and $^1P° - {}^1D$ transitions are greater than a simple scale factor which is all that the general theory of Chapter II can provide. The transformation from one type of transition to the other changes with foil-tilt angle. Another way of phrasing this

is that the functional form of at least some of the excitation parameters with foil tilt is different from one type of transition to another. This observed fact is the reason why the Band theory could not adequately describe both types of transitions. At first this result seems curious since one might expect that the dependence of polarization on quantum number is completely described by the general theory. However, the general theory of Chapter II is an emission theory which made no attempt to explain excitation. This experimentally observed effect, which had not previously been measured, indicates that the excitation process itself is dependent upon the quantum numbers of the excited state. A theory of the excitation process will almost certainly be more complicated than any so far advanced.

The Helium triplet results, as presented in Figure 11, point to the validity, for Helium, of the spin-independence hypothesis. The experiment of Burns et al. (BHG 79) however, indicates that the $2s\,^3S - 3p\,^3P°$ polarization pattern of 3889 Å is not the same as the $2s\,^1S - 3p\,^1P°$ one. One possible explanation is that the spin-independence hypothesis does not hold while another is that the triplet P states are perturbed in some way by the proximity of the triplet D states. The singlets are not nearly so close together. The measurements should be made again in a more complete manner as described in Chapter V so that the behavior of the excitation parameters with foil-tilt angle for both the ^3P

and ^3D states can be examined.

The Helium doubly-excited state transitions show polarization patterns with foil-tilt angle (Figure 9) which do not resemble any of the patterns obtained with the normal states. In fact they more nearly resemble the Nitrogen patterns of Figure 15, though the electron configurations have nothing in common. The negative values of M/I at all tilt angles for the $2p^2\ {}^3P - 2p3d\ {}^3D°$ transition at 3014 Å cannot be explained with the help of Table 7. There are several possible explanations:

1) The assigned quantum numbers for the transition are incorrect.
2) The fine structure does not satisfy the condition that any quantum beats have too high a frequency to resolve.
3) The alignment has its sign opposite to all of the other Helium transitions.

The first alternative seems remote in light of the fact that the transition occurs <u>between</u> states forbidden to autoionize (which is consistent with its narrow line width relative to, for example, the transitions at 2363 Å or 2577 Å) and also that the transitions from the next three higher members of the Rydberg series have been observed. The second alternative must be seriously considered. The author has been unable to obtain any values, either from measurement or calculation, for the fine structure intervals of Helium

doubly-excited states. Since the fine structure of Helium is composed of the spin-spin and spin-other-orbit interactions in addition to the spin-orbit interaction, one might guess that the fine structure intervals would be much larger when the two electrons are closer together as in the doubly-excited case than when one electron is in the 1s shell. It is conceivable that the frequencies have just the size required for the measurements to have been taken at the minimum of a beat. However, the transition is from a $^3D°$ term and only if the beat amplitudes of all three possible frequencies were summed could the value slightly exceed unity which is the necessary condition for M/I to change sign somewhere along a beat. Even if that unlikely situation (i.e., all three frequencies about the same) were the case, the averaging length of the slits combined with the short decay should still yield a positive value for M/I. The conclusion, then, is that in all likelihood, the sign of the alignment of the $2p3d\,^3D°$ term of doubly-excited Helium is opposite to that of all the other measured states.

7.2 Estimation of Relative Polarization Fractions

The polarization fractions of both the 2577 Å and 3014 Å transitions of the Helium doubly-excited states increase dramatically with foil-tilt angle. Yet the polarization of the $2p^2\ ^3P - 2p3d\ ^3P°$ transition at 2818 Å (Appendix 2) is essentially zero through 60° foil tilt. In like manner, several Nitrogen transitions in Table 6

originating from upper levels which do not belong to an S term, show very little polarization at 60° foil tilt. Considering that the polarization fractions of over 30 different transitions have been measured for this project, has any pattern developed which might indicate whether or not a given transition is likely to show large polarization? The answer is "yes," but the validity of any rule determined empirically from what must be considered a small sample, is suspect.

The rule which can be used as an aid for estimating whether or not a given transition is likely to show significant circular polarization at large foil-tilt angle (60°) is based solely upon the upper state of that transition. <u>For a given configuration the term of maximum L yields the largest value of ρ_1^1 while the term of minimum L yields the smallest</u>. No transition from a term of minimum L has been observed which yielded an S/I value greater than 4% at 60° foil tilt. No transition from a term of maximum L has been observed which yielded an S/I value smaller than 9% at 60° foil tilt. If for a given configuration only one L value is permitted, nothing can be concluded about the size of the circular polarization. Of course the value of S/I depends upon $A^1(t)/A^0(t)$ which was given in Table 7 for unresolved fine structure with unresolved (high frequency) quantum beats. The value of L_f for the final state influences the circular polarization fraction through this term. One should evaluate the ratio of A^1/A^0 for the transition of interest since it is

unlikely that a large polarization fraction will be observed if this ratio is small. Furthermore the rule has been written for ρ_1^1 not the circular polarization itself since it may happen that A^1/A^0 is sufficient to reverse the relative sizes of the circular polarization. No example is available from the measured transitions in which more than three terms are possible from a given configuration.

Consider the following two Nitrogen examples from Table 6:

	Transition	S/I @ 60°	A^1/A^0
Example 1	3p ^3D - 3d $^3F°$	-19.0%	-0.73
	3p ^3D - 3d $^3D°$	- 6.3%	-0.23
	3p ^1P - 3d $^1D°$	-19.3%	-0.87
Example 2	3d $^1F°$ - 4f G(9/2)	- 9.3%	-0.79
	3d $^3D°$ - 4f F(7/2)	- 7.8%	-0.73
	3d $^3P°$ - 4f D(5/2)	- 3.1%	-0.69

The first example indicates that a large value of A^1/A^0 can be sufficient for the polarization of a term not having the maximum L value for the configuration to show a polarization larger than that for the term with maximum L. The second example indicates that the size of A^1/A^0 is insufficient to estimate the magnitude of the polarization.

It would have been satisfying to report that a single set of excitation parameters could describe the polarization of a particular ion at some velocity and foil-tilt angle for

all transitions measured. As mentioned in Chapter II this has been observed using a tilted surface rather than a foil for a selection of transitions in Ar II. However, neither the set of N II transitions nor any subset (except the triplet-singlet pairs) could be so described. The empirical rule stated above is a consequence of this fact for had a single set of excitation parameters been sufficient such a relationship would not have been observed. One cannot exclude the possibility that partial resolution of the fine structure was the sole reason why a single set of parameters was insufficient. A survey similar to the one conducted for Nitrogen using a more appropriate element may resolve this matter.

7.3 Conclusion

The acquisition, design and construction of most of the equipment in a new laboratory has opened up a relatively new area of beam-foil spectroscopy to the University of Alberta. This dissertation has presented the first research performed with that facility. The methods employed for data acquisition, remote computer control of experimental equipment and data analysis had not previously been used here and were programmed by the author. For comparison of polarizations at different wavelengths, the determination of the phase of the retarder at these wavelengths is most important and the self-consistent technique for accomplishing this was developed by the author.

Previous sections of this chapter have discussed the conclusions that can be drawn from the results obtained in this study, including both the more general behavior of polarization induced by tilted-foil excitation and the more specific behavior of particular types of transitions. As is often the case in scientific investigation, this work has pointed to some new questions, as well providing answers to some previously asked. The measurements performed for this project have focused on only two variables of the many such combinations which might be imagined. The first is the foil-tilt angle and the second is the transition wavelength which selects those quantum numbers that are of particular interest. Other laboratories are concentrating on different variables and slowly, like the restoration of an ancient mosaic, the pattern of the beam-foil excitation mechanism is struggling to emerge. It is too soon, at least for this writer, to discern the pattern but the next few years may see a clearer image emerge and the resolution of some of the problems posed by this work.

BIBLIOGRAPHY

ACLMM 76 G. Astner, L.J. Curtis, L. Liljeby, S. Mannervik and I. Martinson, J. Phys. B 9, L345 (1976).

AFPS 76 H.J. Andrä, R. Fröhling, H.J. Plöhm and J.D. Silver, Phys. Rev. Lett. 37, 1212 (1976).

AM 67 P.L. Altick and E.N. Moore, Proc. Phys. Soc. 92, 853 (1967).

An 75 H.J. Andrä, Phys. Lett. 54A, 315 (1975).

APGF 77 H.J. Andrä, H.J. Plöhm, A. Gaupp and R. Fröhling, Z. Physik A 281, 15 (1977).

ATW 78 Lloyd Armstrong, Jr., Constantine E. Theodosiou and M.J. Wall, Phys. Rev. A 18, 2538 (1978).

Ba 68 Beam-Foil Spectroscopy, ed. S. Bashkin (Gordon and Breach, New York, 1968).

Ba 73 Proc. Third Int. Conf. Beam-Foil Spectroscopy, ed. S. Bashkin (North-Holland, Amsterdam, 1973); Nucl. Instr. Methods, 110, 1-522 (1973).

Ba 76 Beam-Foil Spectroscopy, ed. S. Bashkin (Springer-Verlag, Berlin, 1976).

Ba 76 Yehuda Band, Phys. Rev. A 13, 2061 (1976).

BCES 74 H.G. Berry, L.J. Curtis, D.G. Ellis and R.M. Schectman, Phys. Rev. Lett. 35, 274 (1974).

BCES 75 H.G. Berry, L.J. Curtis, D.G. Ellis and R.M. Schectman, Phys. Rev. Lett. 35, 274 (1975).

BCES 76 H.G. Berry, L.J. Curtis, D.G. Ellis and R.M. Schectman, in Electron and Photon Interactions With Atoms, ed. Kleinpoppen and McDowell (Plenum Press, New York, 1976), p 515.

BCOWPM 78 J.A. Brink, L.J. Coetzer, J.H.I. Olivier, P. van der Westhuizen, R. Pretorius and W.R. McMurray, Z. Physik A 288, 1 (1978).

BCS 72 H.G. Berry, L.J. Curtis and J.L. Subtil, J. Opt. Soc. Am. 62, 771 (1972).

BCS 75 H.G. Berry, L.J. Curtis and R.M. Schectman, Phys. Rev. Lett. 34, 509 (1975).

BDD 72 H.F. Berry, J. Desesquelles and M. Duffy, Phys. Rev. A 6, 600 (1972).

Be 69 Data Reduction and Error Analysis for the Physical Sciences, Philip R. Bevington (McGraw-Hill, New York, 1969).

Be 75 H.G. Berry, Phys. Scr. 12, 5 (1975).

Be 77 H.G. Berry, Rep. Prog. Phys. 40, 155 (1977).

BGGL 77 H.G. Berry, G. Gabrielse, T. Gay and A.E. Livingston, Phys. Scr. 16, 99 (1977).

BGL 77 H.G. Berry, G. Gabrielse and A.E. Livingston, Appl. Opt. 16, 3200 (1977).

BGLSD 77 H.G. Berry, G. Gabrielse, A.E. Livingston, R.M. Schectman and J. Desesquelles, Phys. Rev. Lett. 38, 1473 (1977).

BH 73 Donal J. Burns and Walter H. Hancock, J. Opt. Soc. Am. 63, 241 (1973).

BHG 79 Donal J. Burns, Ralph D. Hight and Chris H. Greene, Phys. Rev. A, to be published (1979).

BP 78 Robert L. Brooks and Eric H. Pinnington, Phys. Rev. A 18, 1454 (1978).

Br 75 Robert Leslie Brooks, "Quantum Beats in Beam-Foil Spectroscopy," M.Sc. Thesis, University of Alberta (1975).

BS 77 Quantum Mechanics of One- and Two-Electron Atoms, Hans A. Bethe and Edwin E Salpeter (Plenum, New York, 1977).

BT 75 A.K. Bhatia and A. Temkin, Phys. Rev. A 11, 2018 (1975).

Ca 78 Joseph Callaway, Phys. Lett. 66A, 201 (1978).

CG 71 Polarized Light and Optical Measurement, D. Clarke and J.F. Grainger (Pergamon, Oxford, 1971).

CHLPB 77 L.J. Curtis R. Hallin, J.L. Lindskog, J. Pihl and H.G. Berry, Phys. Lett. 60A, 297 (1977).

CKMH 74 D.A. Church, W. Kolbe, M.C. Michel and T. Hadeishi, Phys. Rev. Lett. 33, 565 (1974).

CL 78 M.J. Conneely and Lester Lipsky, J. Phys. B 11, 4135 (1978).

CM 66 R.S. Caswell and L.C. Maximon, "Fortram Programs for the Calculation of Wigner 3j, 6j and 9j Coefficients for Angular Momenta ≤80," NBS Technical Note 409 (U.S. Govt. Printing Office, Washington, D.C., 1966).

CM 75 D.A. Church and M.C. Michel, Phys. Lett. 55A, 167 (1975).

COHB 67 J.W. Cooper, S. Ormondes, C.H. Humphrey and R,G, Burke, Proc. Phys. Soc. 91, 285 (1967).

CRPGL 77 P.G. Christiansen, J.E. Ross, G.J. Pedrazzini, R.B. Gardiner and C. H. Liu, J. Phys. B 10, 3559 (1977).

CS 70 The Theory of Atomic Spectra, E.U. Condon and G.H. Shortley (Cambridge, Cambridge, 1970).

De 71 Jean Desesquelles, Ann. Phys. 6, 71 (1971).

De 79 "Fast Ion Spectroscopy," ed. J. Desesquelles, Jour. de Phys. 40, Colloque C-1 (1979).

Ec 73 T.G. Eck, Phys. Rev. Lett. 31, 270 (1973).

Ec 74 T.G. Eck, Phys. Rev. Lett. 33, 1055 (1974).

Ed 74 Angular Momentum in Quantum Mechanics, A.R. Edmonds (Princeton, Princeton, 1974).

El 73 David G. Ellis, J. Opt. Soc. Am. 63, 1232 (1973).

El 77 David G. Ellis, J. Phys. B 10, 2301 (1977).

FM 73 U. Fano and Joseph H. Macek, Rev. Mod. Phys. 45, 553 (1973).

GB 79 T,J, Gay and H.G. Berry, Phys. Rev. A 19, 952 (1979).

HCDEIM 78 S. Huldt, L.J. Curtis, B. Denne, L. Engström, K. Ishii and I Martinson, Phys. Lett. 66 A. 103 (1978).

He 75 R.M. Herman, Phys. Rev. Lett. 35, 1626 (1975).

HSBGG 77 R.D. Hight, R.M. Schectman, H.G. Berry, G. Gabrielse and R. Gay, Phys. Rev. A 16, 1805 (1977).

IT 78 Keishi Ishii and Michio Tomita, Jour. Phys. Soc. Japan 45, 230 (1978).

Jo 41 R.C. Jones, J. Opt. Soc. Am. 31, 488 (1941).

KD 73 E.J. Knystautas and R. Drouin, Nucl. Instr. Methods 110, 95 (1973).

LAC 77 Lester Lipsky, Russel Anania and M.J. Conneely, Atomic Data and Nuclear Data Tables 20, 127 (1977).

LBC 74 C.H. Liu, S. Bashkin and D.A. Chruch, Phys. Rev. Lett. 33, 993 (1974).

LC 76 Lester Lipsky and M.J. Conneely, Phys. Rev. A 14, 2193 (1976).

Lo 75 M. Lombardi, Phys. Rev. Lett. 35, 1172 (1975).

LS 75 E.L. Lewis and J.D. Silver, J. Phys. B 8, 2697 (1975).

Ma 73 W.C. Martin, J. Phys. Chem. Ref. Data 2, 257 (1973).

MB 76 Joseph Macek and Donal Burns, in Beam-Foil Spectroscopy, ed., S. Bashkin (Springer-Verlag, Berlin, 1976), p. 237.

MBB 70 Proc. Second Int. Conf. Beam-Foil Spectroscopy, ed. I. Martinson, J. Bromander and H.G. Berry (North-Holland, Amsterdam, 1970); Nucl. Instr. Methods 90, 1-371 (1970).

MC 63 R.P. Madden and K. Codling, Phys. Rev. Lett. 10, 516 (1963).

Mu 48 H. Mueller, J. Opt. Soc. Am. 38, 661 (1948).

Pe 42 F. Perrin, J. Chem. Phys. 10, 415 (1942).

RBMW 59 The 3-j and 6-j Symbols, M. Rotenberg, R. Bivens, N. Metropolis and J.K. Wooten (Technology Press, M.I.T., 1959).

Sc 73 G.J. Schultz, Rev. Mod. Phys. 45, 378 and 423 (1973).

Sc 78 H. Schröder, Z. Physik A 284, 125 (1978).

SCDD 76 J.L. Subtil, P. Ceyzériat, A Denis et J. Desesquelles, Jour. de Phys. 37, 1299 (1976).

SDG 75 J.D. Silver, J. Desesquelles and M.L. Gaillard, J. Phys. B 8, L219 (1975).

SK 76 Heinz Schröder and Eckart Kupfer, Z Physik A 279, 13 (1976).

SL 73 J.O. Stoner and J.A. Leavitt, Optica Acta 20, 435 (1973).

SLMH 79 I.A. Sellin, L. Liljeby, S. Mannervik and S. Hultberg, Phys. Rev. Lett. 42, 570 (1979).

SP 76 Beam-Foil Spectroscopy, ed. Ivan A Sellin and David J. Pegg (Plenum, New York, 1976).

SS 68 Tables of Spectral Lines of Neutral and Ionized Atoms, A.R. Striganov and N.S. Sventitskii (Plenum, New York, 1968).

TW 71 J.L. Tech. and J.F. Ward, Phys. Rev. Lett. 27, 367 (1971)

WA 78 W. Wittman and H.J. Andrä, Z. Physik A 288, 335 (1978).

WTAD 72 W. Wittman, K. Tillmann, H.J. Andrä and P. Dobberstein, Z. Physik 257, 279 (1972).

APPENDIX 1

SOME DETAILED CALCULATIONS

A1.1 Derivation of Equation (2.10)

Before commencing the derivation, it would be useful to describe how the phase factors which appear in these expressions may be manipulated. All of the necessary relations follow from identities or symmetries of the 3-j and 6-j symbols.

First, the symmetry of the 3-j symbol permits any even permutation of columns. Odd permutations of columns as well as changing the sign of all elements in the lower row introduce a phase factor of $(-1)^n$, where n is the sum of all elements in the upper row. For example,

$$\begin{pmatrix} j_1 & j_2 & j \\ m_1 & m_2 & m \end{pmatrix} = \begin{pmatrix} j & j_1 & j_2 \\ m & m_1 & m_2 \end{pmatrix} = (-1)^{j_1+j_2+j} \begin{pmatrix} j_1 & j & j_2 \\ m_1 & m & m_2 \end{pmatrix}$$

$$= (1)^{j_1+j_2+j} \begin{pmatrix} j_2 & j & j_1 \\ -m_2 & -m & -m_1 \end{pmatrix} = \begin{pmatrix} j_2 & j_1 & j \\ -m_2 & -m_1 & -m \end{pmatrix} .$$

In addition, the sum of all elements in the lower row is zero. Any combination of the elements of a 3-j symbol, using the above notation, such as $(j_1 \pm m_1)$, $(j_2 \pm m_2)$ or $(j \pm m)$ must be integer so that $(-1)^{2j-2m} = 1$.

A 6-j symbol is invariant to both even and odd permutations of columns as well as the interchange of any 2 elements in the upper row with the 2 elements below them. There are thus 24 equivalent permutations. For example:

$$\begin{Bmatrix} j_1 & j_2 & j_3 \\ j_4 & j_5 & j_6 \end{Bmatrix} = \begin{Bmatrix} j_1 & j_3 & j_2 \\ j_4 & j_6 & j_5 \end{Bmatrix} = \begin{Bmatrix} j_3 & j_4 & j_5 \\ j_6 & j_1 & j_2 \end{Bmatrix} \quad \text{etc.}$$

There are only four sums of three elements in a 6-j symbol which must be able to make a triangle.[1] If any one of these cannot form a triangle the 6-j symbol is zero. In addition, all such sums must be integer. For the example above they are:

$$(j_1,j_2,j_3),\ (j_3,j_4,j_5),\ (j_1,j_5,j_6) \text{ and } (j_2,j_4,j_6).$$

Thus, for the symbol $\begin{Bmatrix} L_f & J_f & S \\ J & L & 1 \end{Bmatrix}$, the phase $(-1)^{2J_f+2S}$ must equal 1 since $L_f + J_f + S$ is always integer and L_f is always integer. An interesting consequence of the above rules for 6-j symbols is that if any element in a 6-j symbol is half-integer then 3 or 4 elements are half integer.

The matrix element of the light emission operator is given by equation (2.9):

---

[1]Three elements j_1, j_2 and j_3 are said to make a triangle if $|j_1-j_2|\le j_3\le|j_1+j_2|$ for any combination of j_1, j_2 and j_3.

$$<J'M'|L(\lambda,\vec{\varepsilon})|JM> = C' \sum_{J_f M_f} \sum_{q_1 q_2} (-1)^{J'-M'+J_f-M_f}$$

$$\times (-1)^{q_1+q_2} \varepsilon_{q_1} \varepsilon^{+}_{-q_2} \begin{pmatrix} J' & 1 & J_f \\ -M' & -q_1 & M_f \end{pmatrix} \begin{pmatrix} J_f & 1 & J \\ -M_f & q_2 & M \end{pmatrix} \tag{A1.1}$$

$$\times <\alpha(LS)J'||D||\alpha(L_fS)J_f><\alpha(L_fS)J_f||D||\alpha(LS)J>.$$

The sum over M_f may be performed by invoking the following:[1]

$$\sum_{m_3} \begin{pmatrix} j_1 & j_2 & j_3 \\ m_1 & m_2 & m_3 \end{pmatrix} \begin{pmatrix} \ell_1 & \ell_2 & j_3 \\ n_1 & n_2 & -m_3 \end{pmatrix} = \sum_{\ell_3 n_3} (-1)^{j_3+\ell_3+m_1+n_1}$$

$$\times (2\ell_3+1) \begin{Bmatrix} j_1 & j_2 & j_3 \\ \ell_1 & \ell_2 & \ell_3 \end{Bmatrix} \begin{pmatrix} \ell_1 & j_2 & \ell_3 \\ n_1 & m_2 & n_3 \end{pmatrix} \begin{pmatrix} j_1 & \ell_2 & \ell_3 \\ m_1 & n_2 & -n_3 \end{pmatrix}.$$

The $-M_f$ which appears in the phase factor of (A1.1) may be changed to $-q_2-M$. Then

$$\sum_{M_f} \begin{pmatrix} J' & 1 & J_f \\ -M' & -q_1 & M_f \end{pmatrix} \begin{pmatrix} 1 & J & J_f \\ q_2 & M & -M_f \end{pmatrix} = \sum_{kq} (-1)^{J_f+k-M'+q_2}$$

$$\times (2k+1) \begin{Bmatrix} J' & 1 & J_f \\ 1 & J & k \end{Bmatrix} \begin{pmatrix} 1 & 1 & k \\ q_2 & -q_1 & q \end{pmatrix} \begin{pmatrix} J' & J & k \\ -M' & M & -q \end{pmatrix} \tag{A1.2}$$

---

[1] Equation (2.19) of RBMW 59.

Using equation (A1.2), equation (A1.1) becomes

$$<J'M'|L(\lambda \cdot \vec{\varepsilon})|JM> = C' \sum_{kqJ_f} \sum_{q_1q_2} (-1)^{J'-2M'+2J_f-M+k}$$

$$\times (-1)^{q_1+q_2} \varepsilon_{q_1} \varepsilon_{\pm q_2} (2k+1) \begin{Bmatrix} J' & 1 & J_f \\ 1 & J & k \end{Bmatrix}$$

$$\times \begin{pmatrix} 1 & 1 & k \\ q_2 & -q_1 & -q \end{pmatrix} \begin{pmatrix} J' & J & k \\ -M' & M & q \end{pmatrix}$$

$$\times <\alpha J'||D||\alpha J_f><\alpha J_f||D||\alpha J>.$$

The sign of q was changed everywhere (q is summed from -k to +k) for later convenience. From the definition of ℓ_q^k one has

$$\sum_{q_1q_2} (-1)^{q_1+q_2} \varepsilon_{q_1} \varepsilon_{\pm q_2} (2k+1)^{\frac{1}{2}} \begin{pmatrix} 1 & 1 & k \\ q_2 & -q_1 & -q \end{pmatrix} = (-1)^k \ell_{-q}^k$$

So

$$<J'M'|L(\lambda,\vec{\varepsilon})|JM> = C' \sum_{J_f} \sum_{kq} (-1)^{2J'+J-M+k}$$

$$\times \ell_{-q}^k (2k+1)^{\frac{1}{2}} \begin{pmatrix} J' & k & J \\ -M' & q & M \end{pmatrix} \begin{Bmatrix} J' & J & k \\ 1 & 1 & J_f \end{Bmatrix}$$

$$\times <\alpha J'||D||\alpha J_f><\alpha J_f||D||\alpha J>. \qquad (A1.3)$$

Since the operator D is not a function of spin, one may write

$$\langle\alpha(LS)J'\|D\|\alpha(L_fS)J_f\rangle = (-1)^{L+S+J_f+1}$$

$$\times\ (2J_f+1)^{\frac{1}{2}}(2J'+1)^{\frac{1}{2}} \begin{Bmatrix} L & J' & S \\ J_f & L_f & 1 \end{Bmatrix} \langle\alpha L\|D\|\alpha L_f\rangle$$

and similarly

$$\langle\alpha(L_fS)J_f\|D\|\alpha(LS)J\rangle = (-1)^{L_f+S+J+1}$$

$$\times\ (2J_f+1)^{\frac{1}{2}}(2J+1)^{\frac{1}{2}} \begin{Bmatrix} L_f & J_f & S \\ J & L & 1 \end{Bmatrix} \langle\alpha L_f\|D\|\alpha L\rangle\ .$$

Substitution into (A1.3) yields

$$\langle J'M'|L(\lambda,\vec{\varepsilon})|JM\rangle = C\sum_{kq}(-1)^{2J'+L+L_f-M+k}$$

$$\times\ \ell^k_{-q}[J\,J'k]^{\frac{1}{2}} \begin{pmatrix} J' & k & J \\ -M' & q & M \end{pmatrix} \sum_{J_f}(-1)^{J_f}[J_f]$$

$$\begin{Bmatrix} J' & J & k \\ 1 & 1 & J_f \end{Bmatrix} \begin{Bmatrix} J' & S & L \\ L_f & 1 & J_f \end{Bmatrix} \begin{Bmatrix} J & S & L \\ L_f & 1 & J_f \end{Bmatrix} \qquad \text{(A1.4)}$$

where $C = C'\ S = C'\,|\langle\alpha L\|D\|\alpha L_f\rangle|^2$.

The sum over J_f can be performed by appealing to the following identity:[1]

[1]Equation (6.2.12) of Ed 74.

$$\sum_k (-1)^{S+k}(2k+1) \begin{Bmatrix} \ell_1 & j_2 & \ell_3 \\ \ell_3' & \ell_2' & k \end{Bmatrix} \begin{Bmatrix} j_2 & j_3 & j_1 \\ \ell_1' & \ell_3' & k \end{Bmatrix} \begin{Bmatrix} \ell_1 & j_3 & \ell_2 \\ \ell_1' & \ell_2' & k \end{Bmatrix}$$

$$= \begin{Bmatrix} j_1 & j_2 & j_3 \\ \ell_1 & \ell_2 & \ell_3 \end{Bmatrix} \begin{Bmatrix} \ell_3 & j_1 & \ell_2 \\ \ell_1' & \ell_2' & \ell_3' \end{Bmatrix}$$

where $S = j_1 + j_2 + j_3 + \ell_1 + \ell_2 + \ell_3 + \ell_1' + \ell_2' + \ell_3'$. Using this equation (A1.4) becomes the desired result:

$$\langle J'M'|L(\lambda,\vec{\varepsilon})|JM\rangle = C \sum_{kq} (-1)^q \, \ell^k_{-q} (-1)^{J'-M'}$$

$$\times \begin{pmatrix} J' & k & J \\ -M' & q & M \end{pmatrix} (-1)^{L+S+J} \, [J\,J'k]^{\frac{1}{2}} \begin{Bmatrix} J' & J & k \\ L & L & S \end{Bmatrix} \begin{Bmatrix} L & L & k \\ 1 & 1 & L_f \end{Bmatrix}.$$

Comparison with equation (2.7) reveals that the reduced matrix element of L^k_q may be written

$$\langle \alpha(LS)J'\|L^k\|\alpha(LS)J\rangle = C \; (-1)^{L+S+J} \, [J\,J'k]^{\frac{1}{2}}$$

$$\begin{Bmatrix} J' & J & k \\ L & L & S \end{Bmatrix} \begin{Bmatrix} L & L & k \\ 1 & 1 & L_f \end{Bmatrix}$$

A1.2 Symmetry Consequences to ρ^k_q

There is one symmetry condition that always applies to the beam-foil source (even with a tilted foil) which simplifies ρ^k_q. That condition is reflection symmetry in the

plane containing the beam and lying perpendicular to the foil-tilt axis. If the z-axis, the axis of quantization, is chosen to lie along the beam and the x-axis is chosen as the foil-tilt axis, then ρ^k_q must be invariant to a change of $x \to -x$. This transformation is equivalent to an inversion followed by a 180° rotation about z, followed by a 180° rotation about y. ρ^k_q must be invariant to an inversion since all of the upper states considered have the same definite parity.

Any spherical tensor transforms under rotations as

$$D(\omega)\, T^k_q\, D^{-1}(\omega) = \sum_{q'=-k}^{k} T^k_{q'}\, D^{(k)}_{q'q}(\omega)$$

In terms of the Euler angles[1] (α,β,γ)

$$D^{(k)}_{q'q}(\alpha,\beta,\gamma) = e^{iq'\gamma}\, d^k_{q'q}(\beta)\, e^{iq\alpha} \tag{A1.5}$$

or

$$D^{(k)}_{q'q}(\pi,\pi,0) = (-1)^{k+q}\, \delta_{q'-q}\, (-1)^q .$$

Applied to ρ^k_q this yields the condition

$$\rho^k_q = (-1)^k\, \rho^k_{-q} . \tag{A1.6}$$

Axial symmetry is nothing more than the demand that

---

[1]See section 1.3 of Ed 74 for definition of Euler angles and section 4.1 for the rotation matrices.

ρ^k_q be invariant to an arbitrary rotation about the z-axis (an α rotation). Equation (A1.5) then demands that q must equal 0. Hence only the ρ^k_0 elements can be non-zero but equation (A1.6) already demands that $\rho^1_0 = 0$, so only ρ^0_0 and ρ^2_0 may be non-zero for a perpendicular foil.

A1.3 Evaluation of the Trace of ρ

The trace of the density matrix is given by

$$\mathrm{Tr}\,\rho = \sum_{JM} \langle\alpha(LS)JM|\rho(0)|\alpha(LS)JM\rangle$$

$$= \sum_{kq}\sum_{JM} (-1)^{J-M+L+S+J+k}\,[J][S]^{-1}\,\rho^k_q \times \begin{pmatrix} J & J & k \\ M & -M & q \end{pmatrix} \begin{Bmatrix} J & J & k \\ L & L & S \end{Bmatrix}.$$

The 3-j symbol demands that q = 0. The sum over k may be written out to yield[1]

$$\mathrm{Tr}\,\rho = \sum_{JM} (-1)^{J-M}(-1)^{J+L+S}\,\rho^0_0\frac{(2J+1)}{(2S+1)} \begin{pmatrix} J & J & 0 \\ M & -M & 0 \end{pmatrix} \begin{Bmatrix} J & J & 0 \\ L & L & S \end{Bmatrix}$$

$$\times \sum_{JM} (-1)^{J-M}(-1)^{J+L+S}\,\rho^2_0\frac{(2J+1)}{(2S+1)} \begin{pmatrix} J & J & 2 \\ M & -M & 0 \end{pmatrix} \begin{Bmatrix} J & J & 2 \\ L & L & S \end{Bmatrix}$$

---

[1] The density matrix may indeed have elements for k>2 but these are not relevant to light emission in the dipole approximation because of the appearance of $\begin{Bmatrix} L & L & k \\ 1 & 1 & L_f \end{Bmatrix}$ which limits k to ≤ 2.

The first sum is $\sqrt{2L + 1}\,\rho_0^0$ while the second sum is zero. This is a consequence of

$$\sum_{M=-J}^{J} (-1)^{J-M} \begin{pmatrix} J & J & 2 \\ M & -M & 0 \end{pmatrix} = 0$$

which results from summing the exact expression for the 3-j symbol for both the half-integer and integer cases. Finally

$$\mathrm{Tr}\ \rho = \sqrt{2L + 1}\,\rho_0^0 \quad .$$

APPENDIX 2

TABULATION OF RESULTS

A2.1 Experimental Conditions and Results for He I Singlets

<u>For Results Shown in Figures 5 and 6</u>

Incident ion energy = 160 ± 5 KeV

Beam velocity = 2.78 ± .04 mm/ns

Beam current = 7 ± 2 μA

Beam diameter = 7 mm

Foil thickness = 5 ± 1 $\mu g/cm^2$

Spectrometer slits = 500 μm

He I $2s\ ^1S - 3p\ ^1P^\circ$ 5016 Å

Foil-tilt angle α (degrees)	M/I	C/I	S/I
0	18.7 ± 0.7[a]	-1.3[a,b]	-0.5 ± 0.4[a]
10	19.9 ± 1.0	2.7	-3.8 ± 0.6
20	15.9 ± 0.8	4.6	-6.2 ± 0.5
30	13.9 ± 1.0	5.5	-9.6 ± 0.6
40	11.1 ± 1.0	4.2	-12.8 ± 0.6
50	6.1 ± 0.8	5.0	-16.7 ± 0.5
60	-1.8 ± 1.0	6.7	-20.6 ± 0.6
70	-2.3 ± 0.9	2.7	-20.6 ± 0.6

a. Values in percent $\Delta = 104^\circ$
b. Uncertainties same as M/I

Band parameters: A=-4.61, B=-1.01, D=-0.15, E=-1.18, F=0.23

He I $2s\,^1S - 4p\,^1P°$ 3965 Å

Foil-tilt angle α (degrees)	M/I	C/I	S/I
0	17.9 ± 0.9[a]	0.5[a,b]	-0.3 ± 0.9[a]
10	15.7 ± 0.8	2.8	-2.8 ± 0.8
20	15.0 ± 0.9	3.2	-7.2 ± 0.9
30	10.8 ± 0.6	5.7	-12.7 ± 0.6
40	7.6 ± 0.5	5.1	-14.2 ± 0.6
50	2.9 ± 0.6	2.8	-17.9 ± 0.7
60	-0.4 ± 0.7	1.0	-19.8 ± 0.7
70	-5.1 ± 1.1	-2.4	-19.1 ± 1.1

a. Values in percent $\Delta = 130°$
b. Uncertainties same as M/I

Band parameters: A=-3.29, B=-1.33, D=-0.07, E=-0.94, F=0.24

He I $2p\,^1P° - 3d\,^1D$ 6678 Å

Foil-tilt angle α (degrees)	M/I	C/I	S/I
0	6.8 ± 0.8[a]	0.2[a,b]	-0.2 ± 0.3[a]
10	7.1 ± 1.0	-0.8	0.6 ± 0.4
20	7.6 ± 0.9	0.7	1.4 ± 0.4
30	5.4 ± 0.7	-1.2	1.6 ± 0.3
40	1.8 ± 0.9	-0.9	-0.3 ± 0.3
50	-2.5 ± 0.7	-1.0	-1.9 ± 0.3
60	-7.1 ± 1.1	-1.0	-5.8 ± 0.4
70	-11.0 ± 1.9	-2.3	-12.1 ± 0.7

a. Values in percent $\Delta = 74°$
b. Uncertainties same as M/I

Band parameters: A=-18.8, B=-0.51, D=0.09, E=-1.61, F=0.56

He I $2p\,^1P^\circ - 4d\,^1D$ 4922 Å

Foil-tilt angle α (degrees)	M/I	C/I	S/I
0	7.3 ± 0.7[a]	-0.3[a,b]	0.0 ± 0.4[a]
10	7.9 ± 0.6	-0.2	0.3 ± 0.4
20	7.3 ± 0.4	-0.8	0.2 ± 0.3
30	4.2 ± 0.5	-2.2	-1.2 ± 0.3
40	1.3 ± 0.6	-1.9	-3.0 ± 0.4
50	-1.6 ± 0.7	-2.3	-5.8 ± 0.4
60	-5.2 ± 0.7	-4.0	-9.7 ± 0.4
70	-7.4 ± 0.7	-4.4	-12.7 ± 0.4

a. Values in percent Δ = 106°
b. Uncertainties same as M/I

Band parameters: A=-17.4, B=-0.46, D=0.19, E=-1.35, F=0.41

He I $2p\,^1P^\circ - 4s\,^1S$ 5048 Å[a]

Foil-tilt angle α (degrees)	M/I	C/I	S/I
0	0.0 ± 0.8[b]	-0.2[b,c]	-0.5 ± 0.5[b]
10	-0.4 ± 0.8	-0.2	0.3 ± 0.5
20	0.3 ± 0.8	-1.7	-0.7 ± 0.5
30	-0.7 ± 0.9	-1.4	0.1 ± 0.5
40	0.3 ± 0.8	-1.4	-0.4 ± 0.4
50	1.2 ± 1.0	0.7	-1.4 ± 0.6
60	0.6 ± 1.0	-1.3	-0.2 ± 0.6
70	-1.1 ± 0.8	-0.1	0.3 ± 0.5

a. Not plotted in figures Δ = 104°
b. Values in percent
c. Uncertainties same as M/I

For Results Shown in Figure 7

Incident ion energy = 160 ± 5 KeV

Beam velocity = 2.78 ± 0.04 mm/ns

Beam current = 7 ± 2 μA

Beam diameter = 5 mm

Foil thickness = 5 ± 1 μg/cm^2

Spectrometer slits = 500 μm

He I 2s ^{1}S - 3p ^{1}P° 5016 Å

Foil-tilt angle α (degrees)	M/I	C/I	S/I
0	16.8 ± 0.6[a]	-0.4[a,b]	0.2 ± 0.4[a]
5	17.2 ± 1.5	-0.2	-1.4 ± 1.0
10	17.9 ± 0.7	0.3	-3.3 ± 0.4
15	16.5 ± 0.7	2.1	-5.2 ± 0.4
20	16.0 ± 0.5	3.3	-6.8 ± 0.3
25	14.8 ± 1.5	3.7	-8.9 ± 0.9
30	13.1 ± 0.7	3.1	-11.0 ± 0.4
35	12.3 ± 1.6	2.7	-13.2 ± 1.0
40	9.8 ± 0.6	3.3	-13.5 ± 0.4
45	7.8 ± 0.5	4.0	-16.6 ± 0.3
50	6.2 ± 0.6	3.8	-16.8 ± 0.4
55	4.1 ± 0.5	3.8	-18.4 ± 0.3
60	0.6 ± 0.6	2.4	-18.8 ± 0.4
65	-0.8 ± 0.5	2.3	-20.5 ± 0.4
70	-5.1 ± 0.7	0.8	-20.6 ± 0.4
75	-8.3 ± 0.8	-0.2	-21.5 ± 0.5
80	-10.6 ± 0.7	-3.8	-22.9 ± 0.5

a. Values in percent
b. Uncertainties same as M/I

Δ = 104°

He I $2p\,^1P^\circ - 4d\,^1D$ 4922 Å

Foil-tilt angle α (degrees)	M/I	C/I	S/I
0	8.2 ± 0.5[a]	-0.4[a,b]	0.4 ± 0.4[a]
5	6.6 ± 0.6	0.0	0.2 ± 0.4
10	7.8 ± 0.5	-1.4	0.8 ± 0.3
15	6.6 ± 0.7	-1.2	0.4 ± 0.4
20	6.0 ± 0.6	-2.2	-0.2 ± 0.4
25	5.4 ± 0.7	-2.6	0.0 ± 0.4
30	5.0 ± 0.6	-2.6	0.9 ± 0.4
35	3.1 ± 0.6	-2.7	-0.4 ± 0.4
40	0.5 ± 0.6	-2.8	-0.8 ± 0.4
45	-1.5 ± 0.7	-3.9	-2.9 ± 0.4
50	-2.3 ± 0.6	-5.4	-4.3 ± 0.4
55	-4.3 ± 0.6	-3.5	-6.6 ± 0.4
60	-7.7 ± 1.0	-4.7	-9.8 ± 0.7
65	-8.4 ± 0.7	-5.8	-11.4 ± 0.5
70	-10.6 ± 1.3	-5.1	-14.8 ± 0.9
75	-10.7 ± 0.8	-7.5	-15.6 ± 0.5
80	-13.9 ± 1.2	-10.1	-19.8 ± 0.8

a. Values in percent

b. Uncertainties same as M/I

$\Delta = 106^\circ$

A2.2 Experimental Conditions for Helium Spectra (Figure 8)

Incident ion energy = 163 ± 5 KeV

Beam velocity =2.81 ± 0.04 mm/ns

Foil thickness = 10 ± 2 μg/cm^2

Spectrometer slits = 500 μm

Instrumental line width = 2.8 Å

Plot resolution = 1 Å per channel

Time normalization = 4.6 sec per point

NOTE: Vertical scale of Figure 8 becomes linear when signal is raised to the 0.5 power (square-root).

A2.3 Experimental Conditions and Results for Helium Double-Excited States (Figure 9)

Incident ion energy = 163 ± 5 KeV

Beam velocity = 2.81 ± 0.04 mm/ns

Beam current = 7 ± 2 μA; except 80° points ≃ 3 μA

Beam diameter = 5 mm

Foil thickness = 10 ± 2 $\mu g/cm^2$

Spectrometer slits = 500 μm

He I 2s2p $^3P^\circ$ - 2p3p ^3D 2577 Å

Foil-tilt angle α (degrees)	M/I	C/I	S/I
0	8.4 ± 0.5[a]	-1.8[a,b]	-1.0 ± 0.8[a]
10	6.3 ± 0.5	-1.0	-5.7 ± 0.8
20	8.2 ± 0.7	-0.8	-9.7 ± 1.1
30	6.8 ± 1.0	-0.4	-15.4 ± 1.5
40	7.3 ± 0.8	-1.4	-18.5 ± 1.2
50	6.7 ± 0.5	-1.0	-25.1 ± 0.8
60	7.0 ± 1.2	-0.7	-32.5 ± 1.9
70	5.8 ± 0.7	-3.5	-36.2 ± 1.1
80	7.7 ± 2.3	-3.0	-39.1 ± 3.5

a. Values in percent

b. Uncertainties same as M/I

Δ = 144°

He I $2p^2\ ^3P - 2p3d\ ^3D°$ 3014 Å

Foil-tilt angle α (degrees)	M/I	C/I	S/I
0	-3.3 ± 0.7[a]	0.0[a,b]	-0.3 ± 0.6[a]
10	-3.3 ± 0.8	1.5	-1.7 ± 0.7
20	-2.8 ± 0.5	0.7	-3.6 ± 0.4
30	-3.7 ± 0.9	-0.1	-6.3 ± 0.7
40	-4.0 ± 1.0	0.7	-8.7 ± 0.8
50	-4.9 ± 0.7	-0.1	-10.5 ± 0.6
60	-4.4 ± 0.9	0.6	-14.0 ± 0.7
70	-6.3 ± 1.1	-1.7	-17.2 ± 0.9
80	-3.2 ± 1.8	-0.1	-19.4 ± 1.5

a. Values in percent $\Delta = 118°$
b. Uncertainties same as M/I

He I $2p^2\ ^3P - 2p3d\ ^3P°$ 2818 Å[a]

Foil-tilt angle α (degrees)	M/I	C/I	S/I
0	0.7 ± 0.9[b]	0.3[b,c]	0.6 ± 0.8[b]
20	1.5 ± 1.0	0.9	-1.2 ± 1.0
40	-0.1 ± 1.4	-1.5	-2.1 ± 1.3
60	1.9 ± 0.7	-0.8	0.1 ± 0.6
He I $2p^2\ ^3P - 2p4d\ ^3D°$ 2562 Å[a] (blend)			
0	-1.3 ± 0.5[b]	0.0[b,c]	0.4 ± 0.7[b]
20	0.2 ± 0.6	0.4	-5.0 ± 0.9
40	-1.8 ± 0.6	-1.6	-12.0 ± 0.9
60	-1.7 ± 1.1	-2.0	-20.9 ± 1.7

a. Not plotted in figure $\Delta = 123°$
b. Values in percent
c. Uncertainties same as M/I $\Delta = 144°$

A2.4 Experimental Conditions and Results for Helium Triplets

<u>For Results Shown in Figures 10 and 11</u>

Incident ion energy = 163 ± 5 KeV

Beam velocity = 2.81 ± 0.04 mm/ns

Beam current = 5 - 7 μA; except 80° points ≃ 3 μA

Beam diameter = 5 mm

Foil thickness: 3889 Å & 5875 Å = 5 ± 1 μg/cm^2

3188 Å = 10 ± 2 μg/cm^2

Spectrometer slits: 3889 Å & 5875 Å = 500 μm

3188 Å = 500 μm @ 0° tilt → 250 μm @ 60° tilt

He I 2s ^{3}S - 3p ^{3}P° 3889 Å[a]

Foil-tilt angle α (degrees)	M/I	C/I	S/I
0	13.6 ± 1.0[b]	-1.0[b,c]	0.2 ± 1.2[b]
10	10.8 ± 0.6	-0.2	-3.0 ± 0.7
20	6.8 ± 0.5	0.1	-5.4 ± 0.6
30	5.0 ± 0.5	-0.2	-6.8 ± 0.6
40	-1.1 ± 0.5	-1.2	-7.5 ± 0.6
50	0.2 ± 0.5	-0.1	-10.6 ± 0.6
60	0.5 ± 0.7	0.0	-9.3 ± 0.9
70	0.3 ± 0.8	-0.1	-15.0 ± 1.0
80	-0.9 ± 0.9	-0.2	-17.4 ± 1.1

a. Measurement perturbed. See text. Δ = 134°
b. Values in percent
c. Uncertainties same as M/I

He I $2s\ ^3S - 4p\ ^3P°$ 3188 Å

Foil-tilt angle α (degrees)	M/I	C/I	S/I
0	16.6 ± 0.6[a]	0.4[a,b]	0.4 0.4[a]
10	17.0 ± 0.6	-0.3	-5.8 0.4
20	14.4 ± 0.6	-0.1	-10.3 0.4
30	12.5 ± 0.6	1.6	-14.4 0.4
40	13.1 ± 0.7	0.3	-19.1 0.5
50	9.8 ± 0.6	0.6	-20.6 0.4
60	6.8 ± 1.0	0.8	-22.1 0.7
70	4.1 ± 0.7	0.4	-22.7 0.5
80	-0.1 ± 1.0	-1.9	-22.0 0.7

a. Values in percent $\Delta = 108°$
b. Uncertainties same as M/I

He I $2p\ ^3P° - 3d\ ^3D$ 5875 Å

Foil-tilt angle α (degrees)	M/I	C/I	S/I
0	4.7 ± 0.8[a]	-0.8[a,b]	0.0 ± 0.4[a]
10	3.6 ± 0.8	-1.6	0.1 ± 0.4
20	3.6 ± 0.7	-0.7	0.1 ± 0.3
30	1.4 ± 0.8	0.5	-0.6 ± 0.4
40	-1.6 ± 0.6	2.0	-2.4 ± 0.3
50	-3.2 ± 1.0	0.1	-4.9 ± 0.5
60	-4.6 ± 0.9	-1.0	-8.9 ± 0.4
70	-9.8 ± 1.4	-1.0	-16.2 ± 0.7
80	-7.9 ± 1.3	-3.3	-20.8 ± 0.6

a. Values in percent $\Delta = 88°$
b. Uncertainties same as M/I

For Results Shown in Figure 12

Incident ion energy = 152 ± 5 KeV

Beam velocity after foil = 2.65 ± 0.04 @ 0°; 2.59 ± 0.04 mm/ns @ 60°

Beam current = 7 ± 1 μA

Beam diameter = 5 mm

Foil thickness = 5 ± 1 μg/cm^2

Spectrometer slits = 500 μm @ 0° tilt; 250 μm @ 60° tilt

He I 2s ^{3}S - 3p ^{3}P° 3889 Å

Position from foil (mm)	0°	60°		
	M/I	M/I	C/I	S/I
0.65	11.2 ± 0.8[a]			
1.00		2.1 ± 0.9[a]	0.3[a,b]	-13.9 ± 1.1[a]
1.15	1.9 ± 0.7			
1.50		-0.5 ± 0.5	-0.5	-11.2 ± 0.6
1.65	-2.8 ± 0.4			
2.00		-1.0 ± 0.8	-1.6	-9.4 ± 0.9
2.15	-2.7 ± 0.6			
2.50		0.1 ± 0.8	0.0	-11.6 ± 0.9
2.65	3.9 ± 0.5			
3.00		4.3 ± 0.7	1.6	-15.5 ± 0.8
3.15	9.9 ± 0.6			
3.50		7.2 ± 0.6	1.6	-20.4 ± 0.7
3.65	15.7 ± 0.6			
4.00		6.1 ± 0.5	2.4	-21.8 ± 0.6
4.15	15.0 ± 0.6			
4.50		5.2 ± 0.6	1.7	-17.2 ± 0.7
4.65	12.3 ± 0.5			
5.00		1.8 ± 0.6	0.3	-13.0 ± 0.7

a. Values in percent
b. Uncertainties same as M/I

Δ = 134°

For Results Shown in Figure 13

Incident ion energy = 162 ± 5 KeV

Beam velocity after foil = 2.74 ± 0.04 @ 0°: 2.56 ± 0.04 mm/ns @ 60°

Beam current = 7 ± 1 μA

Beam diameter = 5 mm

Foil thickness = 10 ± 2 $\mu g/cm^2$

Spectrometer slits = 500 μm @ 0° tilt; 300 μm @ 60° tilt

He I 2s ^3S - 4p $^3P°$ 3188 Å

Position from foil (mm)	0°	60°		
	M/I	M/I	C/I	S/I
10.00		6.8 ± 1.0[a]	0.8[a,b]	-22.1 ± 0.7[a]
10.45	16.6 ± 0.6[a]			
11.50		6.3 ± 1.2	0.6	-20.1 ± 0.8
11.95	10.0 ± 0.9			
13.00		0.5 ± 1.0	-0.1	-14.0 ± 0.7
13.45	0.6 ± 0.8			
14.50		-2.0 ± 0.9	-1.4	-13.6 ± 0.6
14.95	-4.7 ± 0.5			
16.00		1.0 ± 0.8	-1.4	-18.4 ± 0.6
16.45	-0.5 ± 0.8			
17.50		4.1 ± 1.0	-0.9	-24.0 ± 0.7
17.95	8.5 ± 0.6			
19.00		5.3 ± 1.2	-0.3	-24.5 ± 0.8
19.45	16.0 ± 0.9			
20.50		3.6 ± 0.9	0.8	-19.2 ± 0.6
20.95	14.1 ± 0.6			

a. Values in percent

b. Uncertainties same as M/I

Δ = 108°

A2.5 Experimental Conditions for Nitrogen Spectra (Figure 14)

	14a	14b (upper)	14b (lower)	14c
Incident ion energy (KeV):	259(8)	252(8)	259(8)	259(8)
Beam velocity (mm/ns):	1.89(3)	1.86(3)	1.89(3)	1.89(3)
Foil thickness ($\mu g/cm^2$):	10 ± 2	5 ± 1	5 ± 1	10 ± 2
Spectrometer slits (μm):	500	500	300	500
Instrumental line width (Å):	2.8	5.5	3.3	5.5
Plot resolution (A/channel):	1.0	2.0	2.0	2.0
Time normalization (secs):	2.2	2.2	2.2	2.2
Polarizer and retarder:	OUT	IN	IN	OUT

NOTE: Vertical scale of Figure 14 becomes linear when signal is raised to the 0.7 power.

A2.6 Experimental Conditions and Results for N III (Figure 15)

Incident ion energy = 255 ± 8 KeV

Beam velocity = 1.87 ± 0.03 mm/ns

Beam current ≃ 1 μA

Foil thickness = 5 ± 1 $\mu g/cm^2$

Spectrometer slits = 500 μm

Beam diameter = 5 mm

N III $3s\ ^2S - 3p\ ^2P^\circ$ 4097 Å

Foil-tilt angle α (degrees)	M/I	C/I	S/I
0	2.2 ± 0.9[a]	1.4[a,b]	0.0 ± 0.9[a]
20	2.2 ± 1.0	-0.6	-3.1 ± 1.0
40	0.4 ± 0.8	-1.5	-6.2 ± 0.8
60	0.0 ± 0.8	-0.5	-8.2 ± 0.8

a. Values in percent $\Delta = 126°$
b. Uncertainties same as M/I

N III $4f\ ^2F^\circ - 5g\ ^2G$ 4379 Å

Foil-tilt angle α (degrees)	M/I	C/I	S/I
0	3.9 ± 0.7[a]	-0.2[a,b]	-0.3 ± 0.6[a]
10	5.5 ± 1.2	-0.5	-0.9 ± 1.0
20	3.1 ± 1.1	-3.0	-2.0 ± 1.0
30	2.8 ± 1.0	-3.1	-4.5 ± 0.9
40	3.0 ± 1.1	-2.1	-6.9 ± 0.9
50	1.8 ± 1.1	-3.5	-9.3 ± 1.0
60	1.3 ± 1.3	-4.3	-14.1 ± 1.1
70	1.1 ± 0.7	-4.2	-14.3 ± 0.6
80	4.5 ± 1.0	-3.3	-13.7 ± 0.8

a. Values in percent $\Delta = 120°$
b. Uncertainties same as M/I